Non-Linear Moving Least Squares and applications

Summary

José Manuel Ramón García
Director: Dionisio F. Yáñez Avendaño

VNIVERSITAT DE VALÈNCIA

Doctorat en Matemàtiques
Program: Anàlisi numèrica, imatges i simulació
September 2025, Burjassot (València)

Acknowledgments

I would like to thank the people who made my PhD studies an incredible and unforgettable experience. I will keep it in my mind all my life.

First of all, I want to express my gratitude to Dionisio F. Yáñez. He has taught me how to understand all the papers we have had to deal with. Moreover, he has always given tips to express my ideas in a way that it can be understandable for other people, and I was able to give a talk in a congress with clear ideas about the *topic* . He also made me feel I could get my goal and it's something that I'll keep forever.

To Professor Juan Ruiz Álvarez, which was part of our research group, and he has been always there to help me with my research and my papers.

To Professor David Levin, another member of our research groups. Without his ideas it would have been difficult to write down these papers.

Undoubtfully, without the help of all these Professors, the aim of getting a PHD wouldn't have been possible.

To all the members of my Mathematics department, including the staff people, to make me easier to achieve my objective

To Aula Campus my main job, a vocational computer studies center that have never rejected to help me. They have always given me the opportunity of attending Congresses and spend time with my PHD studies and classes as an assistant teacher in Applied Mathematics.

To my family and my friends, for their support in the way that I have spent many weekends working on the project and I haven't had the enough time to be with them. Especially to my mother and my siblings, for always listening and understanding me. And unfortunately to my father that passed away a year ago and he would be very proud of his son.

Thanks to you for making me feel that my adventure has just begun and will be fruitful in the years to come.

Index

1 Introduction

I will present three classic approximation methods that I will use to design new methods with new features that make them novel and at the same time more accurate when they are used to approximate functions that present discontinuities.

1.1 The Weighted Essentially Non-Oscillatory method (WENO)

The Weighted Essentially Non-Oscillatory (WENO) method was developed to solve numerically hyperbolic partial differential equations with discontinuous solutions [23, 28]. The WENO algorithm builds upon the Essentially Non-Oscillatory (ENO) scheme [22], which aims to provide precise, high-order accuracy in smooth regions, while simultaneously preventing unwanted oscillations around discontinuities in solutions of conservation law. The main idea of the WENO method is to build up a weighted combination of several candidate stencils. For a given point, the WENO scheme selects the smoothest stencil by assigning weights that diminish the influence of stencils crossing discontinuities. The smoothness indicators are used to measure the smoothness of the function within each stencil, and the data-dependent weights are computed based on these indicators.

Consider a function $f : [a, b] \to \mathbb{R}$ that we want to approximate within the domain $x_i \in [a, b]$. The WENO reconstruction for the function at x_i is given by:

$$\hat{f}(x_i) = \hat{f}_i = \sum_{k=0}^{r-1} \omega_k p_k(x_i), \tag{1}$$

where r is the number of stencils, p_k are the polynomial approximations from each stencil, and ω_k are the data-dependent weights. The weights ω_k are computed as:

$$\omega_k = \frac{\alpha_k}{\sum_{l=0}^{r-1} \alpha_l}, \tag{2}$$

with

$$\alpha_k = \frac{C_k}{(\epsilon + I_k)^t}, \tag{3}$$

where C_k are the linear weights, I_k are the smoothness indicators, ϵ is a small positive number to avoid division by zero, and t is a parameter typically set to 2 or 4 in order to obtain optimal accuracy at smooth zones. The smoothness indicators I_k were designed in [23] using a measure of the smoothness of the underlying data inspired in the total variation:

$$I_k = \sum_{l=1}^{r-1} \int_{x_{i-1/2}}^{x_{i+1/2}} \Delta x^{2l-1} \left(\frac{d^l}{dx^l} f_k(x) \right)^2 dx, \tag{4}$$

where Δx is the grid spacing. Given the nature of the problem we intend to solve, we will define the smoothness indicators in a different way. This approach is more appropriate considering the scattered distribution of data points we are assuming.

1.2 Moving Least Squares method (MLS)

The Moving Least Squares (MLS) method, that was originally proposed by Shepard in [38] and further developed by Lancaster and Salkauskas in [24], is a powerful mathematical tool for generating smooth surfaces from scattered data points and for approximation of data. The MLS method has been widely applied in various fields such as data approximation [26], image processing [25], and geometric modelling [42], among others.

In the classical MLS approach, the objective is to approximate a function $f : \Omega \subset \mathbb{R}^n \to \mathbb{R}$ given a set of scattered data points:

$$\{(\mathbf{x}_i, f_i)\}_{i=1}^N,$$

where $\mathbf{x}_i \in \mathbb{R}^n$ and $f_i = f(\mathbf{x}_i) \in \mathbb{R}$.

The more general form of the MLS approximation $\hat{f}(\mathbf{x})$ at a point $\mathbf{x} \in \Omega$ is obtained by minimizing a weighted least squares error:

$$J(a(\mathbf{x})) = \sum_{i=1}^{N} \omega(\mathbf{x} - \mathbf{x}_i) \left(f_i - \sum_{j=0}^{m} a_j(\mathbf{x}) \phi_j(\mathbf{x} - \mathbf{x}_i) \right)^2, \tag{5}$$

where $\omega(\mathbf{x} - \mathbf{x}_i)$ is a weight function that decreases with the distance between $\mathbf{x}$ and $\mathbf{x}_i$, ϕ_j are functions as, for example, polynomials, and $a_j(\mathbf{x})$ are the coefficients to be determined. The weight function $\omega(\mathbf{x} - \mathbf{x}_i)$ is designed so that points closer to $\mathbf{x}$ have a larger influence on the approximation.

Despite its effectiveness in smooth regions, the classical MLS method tends to produce oscillations near jump discontinuities. This restriction arises from the fact that the method requires a continuous underlying function, which is not satisfied in the presence of discontinuities. Various strategies have been proposed to address this issue, including modifications to the weight function and the development of methods that adapt to data with discontinuities [16, 31, 32, 40].

In this work, we propose a data-dependent modification to the classical MLS method, inspired by the WENO algorithm [23, 28]. Our purpose is to handle discontinuities more effectively including a data-dependent modification in the minimization problem (5). Our approach can be interpreted as an artificial adjustment of the distances of points near discontinuities, thereby reducing oscillations and improving the accuracy of the approximation.

1.3 Partition of Unit method (PUM)

Kernel-based methods are effective and versatile instruments applied in diverse scientific areas, such as computer-aided geometric design, solving partial differential equations numerically, and image processing. We can find examples [12, 13, 43] of PU method using Radial Basis Functions (RBF) and used for signal processing on graphs, *mesh*-independent surface interpolation, applications in differential geometry and topology and so on. These schemes are satisfactorily used in interpolation, regression, and machine learning due to their easy and quick implementation and their simple generalization for any dimension [11, 12, 13, 27, 42, 43].

The problem consists in finding a good approximation to an unknown function, $f : \Omega \subset \mathbb{R}^n \to \mathbb{R}$, from some data values $F = \{f_i = f(\mathbf{x}_i),\ i = 1, \ldots, N\}$ given a set of arbitrarily distributed points on an open and bounded domain $\Omega \subset \mathbb{R}^n$, $X = \{\mathbf{x}_i \in \Omega,\ i = 1, \ldots, N\}$. RBF method consists of developing the function as a linear combination of a basis of radial functions centered at the data points X. There exists a vast literature about it (see, e.g., [10, 17, 42]), however, the efficiency of the method can be improved in different ways. One approximation, called PUM or PU method (see e.g., [10, 11, 12, 17, 42]), involves partitioning the entire domain into multiple smaller subdomains and applying the RBF method to each of them. Ultimately, a convex combination of these interpolants yields the final approximation. Satisfactory results are obtained when these methods are employed to data originating from continuous functions.

We are going to introduce a non-linear modification of the Partition of Unity Method (NL-PUM). To achieve this, we will replace the PUM weight functions by non-linear ones using the ideas of WENO method. The design of this new method allows us to reduce the oscillations and smearing close to discontinuity zones that the classical PUM method produces.

2 Weighted Essentially Non-Oscillatory Shepard method

2.1 Construction of the non-linear method

We will follow the notation of the paper [LRRY25a]. We assume an open and bounded domain $\Omega \subset \mathbb{R}^n$, a set of N distinct nodes

$$\chi_N = \{\mathbf{x}_i \in \Omega : i = 1, \dots, N\},$$

and a corresponding set of function values

$$\mathcal{F}_N = \{f_i = f(\mathbf{x}_i) : i = 1, \dots, N\},$$

where $f : \Omega \to \mathbb{R}$ is unknown. We define the fill distance as

$$h \equiv \sup_{x \in \Omega} \min_{\mathbf{x}_i \in \chi_N} \|\mathbf{x} - \mathbf{x}_i\|,$$

and consider that the points χ_N are quasi-uniformly distributed in Ω, meaning by *quasi-uniform* the definition 4.6 given in [42].
Consequently, if we consider a non-negative, compactly supported, function $\omega : [0, \infty) \to \mathbb{R}$, and define

$$\omega_i(\mathbf{x}) = \omega\left(\frac{\|\mathbf{x}_i - \mathbf{x}\|}{h}\right), \tag{6}$$

the Shepard's approximant is defined as:

$$\mathcal{I}_{\mathrm{S}}(\mathbf{x}) = \sum_{i=1}^{N} \frac{\omega_i(\mathbf{x})}{\sum_{j=1}^{N} \omega_j(\mathbf{x})} f_i = \sum_{i=1}^{N} W_i(\mathbf{x}) f_i,$$

where $W_i : \Omega \to \mathbb{R}$ are defined as $W_i(\mathbf{x}) = \frac{\omega_i(\mathbf{x})}{\sum_{j=1}^{N} \omega_j(\mathbf{x})}$. It follows that for $i = 1, \dots, N$, we have $0 \leq W_i(\mathbf{x}) \leq 1$, and $\sum_{j=1}^{N} W_j(\mathbf{x}) = 1, \forall \mathbf{x} \in \mathbb{R}^n$.
As described above, Shepard's method is based on the distances between the evaluation point and the given nodes. However, if a discontinuity contaminates the data, or they present a strong gradient, it is then recommended to use only nodes that are free of singularities. To achieve this, the Shepard weights are replaced with non-linear ones, defined as follows:

$$\mathcal{W}_i(\mathbf{x}) = \frac{\alpha_i(\mathbf{x})}{\sum_{j=1}^{N} \alpha_j(\mathbf{x})}, \quad \alpha_i(\mathbf{x}) = \frac{W_i(\mathbf{x})}{(\epsilon + I_i)^t}.$$

The values $\{I_i\}_{i=1}^{N}$ are smoothness indicators, see [39], which identify whether a node is near a discontinuity and, thus, should have a negligible contribution to

the approximation. The parameters ϵ and t are chosen to avoid divition by 0 in ϵ, and to achieve maximal approximation order in t. In our case, we take $\epsilon = 10^{-14}$ and $t = 4$. In the next subsection, we present a way to construct the smoothness indicators. With these ingredients the new WENO-Shepard's method is:

$$\mathcal{I}_{\text{WENO-S}}(\mathbf{x}) = \sum_{i=1}^{N} \mathcal{W}_i(\mathbf{x}) f_i. \tag{7}$$

2.2 The smoothness indicators

We start dividing our domain Ω in some subdomains $\mathcal{S}_i$ with

$$\Omega \subseteq \cup_{i=1}^{N} \mathcal{S}_i,$$

which satisfy that $\mathbf{x}_i \in \mathcal{S}_i$, $i = 1, \ldots, N$. In our case, we define the *stencils* as the balls centered in the data points, $\mathbf{x}_i$, with a determined radius, δ_i i.e.,

$$\mathcal{S}_i = \chi_N \cap B(\mathbf{x}_i, \delta_i) = \{\mathbf{x}_j \in \chi_N : \|\mathbf{x}_j - \mathbf{x}_i\| < \delta_i\}, \quad |\mathcal{S}_i| = N_i \geq 4. \tag{8}$$

To determine the radius, we rely on the general results presented in [17, 26, 43], which assume that $\delta_i = ch$, where we take c as a constant greater than 2 (to assure that the stencils are not empty and, at the same time, if $\mathbf{x}_i$ is close to the discontinuity, to assure that data points from both sides of the discontinuity take part in the approximation) and h is the fill distance.

To design the smoothness indicators, we aim for two properties indicated, for example, in [4]:

1. The order of a smoothness indicator that is free of discontinuities is h^2, i.e.

$$I_i = O(h^2) \text{ if } f \text{ is smooth in } B(\mathbf{x}_i, \delta_i).$$

2. When a discontinuity crosses the stencil $\mathcal{S}_i$ then $I_i \nrightarrow 0$ as $h \to 0$.

Thus, we solve the linear least square problem for each $i = 1, \ldots, N$, and we consider

$$p_i = \underset{p \in \Pi_1(\mathbb{R}^2)}{\arg\min} \sum_{\mathbf{x}_j \in \mathcal{S}_i} (f(\mathbf{x}_j) - p(\mathbf{x}_j))^2,$$

where $\Pi_1(\mathbb{R}^2)$ are the polynomials of degree equal to or less than one, and define

$$I_i = \frac{1}{N_i} \sum_{\mathbf{x}_j \in \mathcal{S}_i} |f(\mathbf{x}_j) - p(\mathbf{x}_j))|. \tag{9}$$

It is clear that the I_i defined in (9) satisfies 1 and 2. The main idea that we are pursuing here is that a smoothness indicator can be defined as the mean of the errors at the points used to fit a polynomial using the least squares method. This indicator provides insight into the quality of the polynomial approximation. In the simplest case, where the data is gridded and the grid size is h, when the data is smooth and the polynomial is of degree 1, the mean error is expected to be of order $O(h^2)$, [17, 26, 43]. This indicates that the error decreases rapidly as the grid becomes finer. However, if the data contains a jump discontinuity, the mean error should be of order $O(1)$, reflecting that the polynomial approximation has difficulty to accurately capture the discontinuity, resulting in a larger error. This contrast in error behavior serves as a useful measure to detect and quantify the smoothness of the underlying data.

2.3 Properties of the new method

In this section, we show some characteristics about our new method. Let us start with the smoothness of the non-linear method:

Theorem 1. *Let $\nu \in \mathbb{N}$, $\Omega \subset \mathbb{R}^n$ and ω be the radial basis function, $\omega(\|\cdot\|) \in \mathcal{C}^\nu(\Omega)$, and let $\mathcal{I}_{\text{WENO-S}}$ be the WENO Shepard's approximation defined in Eq.* (7)*, then $\mathcal{I}_{\text{WENO-S}} \in \mathcal{C}^\nu(\Omega)$.*

Regarding the order of accuracy in the smooth regions, it is evident that the new operator reproduces constants, as it satisfies the condition that:

$$\sum_{i=1}^{N} \mathcal{W}_i(\mathbf{x}) = 1, \ \forall\, \mathbf{x} \in \mathbb{R}^n.$$

As ω is compactly supported, then we have the next theorem [17].

Theorem 2. *Let $\Omega \subset \mathbb{R}^n$. If $f \in \mathcal{C}^1(\overline{\Omega})$, $\chi_N = \{\mathbf{x}_i \in \Omega : i = 1, \ldots, N\}$ are quasi-uniformly distributed with fill distance h, the weight function ω is compactly supported with support size c, then*

$$\|f - \mathcal{I}_{\text{WENO-S}}\|_\infty \leq Ch \max_{\boldsymbol{\xi} \in \overline{\Omega}} |D^{\boldsymbol{\alpha}} f(\boldsymbol{\xi})|, \quad |\boldsymbol{\alpha}| = 1,$$

where C is a constant independent of h.

Let's consider a $(n-1)$-hypersurface Γ defined by a function $\gamma : \mathbb{R}^n \to \mathbb{R}$ being

$$\Omega^+ = \{\mathbf{x} \in \Omega : \gamma(\mathbf{x}) \geq 0\}, \quad \Omega^- = \Omega \setminus \Omega^+.$$

And we suppose that,

$$\tilde{f}(\mathbf{x}) = \begin{cases} f_1(\mathbf{x}), & \mathbf{x} \in \Omega^+, \\ f_2(\mathbf{x}), & \mathbf{x} \in \Omega^-, \end{cases} \tag{10}$$

with $f_1 \in \mathcal{C}^1(\overline{\Omega^+})$ and $f_2 \in \mathcal{C}^1(\overline{\Omega^-})$.

The following Theorem shows that the diffusion area is significantly reduced when using the non-linear WENO-Shepard's method.

Theorem 3. *Let* $\mathbf{x}_0 \in \Omega^+$ *be at distance* $h(1+\epsilon_0)$ *from* Γ*, with* $0 < \epsilon_0 < 1$*. Then*

$$|\tilde{f}(\mathbf{x}_0) - \mathcal{I}_{\text{WENO-S}}(\mathbf{x}_0)| = O(h).$$

2.4 Numerical experiments

In order to study the behaviour in the smooth zones, we will approximate the Franke's function defined as:

$$f(x,y) = \frac{3}{4}e^{-1/4((9x-2)^2+(9y-2)^2)} + \frac{3}{4}e^{-1/49(9x+1)^2-1/10(9y+1)} + \frac{1}{2}e^{-1/4((9x-7)^2+(9y-3)^2)} - \frac{1}{5}e^{-(9x-4)^2-(9y-7)^2} \tag{11}$$

using as nodes the regular grid $\chi_{2^l+1} = \{(i/2^l, j/2^l) : i,j = 0,\ldots,2^l\}$. We denote the fill distance as h_l and the errors as $e_i^l = |f(\mathbf{z}_i) - \mathcal{I}^l(\mathbf{z}_i)|$ with $\{\mathbf{z}_i : 1 \le i \le N_{\text{eval}}\}$ the set of points where we approximate the function.

Thus, in our experiments, we take $\varepsilon = \lfloor \frac{\sqrt{N_l}}{2} \rfloor / \sqrt{2}$ where $N_l = (2^l+1)^2$. The Wendland functions are defined as

$$\begin{aligned} \phi_{W_2}(\|\mathbf{x}\|_2) &= (1-\|\mathbf{x}\|_2)_+^4(4\|\mathbf{x}\|_2+1), \\ \phi_{W_4}(\|\mathbf{x}\|_2) &= (1-\|\mathbf{x}\|_2)_+^6(35\|\mathbf{x}\|_2^2+18\|\mathbf{x}\|_2+3) \end{aligned} \tag{12}$$

In the next table it can be seen that the behaviour of the new algorithm in the smooth zones is analogous to Shepard's method.

Another example based on the piecewise approximation function:
We consider the domain $[0,1]^2$ and a curve $\Gamma = \{(x,y) : \gamma(x,y) = 0\}$, along which we place the discontinuity, where $\gamma : \Omega \to \mathbb{R}$ is a continuous function. Then, we construct $\Omega^+ = \{(x,y) \in [0,1]^2 : \gamma(x,y) \ge 0\}$ and $\Omega^- = [0,1]^2 \setminus \Omega^+$ and define

$$\tilde{f}(x,y) = \begin{cases} 1 + f(x,y), & (x,y) \in \Omega^+, \\ f(x,y), & (x,y) \in \Omega^-, \end{cases} \tag{13}$$

(W2)	Shepard		WENO-Shepard		Shepard		WENO-Shepard	
l	MAE_l	r_l^∞	MAE_l	r_l^∞	RMSE_l	r_l^2	RMSE_l	r_l^2
4	6.1891e-02	-	1.4160e-01	-	1.5976e-02	-	4.4803e-02	
5	2.1657e-02	1.5149	5.4509e-02	1.3773	4.7667e-03	1.7448	1.5903e-02	1.4943
6	1.1315e-02	0.9365	1.7315e-02	1.6545	1.5991e-03	1.5758	4.6052e-03	1.7879
7	5.7795e-03	0.9693	4.6431e-03	1.8989	6.6941e-04	1.2563	9.5190e-04	2.2744
(W4)	Shepard		WENO-Shepard		Shepard		WENO-Shepard	
l	MAE_l	r_l^∞	MAE_l	r_l^∞	RMSE_l	r_l^2	RMSE_l	r_l^2
4	4.7978e-02	-	1.1916e-01	-	1.2350e-02	-	3.6371e-02	-
5	1.6849e-02	1.5097	4.3702e-02	1.4471	3.6356e-03	1.7643	1.2588e-02	1.5307
6	8.8017e-03	0.9368	1.3690e-02	1.6746	1.2311e-03	1.5623	3.6177e-03	1.7989
7	4.4875e-03	0.9719	3.6360e-03	1.9126	5.1835e-04	1.2479	7.3183e-04	2.3055

Tab. 1: Errors and rates using Shepard and WENO-Shepard's methods for Franke's test function on a regular grid.

where f is the Franke's function, *Eq.* (11).
In all the experiments we used 65^2 initial data points and we approximated the data over a regular grid of 120^2 nodes.

As we can appreciate in the figures, it is evident that for the *non-linear* method, the smearing of the discontinuity is reduced.

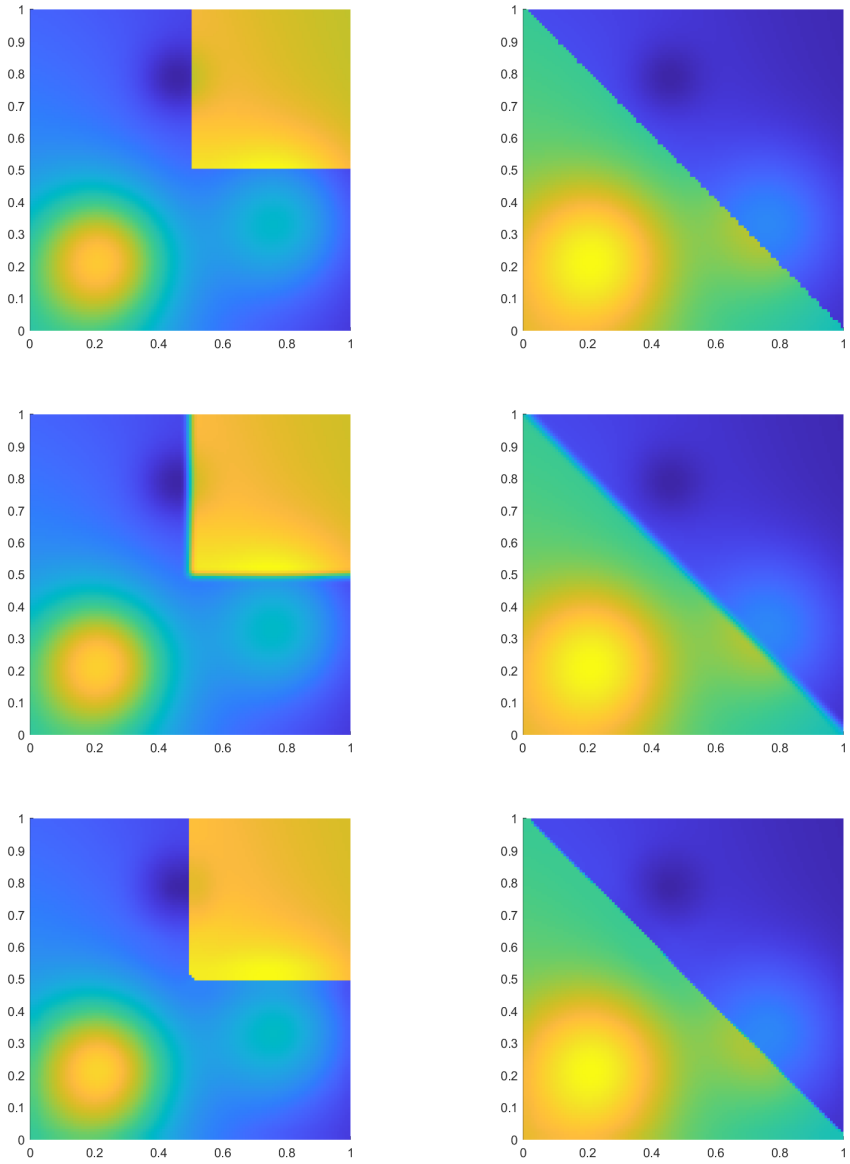

Fig. 1: First row: Cenital view of the original bivariate function $\tilde{f}$, Eq. (13) with discontinuity curve the square with vertices $(0.5, 0.5), (0.5, 1), (1, 0.5), (1, 1)$ (left) and $\gamma_2(x, y) = 1 - x - y$ (right). Second row: cenital view of the approximation using Shepard's method. Third row: cenital view of the approximation using WENO-Shepard. Original data points placed on a regular grid.

3 Data-dependent Moving Least Squares

3.1 Our procedure

We consider $\Omega \subseteq \mathbb{R}^n$ an open set, $\chi_N = \{\mathbf{x}_i \in \Omega : i = 1, \ldots, N\}$, that contains N distinct nodes, and $\mathcal{F}_N = \{f_i = f(\mathbf{x}_i) : i = 1, \ldots, N\}$, that is the corresponding set of function values, where $f : \Omega \to \mathbb{R}$ is unknown. Throughout the section 1 in this *paper [LRRY25b]*, we assume that the nodes are quasi-equally spaced (or equally spaced), and we define the fill distance (see, e.g. [17, 42, 43]) as:

$$h = \sup_{x \in \Omega} \min_{\mathbf{x}_i \in \chi_N} \|\mathbf{x} - \mathbf{x}_i\|, \tag{14}$$

we also choose a non-negative and compactly supported function $\omega : [0, \infty) \to \mathbb{R}$, and define $\omega_i(\mathbf{x}) = \omega(\frac{\|\mathbf{x}_i - \mathbf{x}\|}{h})$, where $\|\cdot\|$ is the Euclidean norm in $\mathbb{R}^n$ (but any other norm can be used).

Let us consider a point $\mathbf{x}_0 \in \Omega$. We particularize the moving least squares problem described in equation (5), to the polynomial approximation of the values $\{f(\mathbf{x}_i)\}_{i=1}^N$. This involves calculating a polynomial of degree less than or equal to d that closely approximates the given values $f(\mathbf{x}_i)$ at the points $\mathbf{x}_i$, and that satisfies the classical least squares problem:

$$\hat{p}_{\mathbf{x}_0} = \arg\min_{p \in \Pi_d(\mathbb{R}^n)} \sum_{i=1}^{N} (f(\mathbf{x}_i) - p(\mathbf{x}_i))^2 \omega_i(\mathbf{x}_0). \tag{15}$$

Then, it is evaluated at $\mathbf{x}_0$, obtaining the approximation

$$f(\mathbf{x}_0) \approx \hat{p}_{\mathbf{x}_0}(\mathbf{x}_0).$$

We can replace the condition that the function $\omega(r)$ is compactly supported with the requirement that it decreases rapidly as $r \to \infty$. In this case, interpolation is achieved if $\omega(0) = \infty$, [26]. There are many formulations for this problem in approximation theory (see e.g., [7, 8, 9, 17, 26]) and in statistics, where it is known as *local polynomial regression* (see e.g., [17, 29]). The core idea of the method is to give more importance to the nodes near the point where we want to approximate. This method is effective because it can reproduce polynomials of degree d, which implies an accuracy order of $d + 1$, and its smoothness depends on the chosen function ω. However, if the data points have a strong gradient or come from a discontinuous function, some oscillations may appear near the discontinuity.

In particular, this paper considers a curve Γ defined as the zero level set of a continuous level-set function $\gamma : \Omega \to \mathbb{R}$. This function γ delineates two distinct sets within the domain Ω

$$\begin{aligned} \Omega^+ &= \{\mathbf{x} \in \Omega : \gamma(\mathbf{x}) \geq 0\}, \\ \Omega^- &= \Omega \setminus \Omega^+. \end{aligned} \tag{16}$$

The unknown function f is defined as:

$$f(\mathbf{x}) = \begin{cases} f_1(\mathbf{x}), & \mathbf{x} \in \Omega^+, \\ f_2(\mathbf{x}), & \mathbf{x} \in \Omega \setminus \Omega^+, \end{cases} \tag{17}$$

with $f_1 \in \mathcal{C}^{d+1}(\overline{\Omega^+})$ and $f_2 \in \mathcal{C}^{d+1}(\overline{\Omega^-})$.

In this *paper*, we replace the functions ω_i in (15), which determine the importance of each node, with a new function $\tilde{\omega}_i$ that assigns a greater weight if the nodes are far from the discontinuity. In this way, we avoid the undesired effects produced by these nodes, and the Gibbs phenomenon is mitigated. The key to the method is to correctly detect the *infected* nodes using *smoothness indicators*, a concept defined in the context of data-dependent methods such as WENO (see e.g., [39]). Therefore, our problem is a weighted least squares problem where the weights depend on different aspects, in this case, two: the distances between the nodes and the point to approximate, and the distance between the isolated discontinuity and the nodes. We could change these particular requirements to others, such as the density of points or the monotonicity of the data.

3.2 The data-dependent MLS method

The MLS problem that we consider, Eq. (15), can be reformulated from an algebraic point of view (see e.g., [29, 30]). We explain it for $n = 2$, but it is similar for any n. Thus, we consider $\Omega \subset \mathbb{R}^2$, $\chi_N = \{\mathbf{x}_i = (x_i, y_i) \in \Omega : i = 1, \ldots, N\}$, the set of polynomials of degree less than or equal to d

$$\Pi_d(\mathbb{R}^2) = \{ \sum_{0 \leq |\boldsymbol{\alpha}| \leq d} a_{(\alpha_0,\alpha_1)} x^{\alpha_0} y^{\alpha_1} : a_{\boldsymbol{\alpha}} \in \mathbb{R}, \boldsymbol{\alpha} = (\alpha_0, \alpha_1) \in \mathbb{N}^2 \},$$

and a basis of $\Pi_d(\mathbb{R}^2)$ defined by (see [15] for a deeper discussion about the use of this base in the minimization problem): Let $\mathbf{x}_0 = (x_0, y_0) \in \Omega$, we define the matrices $\mathbb{X}(\mathbf{x}_0) \in \mathbb{R}^{N \times \binom{d+2}{2}}$, $\mathbb{W}(\mathbf{x}_0) \in \mathbb{R}^{N \times N}$ as:

$$\mathbb{X}(\mathbf{x}_0) = \begin{bmatrix} 1 & (x_1 - x_0) & (y_1 - y_0) & \ldots & (y_1 - y_0)^d \\ 1 & (x_2 - x_0) & (y_2 - y_0) & \ldots & (y_2 - y_0)^d \\ 1 & (x_3 - x_0) & (y_3 - y_0) & \ldots & (y_3 - y_0)^d \\ \vdots & \vdots & \vdots & \ddots & \vdots \\ 1 & (x_N - x_0) & (y_3 - y_0) & \ldots & (y_N - y_0)^d \end{bmatrix},$$

$$\mathbb{W}(\mathbf{x}_0) = \begin{bmatrix} \omega_1(\mathbf{x}_0) & 0 & 0 & \ldots & 0 \\ 0 & \omega_2(\mathbf{x}_0) & 0 & \ldots & 0 \\ 0 & 0 & \omega_3(\mathbf{x}_0) & \ldots & 0 \\ \vdots & \vdots & \vdots & \ddots & \vdots \\ 0 & 0 & 0 & \ldots & \omega_N(\mathbf{x}_0) \end{bmatrix},$$

and suppose that $\mathbb{X}(\mathbf{x}_0)$ has maximum rank, i.e. $m = \binom{d+2}{2}$. If we write

$$\hat{p}_{\mathbf{x}_0}(\mathbf{x}) = \sum_{i=1}^{\binom{d+2}{2}} c_i(\mathbf{x}_0) A_d(\mathbf{x}),$$

with

$$A_d(\mathbf{x}) = [1, (x-x_0), (y-y_0), (x-x_0)^2, (y-y_0)^2, (x-x_0)(y-y_0), \ldots, (x-x_0)^d, \ldots, (y-y_0)^d],$$

then the problem defined in Eq. (15) can be expressed as:

$$\mathbf{c}(\mathbf{x}_0) = \underset{\boldsymbol{\beta} \in \mathbb{R}^{\binom{d+2}{2} \times 1}}{\arg\min} \|\mathbb{W}(\mathbf{x}_0)^{\frac{1}{2}}[f(\mathbf{x}_1), \ldots, f(\mathbf{x}_N)]^T - \mathbb{W}(\mathbf{x}_0)^{\frac{1}{2}} \mathbb{X}(\mathbf{x}_0)\boldsymbol{\beta}\|_2^2, \tag{18}$$

whose solution is

$$\mathbf{c}(\mathbf{x}_0) = (\mathbb{X}(\mathbf{x}_0)^T \mathbb{W}(\mathbf{x}_0) \mathbb{X}(\mathbf{x}_0))^{-1} \mathbb{X}(\mathbf{x}_0)^T \mathbb{W}(\mathbf{x}_0)[f(\mathbf{x}_1), \ldots, f(\mathbf{x}_N)]^T.$$

Therefore, we get that

$$\mathcal{I}_{\mathrm{MLS}}(\mathbf{x}_0) \equiv \hat{p}_{\mathbf{x}_0}(\mathbf{x}_0) = c_0 = [1, 0, \ldots, 0](\mathbb{X}(\mathbf{x}_0)^T \mathbb{W}(\mathbf{x}_0) \mathbb{X}(\mathbf{x}_0))^{-1} \mathbb{X}(\mathbf{x}_0)^T \mathbb{W}(\mathbf{x}_0)\mathbf{f}, \tag{19}$$

where $\mathbf{f} = [f(\mathbf{x}_1), \ldots, f(\mathbf{x}_N)]^T$.

Note 1. Note that if ω is compactly supported, then, there could exist some points $\mathbf{x}_i$ far away from $\mathbf{x}_0$ such that $\omega_i(\mathbf{x}_0) = 0$. In these cases, we denote as:

$$\tilde{\chi}_{N_0} = \{\mathbf{x}_i \in \chi_N : \omega_i(\mathbf{x}_0) > 0\} = \{\mathbf{x}_{0_i} : i = 1, \ldots, N_0\},$$

and construct the same problem, but replacing χ_N by χ_{N_0} in the rest of the paper, we consider that $\omega_i(\mathbf{x}_0) > 0$ if ω is of compact support and $\omega_i(\mathbf{x}_0) > \sigma$ otherwise, for all $i = 1, \ldots, N$. In our experiments, Section 3.4 [13], we have chosen $\sigma = 10^{-10}$.

In the solution of the MLS problem exposed before, we can see that the relevance of the matrix $\mathbb{W}$ is checked, such that weights are assigned depending on the distance of the nodes with respect to the point where we want to obtain the approximation. If the data points present an isolated discontinuity described by an unknown curve Γ, then not only the distance but also the position of the nodes with respect to this curve are relevant. Therefore, in order to take into account these two variables, we construct a different problem by replacing the weight function with a data-dependent one. Thus, we define

$$\tilde{\omega}_i(\mathbf{x}) = \frac{\omega_i(\mathbf{x})}{(\epsilon + I_i)^t} = \frac{\omega(\frac{\|\mathbf{x}-\mathbf{x}_i\|}{h})}{(\epsilon + I_i)^t}, \tag{20}$$

where ϵ and t are two parameters. We use ϵ to avoid zero values in the denominator. Typically, ϵ is set to the machine precision (we take $\epsilon = 10^{-16}$ in our experiments). The purpose of t is to reach the maximum order of accuracy of the approximation at smooth zones (see [39] for a discussion about the use of both parameters in WENO method). Typically, we use $t = 4$, (but we will proof the value needed for t in Theorem 3.4). Finally, the values I_i with $i = 1, \ldots, N$ are the *smoothness indicators*, i.e., the values which mark if one node is close to the discontinuity or not. In our case, we determine a ball centered at the node $\mathbf{x}_i$ with a fixed radius δ denoted by

$$\mathcal{S}_i = \mathcal{S}(\mathbf{x}_i) = B(\mathbf{x}_i, \delta) \cap \chi_N = \{\mathbf{x}_{i_j} \in \chi_N : j = 1, \ldots, N_i\},$$

and impose the same conditions shown in section 2.2.

In this *paper*, we define the smoothness indicators in the following way: First we solve the linear least squares problem:

$$p_i = \underset{p \in \Pi_1(\mathbb{R}^2)}{\arg\min} \sum_{i_j=1}^{N_i} (f(\mathbf{x}_{i_j}) - p(\mathbf{x}_{i_j}))^2, \tag{21}$$

and compute the smoothness indicators as:

$$I_i = \frac{1}{N_i} \sum_{j_i=1}^{N_i} |f(\mathbf{x}_{j_i}) - p_i(\mathbf{x}_{j_i})|. \tag{22}$$

With this definition, I_i satisfies 1 and 2. Now, with the new functions $\tilde{\omega}_i$, defined in (20), we can pose the weighted least squares problem and find its solution. To do so, we define

$$\tilde{\mathbb{W}}(\mathbf{x}_0) = \begin{bmatrix} \tilde{\omega}_1(\mathbf{x}_0) & 0 & 0 & \ldots & 0 \\ 0 & \tilde{\omega}_2(\mathbf{x}_0) & 0 & \ldots & 0 \\ 0 & 0 & \tilde{\omega}_3(\mathbf{x}_0) & \ldots & 0 \\ \vdots & \vdots & \vdots & \ddots & \vdots \\ 0 & 0 & 0 & \ldots & \tilde{\omega}_N(\mathbf{x}_0) \end{bmatrix},$$

and get the new data-dependent approximation DD-MLS as in Eq. (19):

$$\mathcal{I}_{\text{DD-MLS}}(\mathbf{x}_0) \equiv \tilde{\hat{p}}_{\mathbf{x}_0}(\mathbf{x}_0) = \tilde{c}_0 = [1, 0, \ldots, 0](\mathbb{X}(\mathbf{x}_0)^T \tilde{\mathbb{W}}(\mathbf{x}_0) \mathbb{X}(\mathbf{x}_0))^{-1} \mathbb{X}(\mathbf{x}_0)^T \tilde{\mathbb{W}}(\mathbf{x}_0) \mathbf{f}. \tag{23}$$

where $\mathbf{f} = [f(\mathbf{x}_1), \ldots, f(\mathbf{x}_N)]^T$.

If we write $\lambda_i = (\epsilon + I_i)^{-t}$, then we have that $\tilde{\omega}_i$ is a radial function, since

$$\tilde{\omega}_i(\mathbf{x}) = \lambda_i \omega_i(\mathbf{x}) = \lambda_i \omega \left(\frac{\|\mathbf{x} - \mathbf{x}_i\|}{h} \right),$$

with compact support, which assigns small weights (or zero) when the point $\mathbf{x}$ is far from $\mathbf{x}_i$, but also, from the fact that $\lambda_i = O(1)$ or $\lambda_i = O(h^{-2t})$ depending on whether $\mathbf{x}_i$ is close to or far from a discontinuity, the function $\tilde{\omega}_i$ assigns larger weights to *non-infected* points and smaller (close to zero) weights to *infected* ones (meaning by *infected*, nodes that are at a distance smaller than δ from the discontinuity). In other words, we can interpret this data-dependent modification as a change in the distance to the nodes that are close to discontinuities. All the nodes close to the discontinuity are considered to be far from any point and their importance is neglected in the final approximation.

3.3 Properties of the new method

The smoothness of the new approximation operator depends only on the function ω since $\tilde{\omega}_i = \lambda_i \omega$.

Theorem 4. *Let $\nu \in \mathbb{N}$, $\Omega \subset \mathbb{R}^n$, ω be a function with $\omega \in \mathcal{C}^\nu(\Omega)$, then the new approximation defined in Eq.* (23) *is $\mathcal{C}^\nu(\Omega)$.*

The second property is polynomial reproduction. As $\mathbb{X}(\mathbf{x}_0)^T \tilde{\mathbb{W}}(\mathbf{x}_0) \mathbb{X}(\mathbf{x}_0)$ is non-singular, the system has a unique solution. If the data are the discretization of a polynomial of degree less than or equal to d, then the solution of the problem Eq. (15) with $\tilde{\omega}_i$ instead of ω_i is the same. Therefore, the interpolation operator reproduces $\Pi_d(\mathbb{R}^n)$. The next result collects this property.

Theorem 5. *Let $\Omega \subset \mathbb{R}^n$ be an open set, $\mathbf{x}_0 \in \Omega$, $\chi_N = \{\mathbf{x}_i \in \Omega : i = 1, \ldots, N\}$ a set of N distinct nodes and $\mathcal{F}_N = \{f_i = f(\mathbf{x}_i) : i = 1, \ldots, N\}$ a corresponding set of function values with $f \in \Pi_d(\mathbb{R}^n)$. Then the data-dependent MLS approximation defined in Eq.* (23) *satisfies*

$$\tilde{\hat{p}}_{\mathbf{x}_0}(\mathbf{x}_0) = f(\mathbf{x}_0).$$

A direct consequence of this Theorem, is the order of accuracy. If we consider the fill distance h, Eq. (14), then we can assure that if the function is $d + 1$ continuous, the order of accuracy is $O(h^{d+1})$. Thus, we can enunciate the following corollary.

Corollary 6. *Let $\Omega \subset \mathbb{R}^n$. If $f \in \mathcal{C}^{d+1}(\overline{\Omega})$, $\chi_N = \{\mathbf{x}_i \in \Omega : i = 1, \ldots, N\}$ are quasi-uniformly distributed with fill distance h, the weight function ω is compactly*

supported with support size c, then the new approximation defined in Eq. (23) *fulfills*

$$|f(\mathbf{x}_0) - \tilde{\hat{p}}_{\mathbf{x}_0}(\mathbf{x}_0)| \leq Ch^{d+1} \max_{\boldsymbol{\xi} \in \overline{\Omega}} |D^{\boldsymbol{\alpha}} f(\boldsymbol{\xi})|, \quad |\boldsymbol{\alpha}| = d+1, \ \forall \, \mathbf{x}_0 \in \Omega,$$

where C is a constant independent of h.

Finally, we analyze the approximation when some points far enough from the discontinuities are used mixed with *infected* points. In this way, we will suppose that we have at least $m = \binom{d+2}{2}$ data points not marked as *infected*.

Theorem 7. *Let $\Omega \subset \mathbb{R}^2$ be an open set, $\chi_N = \{\mathbf{x}_i \in \Omega : i = 1, \ldots, N\}$ a set of N distinct nodes with fill distance h, and $\mathcal{F}_N = \{f_i = f(\mathbf{x}_i) : i = 1, \ldots, N\}$ the corresponding set of function values with f defined in Eq.* (17)*. Let $\mathbf{x}_0 \in \Omega^+$ and let*

$$\tilde{\chi}_{N_0} = \{\mathbf{x}_i \in \chi_N : \omega_i(\mathbf{x}_0) > 0\} = \{\mathbf{x}_{0_i} \in \chi_N : i = 1, \ldots, N_0\},$$

as the set of points used to calculate the approximation at $\mathbf{x}_0$, with $N_0 \geq \binom{d+2}{2}$. We assume there exist at least $m = \binom{d+2}{2}$ points belonging to $\tilde{\chi}_{N_0}$, denoted by P_d, such that their smoothness indicators are of order h^2, all located within Ω^+. We further assume that the interpolation operator in $\Pi_d(\mathbb{R}^2)$ defined using these points is well-defined, and that a constant independent of h bounds its norm. Then the data-dependent MLS approximation satisfies:

$$|f(\mathbf{x}_0) - \mathcal{I}_{DD\text{-}MLS}(\mathbf{x}_0)| = O(h^{\min\{d+1,\kappa\}}),$$

with $\kappa \geq t$.

3.4 Numerical experiments

We start by analyzing the order of accuracy using the well-known Franke's function (11), using as nodes a regular grid defined by

$$\chi_N = (i/2^l, j/2^l) : i, j = 0, \ldots, 2^l \quad \text{and} \quad N = 2^l + 1.$$

We denote the fill distance by h_l, and the associated errors by $e_i^l = |f(\mathbf{z}_i) - \mathcal{I}^l(\mathbf{z}_i)|$, where $\{\mathbf{z}_i : 1 \leq i \leq N_{\text{eval}}\}$ is a regular grid in $[0.025, 0.975]^2$, and represents the set of evaluation points at which the function is approximated with $N_{eval} = 120^2$ points.

We will use the function Wendland $\mathcal{C}^2$ (W2) defined in (12).

Therefore, when the data points are placed on a regular grid, the order of accuracy must be close to 4 in both linear and data-dependent cases. These results

	MLS^2_{W2}		$\text{DD-MLS}^2_{\text{W2}}$		MLS^2_{W2}		$\text{DD-MLS}^2_{\text{W2}}$	
l	MAE_l	r_l^∞	MAE_l	r_l^∞	RMSE_l	r_l^2	RMSE_l	r_l^2
4	2.9459e-02		6.2989e-02		4.5011e-03		1.2700e-02	
5	3.4607e-03	3.1049	9.5840e-03	2.7299	4.0810e-04	3.4805	1.5139e-03	3.0837
6	2.5977e-04	3.7728	9.5542e-04	3.3594	2.7858e-05	3.9111	1.3019e-04	3.5747
7	1.7035e-05	3.9115	5.1915e-05	4.1814	1.7626e-06	3.9629	5.6006e-06	4.5168

Tab. 2: Errors and rates using linear and data-dependent MLS methods for Franke's test function evaluated at grid points.

are shown in Table 2. We can see that the error is slightly smaller when the linear version of the MLS is employed.

Let us see another example, we approximate some functions with discontinuities as we have defined in Eq. (17). We start by approximating the function, g on $[0,1]^2$, defined in [3]:

$$g(x,y) = \begin{cases} -(x+y+1)\cos(4x) + \sin(4(x+y)), & (x-0.5)^2 + (y-0.5)^2 \geq 0.1, \\ \exp\left(-10\left((x-0.5)^2 + (y-0.5)^2\right)\right), & (x-0.5)^2 + (y-0.5)^2 < 0.1, \end{cases} \tag{24}$$

using $N = 65^2$ grid data points, Figure 2.a) using the linear method, and Figure 2.b), using W2 (note that the figures in the second row are just a rotation of those in the first row). When a polynomial of degree $d \geq 2$ is used, we can see that some oscillations appear close to the discontinuities, Figure 2.a), in the linear case. This phenomenon is not avoided even if we refine the mesh. We can observe that these non-desired oscillations disappear when the data-dependent method is employed, Figure 2.b). This result is very similar when the data points are pseudorandom, Figure 2.c) and Figure 2.d).

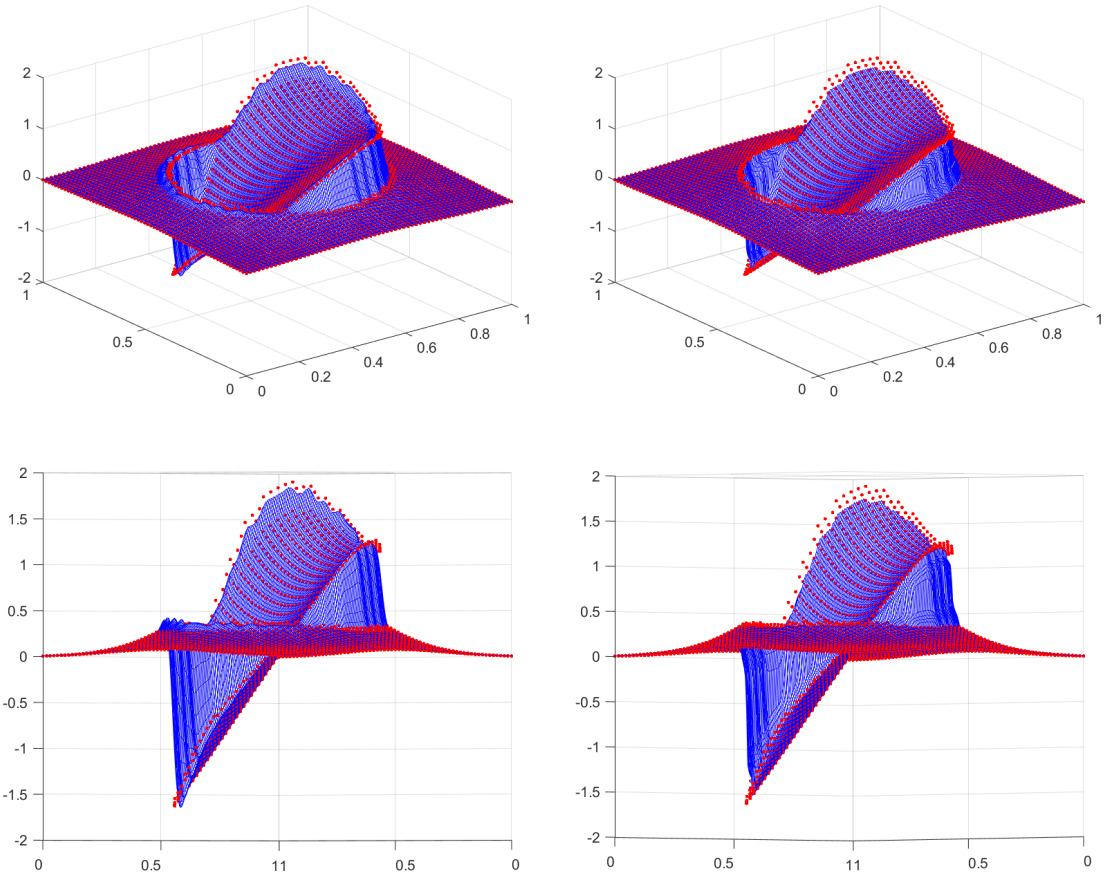

a) MLS^2_{W2} b) $\text{DD-MLS}^2_{\text{W2}}$

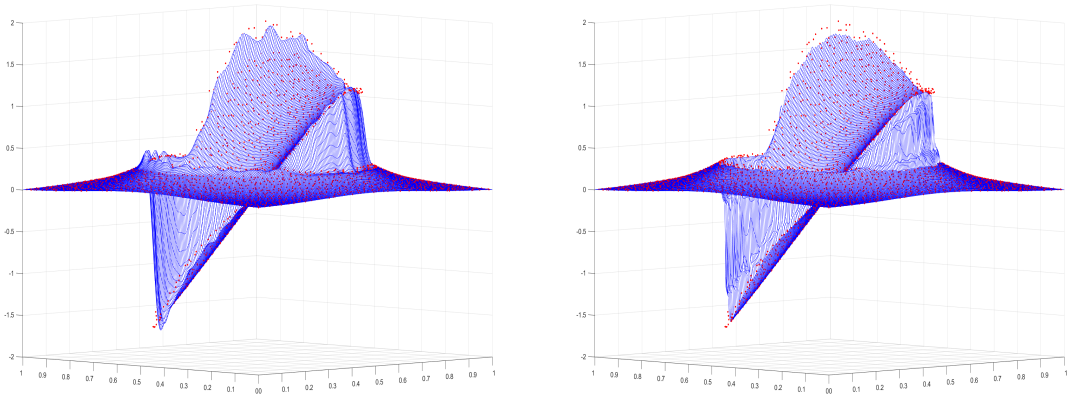

c) MLS^2_{W2} d) $\text{DD-MLS}^2_{\text{W2}}$

Fig. 2: Approximation to the function g, Eq. (24), using linear and data-dependent MLS with different $\omega(x)$ functions [43] and the class of polynomials $\Pi_2(\mathbb{R}^2)$. Red points: original function, blue lines: approximation.

4 Non-linear Partition of Unity method

4.1 Partition of Unity Approximation

The partition of unity method (PUM) is proposed to facilitate efficient computation using meshfree approximation methods. The approach is straightforward: it involves decomposing the large problem into smaller subproblems while preserving the order of accuracy. Let $\Omega \subset \mathbb{R}^n$ represent our open and bounded domain. First of all, we define the fill distance as in section 2.1. We partition our bounded domain into M subdomains Ω_j such that [12, 43]:

- The domain is contained in the union of the subdomains, i.e.
$$\Omega \subseteq \bigcup_{j=1}^{M} \Omega_j.$$
- For every $\mathbf{x} \in \Omega$ the number of subdomains Ω_j with $\mathbf{x} \in \Omega_j$ is bounded by a global constant K.
- There exists a constant $C_r > 0$ and an angle $\theta \in (0, \pi/2)$ such that every patch $\Omega_j \cap \Omega$ satisfies an interior cone condition with angle θ and radius $r = C_r h_{X,\Omega}$.
- The local fill distance h_{X_j,Ω_j} with $X_j = \Omega_j \cup X$ is uniformly bounded by the global fill distance $h_{X,\Omega}$.

This is called a regular covering for (Ω, X), [42]. For this covering, we choose a partition of unity, i.e. a family of compactly supported, non-negative, continuous functions, $w_j : \Omega_j \to \mathbb{R}$ with

$$\sum_{j=1}^{M} w_j(\mathbf{x}) = 1 \ \forall \ \mathbf{x} \in \Omega, \quad \operatorname{supp}(w_j) \subseteq \Omega_j,$$

where $\operatorname{supp}(w_j) = \overline{\{\mathbf{x} \in \Omega_j \mid w_j(\mathbf{x}) \neq 0\}}$, and define the global interpolator as:

$$\mathcal{I}_{\mathrm{PUM}}(f)(\mathbf{x}) = \sum_{j=1}^{M} w_j(\mathbf{x}) \mathcal{I}_j(f)(\mathbf{x}), \tag{25}$$

where $\mathcal{I}_j(f) : \Omega_j \to \mathbb{R}$ is a local RBF interpolant on each sudomain Ω_j.

A simple way, suggested in [12, 17], to construct PUM is to consider Shepard's approximation, i.e.

$$w_j(\mathbf{x}) = \frac{\varphi_j(\mathbf{x})}{\sum_{k=1}^{M} \varphi_k(\mathbf{x})}, \quad j = 1, \ldots, M, \tag{26}$$

where φ_j are compactly supported, with their support contained in Ω_j, and can be chosen,for example, as Wendland functions [42].

4.2 Non-linear partition of unity method

We construct a non-linear PUM starting with the interpolator $\mathcal{I}_{\text{PUM}}(f)$, Eq. (25):

$$\mathcal{I}_{\text{PUM}}(f)(\mathbf{x}) = \sum_{j=1}^{M} w_j(\mathbf{x})\mathcal{I}_j(f)(\mathbf{x}),$$

replacing the weight functions w_j described in Eq. (26) by non-linear ones using the ideas of WENO method:

$$\mathcal{W}_j(\mathbf{x}) = \frac{\alpha_j(\mathbf{x})}{\sum_{k=1}^{M}\alpha_k(\mathbf{x})}, \text{ with } \alpha_j(\mathbf{x}) = \gamma_j\varphi_j(\mathbf{x}) = \frac{\varphi_j(\mathbf{x})}{(\epsilon + I_j)^t},$$

where $0 < \gamma_j = (\epsilon + I_j)^{-t}$ is a constant, and φ_j are compactly supported functions with support on Ω_j. Note that the new functions α_j are compactly supported. The constant $\epsilon = 10^{-14}$ is set to avoid non-zero denominators. The parameter t is relevant to correctly detect the discontinuities and we choose $t = 6$. Finally, I_j, $j = 1, \ldots, M$ are the smoothness indicators. To construct them, we consider

$$\mathcal{S}_j = \Omega_j \cap X = \{\mathbf{x}_{j_i} \in \Omega_j \cap X : i = 1, \ldots, N_j\},$$

with $N_j > 3$, and the linear least square problem

$$p_j = \underset{p\in\Pi_1(\mathbb{R}^2)}{\arg\min} \sum_{i=1}^{N_j}(f(\mathbf{x}_{j_i}) - p(\mathbf{x}_{j_i}))^2,$$

where $\Pi_1(\mathbb{R}^2)$ is the set of polynomials of degree less than or equal to one, and define

$$I_j = \frac{1}{N_j}\sum_{i=1}^{N_j}|f(\mathbf{x}_{j_i}) - p_j(\mathbf{x}_{j_i})|, \tag{27}$$

then I_j satisfies the conditions shown in section 2.2.

Therefore, the new non-linear operator will be:

$$\mathcal{I}_{\text{NL-PUM}}(f)(\mathbf{x}) = \sum_{j=1}^{M}\mathcal{W}_j(\mathbf{x})\mathcal{I}_j(f)(\mathbf{x}). \tag{28}$$

The key to this new method is that it gives a greater weight to the data placed in smooth regions, while neglecting data located near the discontinuity, as this data is multiplied by a weight of order $O(h^{2t})$.

4.3 Properties of the new NL-PUM

Firstly we define a radial function $\Phi : \Omega \to \mathbb{R}$ when there exists a univariate function $\phi : [0, \infty[\to \mathbb{R}$ such that

$$\Phi(\mathbf{x}) = \phi(\|\mathbf{x}\|_2), \quad \forall\, \mathbf{x} \in \Omega,$$

with $\|\cdot\|_2$ the Euclidian norm in $\mathbb{R}^n$. Now, we denote as $\Phi_i(\mathbf{x}) = \phi(\|\mathbf{x} - \mathbf{x}_i\|_2)$, $i = 1, \ldots, N$.

As the new interpolator, Eq. (28), is defined in the same way as PUM, multiplying the compactly supported functions by constants (that are dependent on the data $F = \{f_i\}_{i=1}^N$) then the smoothness of the new operator is similar to PUM, in the sense that its smoothness is solely determined by the smoothness of the functions $\varphi(\|\cdot\|_2)$ and $\phi(\|\cdot\|_2)$.

Secondly, we determine the order of accuracy when we apply $\mathcal{I}_{\text{NL-PUM}}(f)$ to data that comes from a function which is piecewise continuous, i.e. we suppose an open and bounded domain $\Omega \subset \mathbb{R}^n$ and consider a function $\zeta : \mathbb{R}^n \to \mathbb{R}$, $\zeta \in \mathcal{C}^1$ and the sets

$$\Gamma = \{\mathbf{x} \in \Omega : \zeta(\mathbf{x}) = 0\}, \quad \Omega^+ = \{\mathbf{x} \in \Omega : \zeta(\mathbf{x}) \geq 0\}, \quad \Omega^- = \Omega \setminus \Omega^+,$$

that is to say that Ω is divided into two subsets, $\Omega = \Omega^+ \cup \Omega^-$. Let us assume that our data originates from a function of the type:

$$f(\mathbf{x}) = \begin{cases} f_+(\mathbf{x}), & \mathbf{x} \in \Omega^+, \\ f_-(\mathbf{x}), & \mathbf{x} \in \Omega^-, \end{cases}$$

with $f_\pm \in \mathcal{C}^k(\overline{\Omega^\pm})$, $k \in \mathbb{N}$, but

$$\lim_{\mathbf{x} \to \mathbf{x}_0 \in \Gamma} f_-(\mathbf{x}) \neq f_+(\mathbf{x}_0),$$

then our scattered data $X = \{\mathbf{x}_i\}_{i=1}^N$ are divided in two $X_\pm = X \cap \Omega^\pm$. We select our partition $\{\Omega_j\}_{j=1}^M$ as in Section 4.1 and define patches that are contaminated by a discontinuity as follows.

Definition 1 (Contaminated patches)**.** Using the notation presented above, $\Omega_k \in \{\Omega_j\}_{j=1}^M$ is a contaminated patch if there exist $k = 1, \ldots, M$ such that $\Omega_k \cap X_+ \neq \emptyset$ and $\Omega_k \cap X_- \neq \emptyset$.

We determine if a subset $\Omega_k \in \{\Omega_j\}_{j=1}^M$ is a contaminated patch if $I_k > h = h_{X,\Omega}$.

Also, the points close to the discontinuity will be marked using the following definition.

Definition 2 (Discontinuity points)**.** Using the notation above presented, let $\mathbf{x} \in \Omega$ be a point of the domain, $\varepsilon > 0$ be a fixed threshold and

$$S(\mathbf{x}) = \{j \in \{1, \dots, M\} : \mathbf{x} \in supp(\Omega_j),\ \varphi_j(\mathbf{x}) > \varepsilon\},$$
$$\tilde{S}(\mathbf{x}) = \{j \in \{1, \dots, M\} : \mathbf{x} \in supp(\Omega_j),\ \Omega_k \cap X_+ \neq \emptyset,\ \Omega_k \cap X_- \neq \emptyset,\ \varphi_j(\mathbf{x}) > \varepsilon\},$$

then $\mathbf{x}$ is a discontinuity point if

$$S(\mathbf{x}) = \tilde{S}(\mathbf{x}).$$

This definition means that a point is a discontinuity point only if all the patches used to interpolate at that point are contaminated.

We refer to the space (see [12, 17]):

$$\mathcal{C}^{2k}_{\nu}(\mathbb{R}^n) = \{f \in \mathcal{C}^{2k} : D^{\boldsymbol{\beta}} f(\mathbf{x}) = O(\|\mathbf{x}\|_2^{\nu}),\ \text{as } \|\mathbf{x}\|_2 \to 0 \ \text{ if } |\boldsymbol{\beta}| = 2k\},$$

and we define k-stable as:

Definition 3 (k-stable)**.** We assume that the partition of unity function is k-stable. This is, each $w_j \in \mathcal{C}^k(\mathbb{R}^n)$ and for every multi-index $\boldsymbol{\alpha}$ with $|\boldsymbol{\alpha}| \leq k$ the following inequality is satisfied:

$$\|D^{\boldsymbol{\alpha}} w_j\|_{\infty,\Omega_j} \leq \frac{C_{\boldsymbol{\alpha}}}{\delta_j^{|\boldsymbol{\alpha}|}},$$

where $C_{\boldsymbol{\alpha}}$ is some positive constant and δ_j is the diameter of

$$\delta_j = \sup_{\mathbf{x},\mathbf{y} \in \Omega_j} \|\mathbf{x} - \mathbf{y}\|_2,$$

with these restrictions over the covering and the partition of unity function, we show the following theorem [17].

Let Φ be a smoothness function and its native space $\mathcal{N}_\Phi$ [17], where

$$\mathcal{N}_\Phi(\Omega) := span\{\Phi(\cdot - \mathbf{x}), \mathbf{x} \in \Omega\}$$

Theorem 8. *Suppose $\Omega \subseteq \mathbb{R}^n$ is open and bounded, and let $X = \{\mathbf{x}_i\}_{i=1}^N \subseteq \Omega$. Let $\Phi \in \mathcal{C}^{2k}_{\nu}(\mathbb{R}^n)$ be strictly positive definite. Let $\{\Omega_j\}_{j=1}^M$ be a regular covering for (Ω, X) and let $\{w_j\}_{j=1}^M$ be k-stable for $\{\Omega_j\}_{j=1}^M$.*
Then, if $\mathbf{x} \in \Omega_+$, it is not a discontinuity point, and $f_\pm \in \mathcal{N}_\Phi(\Omega_\pm)$, the error between f and its non-linear partition of unity interpolant, with $t \geq k/2 + \nu/4$ can be bounded by

$$|f(\mathbf{x}) - \mathcal{I}_{\text{NL-PUM}}(f)(\mathbf{x})| \leq C h^{k+\frac{\nu}{2}} \|f\|_{\mathcal{N}_\Phi(\Omega_+)}.$$

Analogously, if $\mathbf{x} \in \Omega_-$ and it is not a discontinuity point.

In other words, if $\mathbf{x} \in \Omega$ and there exists, at least, a patch Ω_k free of discontinuities, then the order of accuracy is conserved.

4.4 Numerical experiments

We begin by analyzing the order of accuracy using the widely recognized Franke's function, Eq.(11), using as data points a regular grid defined by $\chi_N = \{(i/2^l, j/2^l) : i, j = 0, \ldots, 2^l\}$ where $N = 2^l + 1$, and a set of N^2 Halton's scattered data points. We denote the fill distance by h_l, and the errors by $e_k^l = |f(\hat{\mathbf{x}}_k) - \mathcal{I}^l(\hat{\mathbf{x}}_k)|$, where $\{\hat{\mathbf{x}}_k\}_{k=1}^{60}$ is a regular grid in $[0, 1]^2$.

In the first example, we choose the Matérn function, ϕ_{M_2} for the RBF problems, and the Wendland $\mathcal{C}^2$ function ϕ_{W_2}, for the partition of unity [1]. We present the results in the Table 3, and it is clear that they are very similar for both the linear and non-linear methods.

	Grid points				Halton's points			
	PUM		NLPUM		PUM		NLPUM	
l	MAE_l	r_l^∞	MAE_l	r_l^∞	MAE_l	r_l^∞	MAE_l	r_l^∞
4	7.5944e-03	-	2.8436e-01	-	1.4157e-02	-	2.6937e-02	-
5	1.6541e-03	2.1989	8.6890e-02	1.7105	2.6921e-03	2.1831	2.9567e-03	2.9058
6	3.7494e-04	2.1413	8.8016e-05	9.9472	9.1058e-04	2.3481	6.6469e-04	3.2331
7	1.1278e-04	1.7332	2.6376e-05	1.7385	2.0617e-04	1.9743	3.0466e-04	1.0369
8	2.8906e-05	1.9640	7.0429e-06	1.9050	6.0296e-05	1.4750	7.9830e-05	1.6068
	PUM		NLPUM		PUM		NLPUM	
l	RMSE_l	r_l^2	RMSE_l	r_l^2	RMSE_l	r_l^2	RMSE_l	r_l^2
4	1.3800e-03	-	9.6360e-02	-	6.8732e-03	-	9.6360e-02	-
5	2.2904e-04	2.5910	4.7798e-03	4.3334	3.3489e-04	2.2581	4.7798e-03	3.9740
6	5.8939e-05	1.9583	1.5566e-05	8.2624	3.8497e-05	2.7589	1.5566e-05	4.6860
7	1.8977e-05	1.6350	1.9141e-06	3.0236	5.9659e-06	1.8766	1.9141e-06	2.4782
8	4.0380e-06	2.2325	2.5281e-07	2.9206	7.4670e-07	1.7219	2.5281e-07	2.4933

Tab. 3: Errors and rates using PUM and NLPUM for Franke's test function: the two first columns evaluated at grid points and the two final columns evaluated at Halton's points. For RBF problems the $\mathcal{C}^2$ Matérn function ϕ_{M_2} has been used, and for partition of unity the Wendland function ϕ_{W_2} is used, i.e. $\varphi_j = \phi_{W_2}$, for all j.

Let us now consider the following function with discontinuities:

$$f_1(x,y) = \begin{cases} 1 + f(x,y), & x^2 + y^2 - 0.5^2 \geq 0, \\ f(x,y), & x^2 + y^2 - 0.5^2 < 0. \end{cases} \tag{29}$$

where the discontinuity curve is given by the zero set of:

$$\zeta_1(x,y) = x^2 + y^2 - 0.5^2.$$

In this case, we plot in Fig. 3 the result of the experiment with $L = 120^2$ equidistant points in the square $[0,1]^2$. It is clear, Fig. 3 right column, that the NL-PUM presents an adequate behaviour close to the discontinuities whereas the PUM produces some oscillations. When the figure is rotated (Fig. 3 rows 2 and 3), the differences become even more evident.

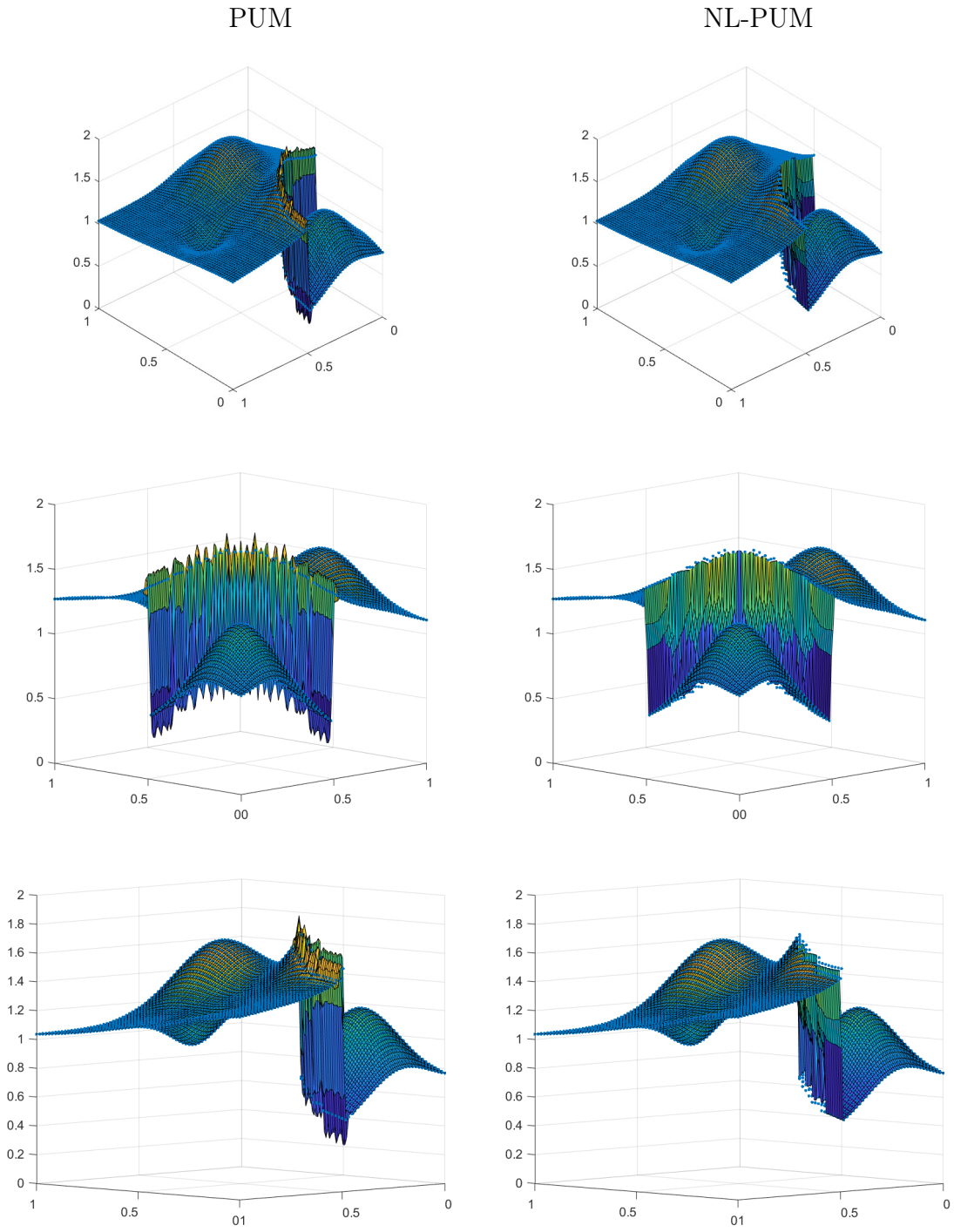

Fig. 3: Approximation of the function f_1 using PUM, and NL-PUM at grid points where we use ϕ_{M_2} for the RBF problems and ϕ_{W_2} for the partition of unity. Second and third rows are rotations of the plots presented in the first row.

5 Conclusions and future perspectives

WENO-Shepard's represents a significant advancement in the interpolation of scattered data, particularly in approximating piecewise smooth functions with discontinuities. Through a non-linear modification of the weight functions, the method demonstrates a remarkable ability to reduce diffusion effects near discontinuities, a common issue with the linear Shepard's method. Numerical experiments show that the proposed method maintains accuracy in smooth regions while substantially improving the quality of approximation near discontinuities. These features make it a versatile tool for scientific applications requiring the handling of complex datasets.

In the study of the DD-MLS, we have introduced a novel approach to the MLS problem (15) by replacing the traditional weight functions with new functions that assign greater weight to nodes farther from discontinuities, while still assigning smaller weights to nodes far from the point of approximation. This adjustment effectively mitigates the Gibbs phenomenon and reduces the smearing of discontinuities in the final approximation of the original data.

Our method uses smoothness indicators to accurately identify *infected* nodes, i.e. those affected by the presence of discontinuities, in a way inspired by the WENO method. These results in a DD-MLS problem where the weights are influenced by both the distances between nodes and the point of approximation, and the distances between isolated discontinuities and the nodes. We think these criteria could be adapted to other requirements, such as point density or monotonicity, we will explore these ideas to improve the MLS method in future research.

We have introduced a NL-PUM. We believe this is the first time such an approach has been presented in the literature. The design of the new method aims to mitigate the oscillations and smearing around discontinuity zones that the classical PUM method produces. Thus, the NL-PUM presented in this study marks a substantial improvement in PUM techniques, offering a robust solution to the numerical artifacts that appear when discontinuities are introduced in the datasets on which the classical PUM has been tested. The new method is founded on integrating Radial RBF interpolation with WENO techniques, improving the results obtained by traditional PUM algorithms close to the discontinuities. By dynamically adjusting weights through smoothness indicators, the NL-PUM selectively conserves accuracy in smooth regions while minimizing oscillations and smearing near discontinuities.

While the NL-PUM demonstrates promising capabilities, it also presents certain limitations, such as its reliance on well-tuned parameters. These factors highlight the need for further research to optimize and simplify the method. Future work could focus on automating parameter selection, extending the framework to higher-dimensional problems, and exploring its application in practical contexts

such as image processing and fluid dynamics.

Contributions

[LRRY25a] D. Levin, J. M. Ramón, J. Ruiz, D. F. Yáñez, (2025): "Weighted Essentially Non-Oscillatory Shepard method." *Numer. Algorithms,* https://doi.org/10.1007/s11075-025-02141-6

[LRRY25b] D. Levin, J. M. Ramón, J. Ruiz, D. F. Yáñez, (2025): "Data-dependent moving least squares." *Appl. Numer. Math.*, 216, 56–75, https://doi.org/10.1016/j.apnum.2025.05.002

[RRY26] J. M. Ramón, J. Ruiz, D. F. Yáñez, (2026): "Non-linear Partition of Unity method." *J. Comput. Appl. Math.*, https://doi.org/10.1016/j.cam.2025.116891

References

[1] S. Amat, D. Levin, J. Ruiz, D. F. Yáñez (2024): "Non-linear WENO B-spline based approximation method", *Numer. Algorithms*, 98, 1141–1169.

[2] S. Amat, J. Ruiz, C.W. Shu, D. F. Yáñez (2020): "A new WENO-2r Algorithm with progressive order of accuracy close to discontinuities", *SIAM J. Numer. Anal.* 58(6), 3448–3474.

[3] A. Amir, D. Levin (2021): "Reconstructing piecewise smooth bivariate functions from scattered data", *Jaen J. Approx.*, 12, 155–173.

[4] F. Aràndiga, A. M. Belda, P. Mulet (2010): "Point-Value WENO Multiresolution Applications to Stable Image Compression", *J. Sci. Comput.*, 43(2), 158–182.

[5] F. Aràndiga, R. Donat (2000): "Nonlinear multiscale decompositions: The approach of Ami Harten", *Numer. Algorithms*, 23:175–216.

[6] A. Baeza, R. Bürger, P. Mulet, D. Zorío (2019): "Central WENO schemes through a global average weight", *J. Sci. Comput.* 78, 499–530.

[7] G. Backus, F. Gilbert (1967): "Numerical applications of a formalism for geophysical inverse problems", *Geophys. J.R. Astr. Soc.* 13, 247–276.

[8] G. Backus, F. Gilbert (1968): "The resolving power of gross Earth data", *Geophys. J.R. Astr. Soc.* 16, 169–205.

[9] L. Bos, K. Salkauskas (1989): "Moving least-squares are Backus-Gilbert optimal", *J. Approx. Theory* 59, 267–275.

[10] M. D. Buhmann: Radial Basis Functions: Theory and Implementations, Cambridge University Press. 2003.

[11] R. Cavoretto, A. De Rossi (2015): "A trivariate interpolation algorithm using a cube-partition searching procedure", *SIAM J. Sci. Comput.* 37, A1891–A1908.

[12] R. Cavoretto, A. De Rossi, E. Perracchione (2016): "Efficient computation of partition of unity interpolants through a block-based searching technique", *Comput. Math. Appl.* 71, 2568–2584.

[13] R. Cavoretto, A. De Rossi, E. Perracchione, S. Lancellotti (2022): "Software Implementation of the Partition of Unity Method", *Dolomites Research Notes on Approximation*, 15(2), 35–46.

[14] F. Dell'Accio, F. Di Tommaso, F. Larosa (2024): "The Multinode Shepard Method: MATLAB Implementation", *J. Approx. Softw.*, 1.

[15] F. Dell'Accio, F. Di Tommaso, N. Siar (2021): "On the numerical computation of bivariate Lagrange polynomials", *Appl. Math. Lett.,* 112, art. 106885.

[16] M. K. Esfahani, S. De Marchi, F. Marchetti (2023): "Moving Least Squares Approximation using Variably Scaled Discontinuous Weight Function", *arXiv preprint arXiv:2302.02707.*

[17] G. E. Fasshauer: Meshfree Approximation Methods with Matlab, World Scientific Publishing, Singapore. 2007.

[18] D. Gottlieb, C-W. Shu (1997): "On the Gibbs phenomenon and its resolution", *SIAM Rev.*, 39(4), 644–668.

[19] J.H. Halton (1960): "On the efficiency of certain quasi-random sequences of points in evaluating multi-dimensional integrals", *Numer. Math.*, 2, 84–90.

[20] R.L. Hardy (1971): "Multiquadric equations of topography and other irregular surfaces", *J. Geophys. Res.*, 76(8), 1905—1915.

[21] A. Harten (1996): "Multiresolution representation of data: a general framework", *SIAM J. Numer. Anal.*, 33(3) 1205–1256.

[22] A. Harten, B. Engquist, S. Osher, S. R. Chakravarthy (1987): "Uniformly high order accurate essentially non-oscillatory schemes, III", *J. Comput. Phys.,* 71(2), 231–303.

[23] G. Jiang, C.-W. Shu (1996): "Efficient Implementation of Weighted ENO Schemes", *J. Comput. Phys.*, 126(1), 202–228.

[24] P. Lancaster, K. Salkauskas (1981): "Surfaces generated by moving least squares methods", *Math. Comput.*, 37(155), 141–158.

[25] Y. J. Lee, G. Wolberg, S. Y. Shin (1997): "Image morphing using moving least squares", *Proceedings of the 24th annual conference on Computer graphics and interactive techniques,* ACM Press/Addison-Wesley Publishing Co., 21–28.

[26] D. Levin (1998): "The approximation power of Moving least-squares", *Math. Comput.* 67, 224.

[27] D. Levin (2004): "Mesh-independent surface interpolation", Geometric modeling for scientific visualization 37–49.

[28] X.-D. Liu, S. Osher, T. Chan (1994): "Weighted Essentially Non-oscillatory Schemes", *J. Comput. Phys.*, 115, 200–212.

[29] C. Loader: Local Regression and likelihook, Springer, New York. 1999

[30] S. López-Ureña, D. F. Yáñez (2024): "Subdivision schemes based on weighted local polynomial regression. A new technique for the convergence analysis", *J. Sci. Comput.*, 100(10).

[31] S. De Marchi, G. Elefante, F. Marchetti (2021): "Stable discontinuous mapped bases: the Gibbs-Runge-Avoiding Stable Polynomial Approximation (GRASPA) method", *Comput. Appl. Math.*, 40(8), 299.

[32] S. De Marchi (2022): "Mapped Polynomials and Discontinuous Kernels for Runge and Gibbs Phenomena", *SEMA SIMAI Springer Series,* 29, 3–43.

[33] B. Matérn (1960): "Spatial Variation: Stochastic Models and Their Application to Some Problems in Forest Surveys and Other Sampling Investigations", *Meddelanden fran Statens Skogsforskningsinstitut, Stockholm, Sweden* 49, 1—144.

[34] P. Mulet, J. Ruiz, C.W. Shu, D. F. Yáñez (2024): "A non-separable progressive multivariate WENO-2r point value", *App. Numer. Math., 204*, 26–47.

[35] E.A. Nadaraya (1964): "On estimating regression", *Theory Probab. Appl.* 9, 141-–142.

[36] E. Parzen (1962): "On estimation of a probability density function and mode", *Ann. Math. Statist.* 33, 1065-–1076.

[37] M. Rosenblatt (1956): "Remarks on some nonparametric estimates of a density function", *Ann. Math. Statist.* 27, 832—837.

[38] D. Shepard (1968): "A two-dimensional interpolation function for irregularly-spaced data", *Proceedings of the 1968 23rd ACM national conference.*, 517–524.

[39] C.-W. Shu (1999): "High Order Weighted Essentially Nonoscillatory Schemes for Convection Dominated Problems", *SIAM Review*, 51(1), 82–126.

[40] W. Y. Tey, N. A. C. Sidik, Y. Asako, M. W. Muhieldeen, O. Afshar (2021): "Moving Least Squares Method and its Improvement: A Concise Review", *J. Appl. Comput. Mech.,* 7(2), 883–889.

[41] G. S. Watson (1964): "Smooth regression analysis", *Sankhya*, Series A 26, 359–372.

[42] H. Wendland: Scattered Data Approximation, Cambridge University Press, 2004.

[43] H. Wendland (2002): "Fast Evaluation of Radial Basis Functions: Methods based on partition of unity", *Approximation Theory X: Wavelets, Splines and Applications*, Vanderbilt University Press, Nashville, TN, 473–483.

[44] H. Wendland (1995): "Piecewise polynomial, positive definite and compactly supported radial functions with minimal degree", *Adv. in Comput. Math.*, 4, 389–396.

Appendices

Numerical Algorithms
https://doi.org/10.1007/s11075-025-02141-6

RESEARCH

Weighted essentially non-oscillatory shepard method

David Levin[1] · José M. Ramón[2] · Juan Ruiz-Álvarez[3] · Dionisio F. Yáñez[2]

Received: 14 January 2025 / Accepted: 20 June 2025

Abstract

Shepard's method is a fast algorithm that has been classically used to interpolate scattered data in several dimensions. This is an important and well-known technique in numerical analysis founded in the main idea that data that is far away from the approximation point should contribute less to the resulting approximation. Approximating piecewise smooth functions in $\mathbb{R}^n$ near discontinuities along a hypersurface in $\mathbb{R}^{n-1}$ is challenging for the Shepard's method or any other linear technique for sparse data due to the inherent difficulty in accurately capturing sharp transitions. This article is devoted to constructing a non-linear Shepard's method using the basic ideas that arise from the weighted essentially non-oscillatory interpolation method (WENO). The proposed method aims to enhance the accuracy and reduce the smearing of the traditional Shepard's method by incorporating WENO's adaptive and non-linear weighting mechanism. To address this challenge, we non-linearly modify the weight function in a general Shepard's method, considering any weight function, rather than relying solely on the inverse of the distance squared. This approach effectively reduces the smearing of discontinuities providing a sharper approximation. The numerical experiments presented demonstrate the superior performance of the new method close to the discontinuities and confirm the theoretical results exposed in this manuscript.

David Levin, José M. Ramón, Juan Ruiz-Álvarez and Dionisio F. Yáñez contributed equally to this work.

✉ Dionisio F. Yáñez
Dionisio.Yanez@uv.es

David Levin
levindd@gmail.com

José M. Ramón
Jose.Manuel.Ramon@uv.es

Juan Ruiz-Álvarez
juan.ruiz@upct.es

1 School of Mathematical Sciences, Tel-Aviv University, Tel-Aviv, Israel

2 Departamento de Matemáticas, Universidad de Valencia, Valencia, Spain

3 Departamento de Matemática Aplicada y Estadística, Universidad Politécnica de Cartagena, Cartagena, Spain

Published online: 27 June 2025

Keywords Shepard's method · Improved adaption to discontinuities · Approximation of discontinuous data · Several dimensions

1 Introduction

The Shepard's method, introduced by Donald Shepard in 1968 [1], is a widely used algorithm for approximating or interpolating scattered data in multiple dimensions. Shepard's method constructs an approximation of a continuous function by assigning weights to data points that are inversely proportional to the distance from the interpolation point. The method's fundamental principle is that data points closer to the interpolation point have a greater influence on the estimated value, while points farther away contribute less. Thus, traditionally, the weight function in the Shepard's method is the inverse of the squared distance, which is shifted to the data sites. However, this weight function, which is also often radial and strictly positive definite, can be generalized to any function, such as Gaussian [2], inverse multiquadric [3], Matérn [4], and Wendland functions [5, 6]. These functions can have compact or global support, and form a partition of unity to ensure the interpolation's accuracy and stability [7]. Thus, the Shepard's method is also considered a *partition of unity method* [7]. In Shepard's method, the compact support of the weight function can also be relaxed to a condition of rapid decay as the distance goes to infinity. Interpolation is achieved if the weight function goes to infinity when the distance goes to zero.

Putting it simple, the Shepard's method is the simplest version of the moving least squares method, where, instead of fitting a polynomial, a data value is used (see for example [8, 9] for modern implementations of the method). In the statistics literature Shepard's method is known as *kernel method* [10–13].

Shepard's method has found a wide array of applications in fields that require interpolation or approximation of data from irregularly spaced data sites to generate continuous surfaces. This need is prevalent in various domains where empirical data are collected at scattered locations. In his seminal paper [1], Shepard mentions several possible applications of his method. For instance, in meteorology, Shepard's method can be used to interpolate weather data from observation stations to produce continuous surfaces of temperature, rainfall, or atmospheric pressure across a region, so it can be useful for weather forecasting and climate modelling. In geography, the method can be applied to create continuous elevation surfaces, or digital elevation models, from sampled altitudes at surveyed points, providing useful information for topographic analysis. In city and regional planning, Shepard's method can help to interpolate data related to urban development, such as population density or infrastructure data, or to generate maps for decision-making or land-use planning. Similarly, in biology, this technique can be employed to interpolate ecological or environmental data, such as the distribution of species across a landscape, from scattered observation points, allowing for more accurate ecological modelling. In general, this technique can be used whenever the data distribution is irregular, making it a useful numerical tool for a wide range of scientific and practical applications.

Talking about its computational performance, the Shepard's method behaves well when approximating or interpolating data obtained from smooth functions, such as

the Franke's function. However, it tends to produce non desirable smearing effects near discontinuities, which can significantly degrade the approximation quality. This limitation has motivated us to explore alternative approaches that can handle discontinuities more effectively.

In this article, we propose a non-linear Shepard's method that aims to mitigate the smearing of discontinuities. By modifying the weight function non-linearly, we achieve results near discontinuities that are comparable to the performance of Shepard's method in smooth regions, while reducing the smearing introduced near jump discontinuities. To make Shepard's method adaptive in the presence of discontinuities, we use appropriate smoothness indicators to detect these discontinuities and modify the weight function accordingly. This adaptation allows the method to maintain high accuracy in smooth regions while effectively handling discontinuities, resulting in a more robust approximation technique. Other strategies can be found in the literature in the numerical resolution of partial differential equations (PDE), [14, 15].

The paper is organized as follows: The second section discusses the construction of the non-linear method. We prove some properties in Section 3. Section 4 presents a series of numerical experiments comparing the performance of the linear and non-linear methods and checking the theoretical results. Finally, some conclusions are offered in Section 5.

2 Construction of the non-linear method

We assume an open and bounded domain $\Omega \subseteq \mathbb{R}^n$, a set of N distinct nodes

$$\chi_N = \{\mathbf{x}_i \in \Omega : i = 1, \ldots, N\}$$

and a corresponding set of function values

$$\mathcal{F}_N = \{f_i = f(\mathbf{x}_i) : i = 1, \ldots, N\},$$

where $f : \Omega \to \mathbb{R}$ is unknown. We define the fill distance as

$$h \equiv \sup_{x \in \Omega} \min_{\mathbf{x}_i \in \chi_N} \|\mathbf{x} - \mathbf{x}_i\|,$$

and consider that the points χ_N are quasi-uniformly distributed in Ω, meaning by *quasi-uniform* the definition 4.6 given in [5], that we reproduce here for completeness.

Definition 1 The separation distance of $\chi_N = \{\mathbf{x}_1, \ldots, \mathbf{x}_N\}$ is defined by

$$q_{\chi_N} := \frac{1}{2} \min_{i \neq j} \|\mathbf{x}_i - \mathbf{x}_j\|_2.$$

A set χ_N of data sites is said to be quasi-uniform with respect to a constant $c_{\text{qu}} > 0$ if

$$q_{\chi_N} \leq h \leq c_{\text{qu}} q_{\chi_N}. \tag{1}$$

Equation (1) holds trivially for any finite point set for a sufficiently large constant c_{qu}. Thus, the quasi-uniformity assumption gains its full meaning only in an asymptotic context. In this framework, the condition ensures a balanced refinement of the point distribution and prevents clustering or sparsity.

Shepard's method can be viewed as a special case of the moving least squares technique (see [16]), where the degree of the polynomial is zero, i.e., a constant. Consequently, if we consider a non-negative, compactly supported, radial function $\omega : \Omega \to \mathbb{R}$, and define

$$\omega_i(\mathbf{x}) = \omega\left(\frac{\|\mathbf{x}_i - \mathbf{x}\|}{h}\right), \tag{2}$$

the Shepard's approximant is defined as:

$$\mathcal{I}_S(\mathbf{x}) = \sum_{i=1}^{N} \frac{\omega_i(\mathbf{x})}{\sum_{j=1}^{N} \omega_j(\mathbf{x})} f_i = \sum_{i=1}^{N} W_i(\mathbf{x}) f_i,$$

where $W_i : \Omega \to \mathbb{R}$ are defined as $W_i(\mathbf{x}) = \frac{\omega_i(\mathbf{x})}{\sum_{j=1}^{N} \omega_j(\mathbf{x})}$. It follows that for $i = 1, \ldots, N$, we have $0 \leq W_i(\mathbf{x}) \leq 1$, and $\sum_{j=1}^{N} W_j(\mathbf{x}) = 1, \forall \mathbf{x} \in \mathbb{R}^n$. We call the W_i "*optimal Shepard weights*".

As described above, Shepard's method is based on the distances between the evaluation point and the given nodes. However, if a discontinuity contaminates the data, or they present a strong gradient, it is then recommended to use only nodes that are free of singularities. To achieve this, the optimal Shepard weights are replaced with non-linear ones, defined as follows:

$$\mathcal{W}_i(\mathbf{x}) = \frac{\alpha_i(\mathbf{x})}{\sum_{j=1}^{N} \alpha_j(\mathbf{x})}, \quad \alpha_i(\mathbf{x}) = \frac{W_i(\mathbf{x})}{(\epsilon + I_i)^t}.$$

The values $\{I_i\}_{i=1}^{N}$ are smoothness indicators, see [17], which identify whether a node is near a discontinuity and thus should have a negligible contribution to the approximation. The parameters ϵ and t are chosen to achieve maximal approximation order. In our case, we take $\epsilon = 10^{-14}$ and $t = 4$. In the next subsection, we present a way to construct the smoothness indicators. With these ingredients the new WENO-Shepard's method is:

$$\mathcal{I}_{\text{WENO-S}}(\mathbf{x}) = \sum_{i=1}^{N} \mathcal{W}_i(\mathbf{x}) f_i. \tag{3}$$

2.1 The smoothness indicators

We start dividing our domain Ω in some subdomains $\mathcal{S}_i$ with

$$\Omega \subseteq \cup_{i=1}^{N} \mathcal{S}_i,$$

which satisfy that $\mathbf{x}_i \in \mathcal{S}_i$, $i = 1, \ldots, N$. In our case, we define the *stencils* as the balls centered in the data points, $\mathbf{x}_i$ with a determined radius, δ_i i.e.,

$$\mathcal{S}_i = \chi_N \cap B(\mathbf{x}_i, \delta_i) = \{\mathbf{x}_j \in \chi_N : \|\mathbf{x}_j - \mathbf{x}_i\| < \delta_i\}, \quad |\mathcal{S}_i| = N_i \geq 4. \tag{4}$$

Note that the stencils $\mathcal{S}_i$ contain a finite number of data sites used for the local least squares fit.

To determine the radius, we rely on the general results presented in [6, 7, 16], which assume that $\delta_i = ch$ where we take c as a constant greater than 2 (to assure that the stencils are not empty and, at the same time, if $\mathbf{x}_i$ is close to the discontinuity, to assure that data points from both sides of the discontinuity take part in the approximation) and h is the fill distance.

To design the smoothness indicators, we aim for two properties indicated, for example, in [18]:

P1 The order of a smoothness indicator that is free of discontinuities is h^2, i.e.

$$I_i = O(h^2) \text{ if } f \text{ is smooth in } \mathcal{S}_i.$$

P2 When a discontinuity crosses the stencil $\mathcal{S}_i$ then $I_i \nrightarrow 0$ as $h \to 0$.

Thus, we solve the linear least square problem for each $i = 1, \ldots, N$,

$$p_i = \underset{p \in \Pi_1(\mathbb{R}^2)}{\arg\min} \sum_{\mathbf{x}_j \in \mathcal{S}_i} (f(\mathbf{x}_j) - p(\mathbf{x}_j))^2,$$

and define

$$I_i = \frac{1}{N_i} \sum_{\mathbf{x}_j \in \mathcal{S}_i} |f(\mathbf{x}_j) - p(\mathbf{x}_j))|. \tag{5}$$

It is clear that the I_i defined in (5) satisfy **P1** and **P2**. The main idea that we are pursuing here is that a smoothness indicator can be defined as the mean of the errors at the points used to fit a polynomial using the least squares method. This indicator provides insight into the quality of the polynomial approximation. In the simplest case, where the data is gridded and the grid size is h, when the data is smooth and the polynomial is of degree 1, the mean error is expected to be of order $O(h^2)$, [6, 7, 16]. This indicates that the error decreases rapidly as the data becomes finer. However, if the data contains a jump discontinuity, the mean error should be of order $O(1)$, reflecting that the polynomial approximation has difficulty to accurately capture the discontinuity, resulting in a larger error. This contrast in error behavior serves as a useful measure to detect and quantify the smoothness of the underlying data. With these definitions we can prove some properties about the smoothness, the order of accuracy, and the behaviour close to the discontinuities presented by the approximant.

3 Properties of the new method

In this section, we prove some characteristics about our new method. Principally, we want to conserve the properties of the linear one, Shepard's method, and to improve the approximation in the zones close to the discontinuities. Let us start with the smoothness of the non-linear method. In this case, from the expression of the smoothness indicator, (5), we can see that it is a number independent of the variable x. Then, we only need the smoothness of the weight function $\omega(\|\cdot\|)$. This is similar to the linear Shepard's operator. We can summarize this property with the following result (Th. 1).

Theorem 1 *Let $\nu \in \mathbb{N}$, $\Omega \subset \mathbb{R}^n$ and ω be the radial basis function, $\omega(\|\cdot\|) \in \mathcal{C}^\nu(\Omega)$, and let $\mathcal{I}_{\text{WENO-S}}$ be the WENO Shepard's approximation defined in (3), then $\mathcal{I}_{\text{WENO-S}} \in \mathcal{C}^\nu(\Omega)$.*

Regarding the order of accuracy in the smooth regions, it is evident that the new operator reproduces constants, as it satisfies the condition that:

$$\sum_{i=1}^{N} \mathcal{W}_i(\mathbf{x}) = 1, \ \ \forall\, \mathbf{x} \in \mathbb{R}^n.$$

As ω is compactly supported, then we have the next theorem [7].

Theorem 2 *Let $\Omega \subset \mathbb{R}^n$. If $f \in \mathcal{C}^1(\overline{\Omega})$, $\chi_N = \{\mathbf{x}_i \in \Omega : i = 1, \ldots, N\}$ are quasi-uniformly distributed with fill distance h, the weight function ω is compactly supported with support size c, then*

$$\|f - \mathcal{I}_{\text{WENO-S}}\|_\infty \leq Ch \max_{\boldsymbol{\xi} \in \overline{\Omega}} |D^{\boldsymbol{\alpha}} f(\boldsymbol{\xi})|, \quad |\boldsymbol{\alpha}| = 1,$$

where C is a constant independent of h.

Remark 1 We take the support size of ω to be c, (note that support of ω_i is ch) as it is a reasonable support to assure that we have enough function values f_i, and to minimize the smearing introduced by the new method.

Finally, we analyze the behaviour of the operator $\mathcal{I}_{\text{WENO-S}}$ close to the discontinuities. For this purpose, we consider a $(n-1)$-hypersurface Γ defined by a function $\gamma : \mathbb{R}^n \to \mathbb{R}$ being

$$\Omega^+ = \{\mathbf{x} \in \Omega : \gamma(\mathbf{x}) \geq 0\}, \quad \Omega^- = \Omega \setminus \Omega^+,$$

and we suppose that

$$\tilde{f}(\mathbf{x}) = \begin{cases} f_1(\mathbf{x}), \ \mathbf{x} \in \Omega^+, \\ f_2(\mathbf{x}), \ \mathbf{x} \in \Omega^-, \end{cases} \tag{6}$$

with $f_1 \in \mathcal{C}^1(\overline{\Omega^+})$ and $f_2 \in \mathcal{C}^1(\overline{\Omega^-})$.

Remark 2 **Diffusion in Shepard's method** When applying the linear Shepard's method to discontinuous data with a radial weight function ω of support c, the resulting approximation exhibits a significant diffusion at all points within a distance $\leq ch$ from the discontinuity Γ.

The following Theorem shows that the diffusion area is significantly reduced when using the non-linear WENO-Shepard's method. We use the above definitions of Γ, Ω^+ and Ω^- and of $\tilde{f}$ defined in (6). We consider a weight function ω of support size c, (as explained in Section 2.1, we take $c \geq 2$), and such that $\omega(c - \epsilon_0) \geq C_0 > 0$. We further assume that Γ is a smooth hypersurface.

Theorem 3 *Let* $\mathbf{x}_0 \in \Omega^+$ *be at distance* $h(1+\epsilon_0)$ *from* Γ*, with* $0 < \epsilon_0 < 1$*. Then*

$$|\tilde{f}(\mathbf{x}_0) - \mathcal{I}_{\text{WENO-S}}(\mathbf{x}_0)| = O(h).$$

Proof Define the support of data points respect to $\mathbf{x}_0$ as

$$S(\mathbf{x}_0) = \{\mathbf{x}_i \in \chi_N : \omega_i(\mathbf{x}_0) > 0\}.$$

It turns out that for any point $\mathbf{x}_i \in S(\mathbf{x}_0) \cap \Omega^-$ the smoothness indicator I_i is $O(1)$. Furthermore, there exist points $\mathbf{x}_i \in S(\mathbf{x}_0) \cap \Omega^+$ such that the smoothness indicator I_i is $O(h^2)$ as $h \to 0$. To prove this we examine the ball of radius ch centered at $\mathbf{x}_0$, $B(\mathbf{x}_0, ch)$. We also consider all the points in Ω^+ that are at least at a distance ch away from Γ, and denote this set as D^+. Since $\mathbf{x}_0 \in \Omega^+$, and is located at a distance $h(1+\epsilon_0)$ from Γ, and given that Γ is smooth, it follows that for sufficiently small h, the intersection $D^+ \cap B(\mathbf{x}_0, ch)$ contains a ball of diameter $h(1+\epsilon_0)$. Such a ball must contain a point $\mathbf{x}_i \in S(\mathbf{x}_0) \cap \Omega^+$, and for such a point $I_i = O(h^2)$ as $h \to 0$.

We define $\mathcal{K} = \{i : I_i = O(1), 1 \leq i \leq N\}$. It follows that

$$\alpha_i(\mathbf{x}) = \begin{cases} O(1), & i \in \mathcal{K}, \\ O(h^{-2t}), & i \notin \mathcal{K}, \end{cases}$$

therefore

$$\sum_{i=1}^{N} \alpha_i(\mathbf{x}_0) = O(h^{-2t}) \quad \text{and} \quad \mathcal{W}_i(\mathbf{x}_0) = O(h^{2t}) \quad \text{for} \quad i \in \mathcal{K}.$$

Then, we get

$$\begin{aligned} \tilde{f}(\mathbf{x}_0) - \mathcal{I}_{\text{WENO-S}}(\mathbf{x}_0) &= \sum_{i=1}^{N} \mathcal{W}_i(\mathbf{x}_0)(\tilde{f}(\mathbf{x}_0) - \tilde{f}_i) \\ &= \sum_{i \notin \mathcal{K}} \mathcal{W}_i(\mathbf{x}_0)(f_1(\mathbf{x}_0) - f_1(\mathbf{x}_i)) + \sum_{i \in \mathcal{K}} \mathcal{W}_i(\mathbf{x}_0)(\tilde{f}(\mathbf{x}_0) - \tilde{f}_i) \\ &= \sum_{i \notin \mathcal{K}} \mathcal{W}_i(\mathbf{x}_0) O(h) + \sum_{i \in \mathcal{K}} O(h^{2t})(\tilde{f}(\mathbf{x}_0) - \tilde{f}_i) \\ &= O(h). \end{aligned}$$

The same result holds if $\mathbf{x}_0 \in \Omega^-$ is at distance $h(1+\epsilon_0)$ from Γ. □

4 Numerical experiments

In this section, we perform some numerical tests to check the theoretical results stablished in the previous section. We divide this section in two parts: firstly, we analyze the order of accuracy in the smooth regions of the data. Secondly, we use a function with a jump discontinuity defined by a curve. All the examples are designed within the domain $[0,1]^2 \subset \Omega \subseteq \mathbb{R}^2$.

4.1 Order of accuracy

In order to study the behaviour in the smooth zones, we will approximate the Franke's function defined as

$$\begin{aligned} f(x,y) =& \frac{3}{4}e^{-1/4((9x-2)^2+(9y-2)^2)} + \frac{3}{4}e^{-1/49(9x+1)^2-1/10(9y+1)} \\ &+ \frac{1}{2}e^{-1/4((9x-7)^2+(9y-3)^2)} - \frac{1}{5}e^{-(9x-4)^2-(9y-7)^2}, \end{aligned} \tag{7}$$

using as nodes the regular grid $\chi_{2^l+1} = \{(i/2^l, j/2^l) : i, j = 0, \ldots, 2^l\}$, and a set of $N_l = (2^l+1)^2$ Halton scattered data points [19]. We denote the fill distance as h_l and the errors as $e_i^l = |f(\mathbf{z}_i) - \mathcal{I}^l(\mathbf{z}_i)|$ with $\{\mathbf{z}_i : 1 \le i \le N_{\text{eval}}\}$ the set of points where we approximate the function. Finally we denote the maximum, discrete ℓ^2 norms and rates as:

$$\begin{aligned} &\text{MAE}_l = \max_{i=1,\ldots,N_{\text{eval}}} e_i^l, \quad \text{RMSE}_l = \left(\frac{1}{N_{\text{eval}}}\sum_{i=1}^{N_{\text{eval}}}(e_i^l)^2\right)^{\frac{1}{2}}, \\ &r_l^\infty = \frac{\log(\text{MAE}_{l-1}/\text{MAE}_l)}{\log(h_{l-1}/h_l)}, \quad r_l^2 = \frac{\log(\text{RMSE}_{l-1}/\text{RMSE}_l)}{\log(h_{l-1}/h_l)}. \end{aligned} \tag{8}$$

In these examples, as the fill distance is an approximation, we replace the division of h in (2) by a shape parameter, ε depending on the number of data, [20]. Therefore, we use the $\mathcal{C}^2$ and $\mathcal{C}^4$ Wendland's compactly supported functions (see [21] or chapter 11 in [7]) defined as

$$\begin{aligned} \omega_i^{\text{W2}}(\mathbf{x}) &= \omega^{\text{W2}}(\|\mathbf{x}-\mathbf{x}_i\|\varepsilon) = (1-\|\mathbf{x}-\mathbf{x}_i\|\varepsilon)_+^4(4\|\mathbf{x}-\mathbf{x}_i\|\varepsilon+1), \\ \omega_i^{\text{W4}}(\mathbf{x}) &= \omega^{\text{W4}}(\|\mathbf{x}-\mathbf{x}_i\|\varepsilon) = (1-\varepsilon r)_+^6(35(\|\mathbf{x}-\mathbf{x}_i\|\varepsilon)^2+18\|\mathbf{x}-\mathbf{x}_i\|\varepsilon+3), \end{aligned} \tag{9}$$

where the cutoff function $(\cdot)_+ : \mathbb{R} \to \mathbb{R}$ is defined as:

$$(x)_+ = \begin{cases} x, & x \ge 0, \\ 0, & x < 0. \end{cases}$$

Table 1 Errors and rates using Shepard and WENO-Shepard's methods for Franke's test function (7) on a regular grid

(W2)	Shepard		WENO-Shepard		Shepard		WENO-Shepard	
l	MAE_l	r_l^∞	MAE_l	r_l^∞	RMSE_l	r_l^2	RMSE_l	r_l^2
4	6.1891e-02	–	1.4160e-01	–	1.5976e-02	-	4.4803e-02	
5	2.1657e-02	1.5149	5.4509e-02	1.3773	4.7667e-03	1.7448	1.5903e-02	1.4943
6	1.1315e-02	0.9365	1.7315e-02	1.6545	1.5991e-03	1.5758	4.6052e-03	1.7879
7	5.7795e-03	0.9693	4.6431e-03	1.8989	6.6941e-04	1.2563	9.5190e-04	2.2744
(W4)	Shepard		WENO-Shepard		Shepard		WENO-Shepard	
l	MAE_l	r_l^∞	MAE_l	r_l^∞	RMSE_l	r_l^2	RMSE_l	r_l^2
4	4.7978e-02	–	1.1916e-01	–	1.2350e-02	–	3.6371e-02	–
5	1.6849e-02	1.5097	4.3702e-02	1.4471	3.6356e-03	1.7643	1.2588e-02	1.5307
6	8.8017e-03	0.9368	1.3690e-02	1.6746	1.2311e-03	1.5623	3.6177e-03	1.7989
7	4.4875e-03	0.9719	3.6360e-03	1.9126	5.1835e-04	1.2479	7.3183e-04	2.3055

Table 2 Errors and rates using Shepard and WENO-Shepard's methods for Franke's test function (7) evaluated on Halton points

(W2)	Shepard		WENO-Shepard		Shepard		WENO-Shepard	
l	MAE_l	r_l^∞	MAE_l	r_l^∞	RMSE_l	r_l^2	RMSE_l	r_l^2
4	1.0652e-01	–	1.5273e-01	–	2.0217e-02	–	4.8709e-02	
5	6.2913e-02	0.6926	6.5045e-02	1.1227	8.1166e-03	1.2003	1.7523e-02	1.3446
6	2.9851e-02	1.6150	2.6824e-02	1.9188	3.5854e-03	1.7699	6.0397e-03	2.3074
7	1.3749e-02	1.0304	1.4274e-02	0.8385	1.8125e-03	0.9067	2.1831e-03	1.3525
(W4)	Shepard		WENO-Shepard		Shepard		WENO-Shepard	
l	MAE_l	r_l^∞	MAE_l	r_l^∞	RMSE_l	r_l^2	RMSE_l	r_l^2
4	1.0459e-01	–	1.3537e-01		1.7996e-02	–	4.0106e-02	
5	6.2727e-02	0.6724	6.1287e-02	1.0422	7.5610e-03	1.1405	1.4581e-02	1.3308
6	3.0973e-02	1.5286	2.6223e-02	1.8390	3.5886e-03	1.6144	5.3386e-03	2.1765
7	1.3367e-02	1.1169	1.3816e-02	0.8517	1.8699e-03	0.8664	2.1466e-03	1.2109

Thus, in our experiments, we take $\varepsilon = \lfloor \frac{\sqrt{N_l}}{2} \rfloor / \sqrt{2}$. In Tables 1 and 2 we present a grid refinement analysis in the l^2 and the l^∞ norms, using the errors and rates presented in (8). Table 1 presents the errors and rates obtained for Franke's function in (7) using a regular grid, and Table 2 presents the corresponding errors and rates for Halton's points. We can see that the numerical order of accuracy (order one) is the one expected in the linear and non-linear methods (and sometimes better than the order expected in the case of the non-linear method). The results are very similar, therefore, the behaviour of the new algorithm in the smooth zones is analogous to Shepard's method. In terms of the norm of the error, the linear method obtains a very slight advantage for this experiment at the smooth zones.

4.2 Approximation of piecewise smooth functions

We consider the domain $[0, 1]^2$ and a curve $\Gamma = \{(x, y) : \gamma(x, y) = 0\}$, along which we place the discontinuity, where $\gamma : \Omega \to \mathbb{R}$ is a continuous function. Then we construct $\Omega^+ = \{(x, y) \in [0, 1]^2 : \gamma(x, y) \geq 0\}$ and $\Omega^- = [0, 1]^2 \setminus \Omega^+$ and define

$$\tilde{f}(x, y) = \begin{cases} 1 + f(x, y), & (x, y) \in \Omega^+, \\ f(x, y), & (x, y) \in \Omega^-, \end{cases} \tag{10}$$

where f is the Franke's function, (7). We compute three experiments with

$$\gamma_2(x, y) = 0.25^2 - x^2 - y^2, \quad \gamma_1(x, y) = 1 - x - y,$$

and finally with a square with vertices (0.5, 0.5), (0.5, 1), (1, 0.5), (1, 1), for a regular grid and Halton scattered data points. In all the experiments we used 65^2 initial data points and we approximated the data over a regular grid of 120^2 nodes. We present the results in Figs. 1, 2, 3, and 4. It is clear that in all cases, the non-linear method avoids the smearing effects close to the discontinuities. Let us focus on Fig. 1, where

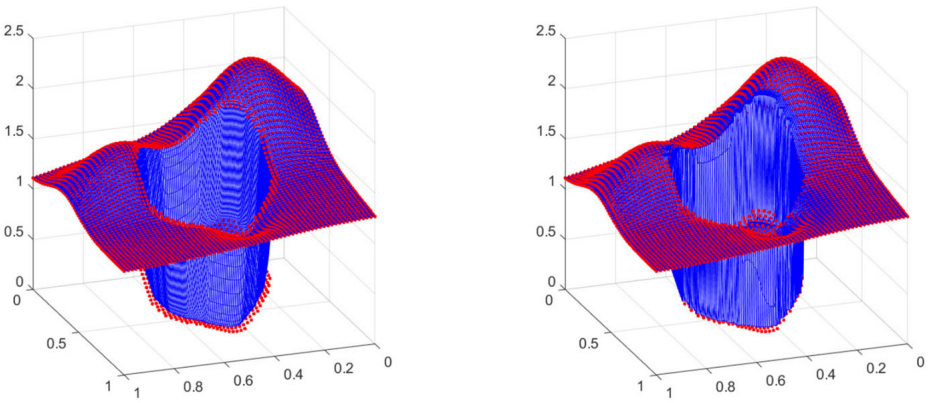

Fig. 1 Approximation to function $\tilde{f}$, (10) with $\gamma_1(x, y) = 0.25^2 - x^2 - y^2$ using Shepard's method (left) and WENO-Shepard's (right)

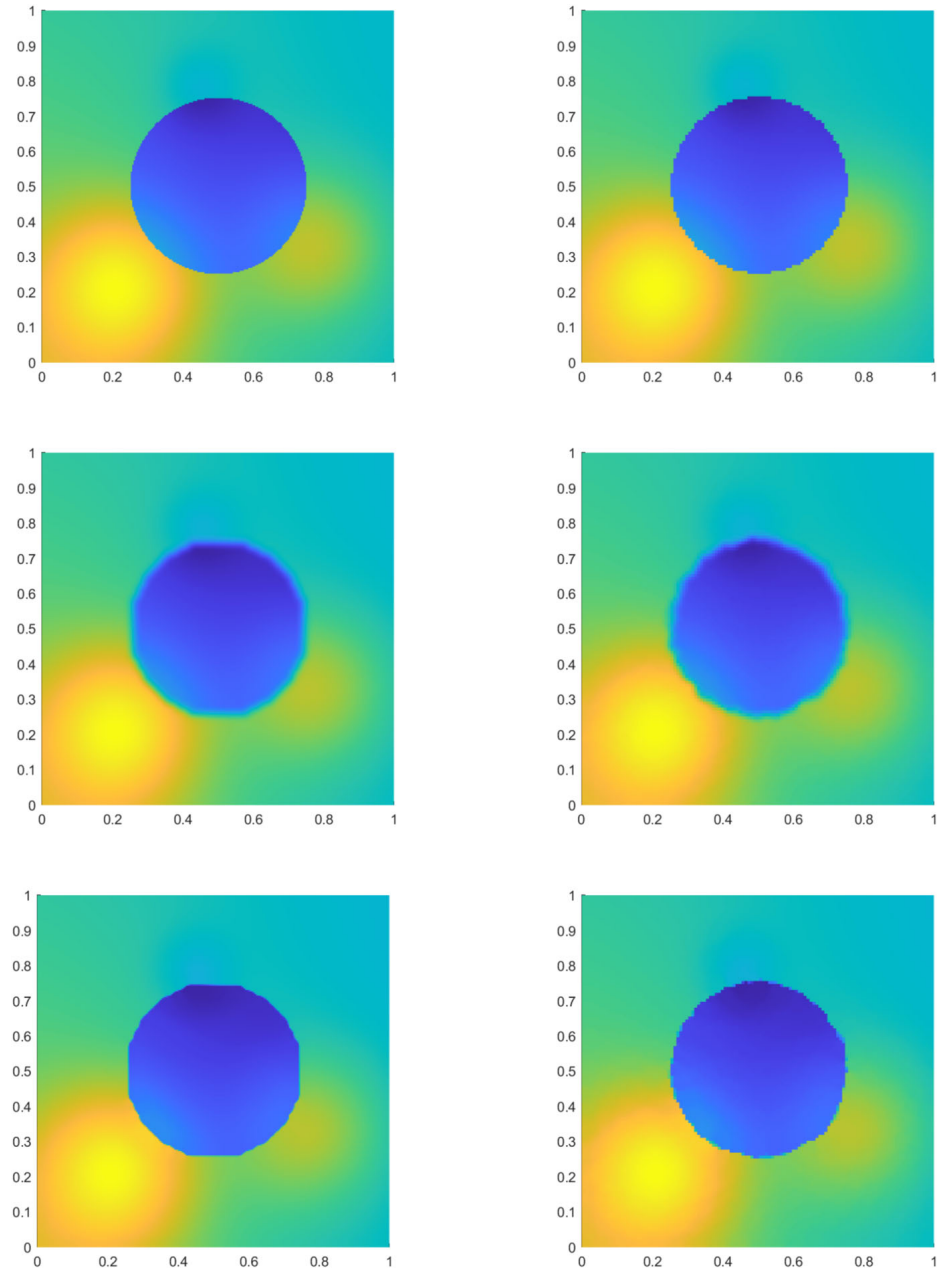

Fig. 2 First row: Cenital view of the original bivariate function $\tilde{f}$, (10) with discontinuity curve $\gamma_1(x, y) = 0.25^2 - x^2 - y^2$. Second row: cenital view of the approximation using Shepard's method. Third row: cenital view of the approximation using WENO-Shepard. Left column: Original data points placed on a regular grid. Right column: Original data are Halton's points

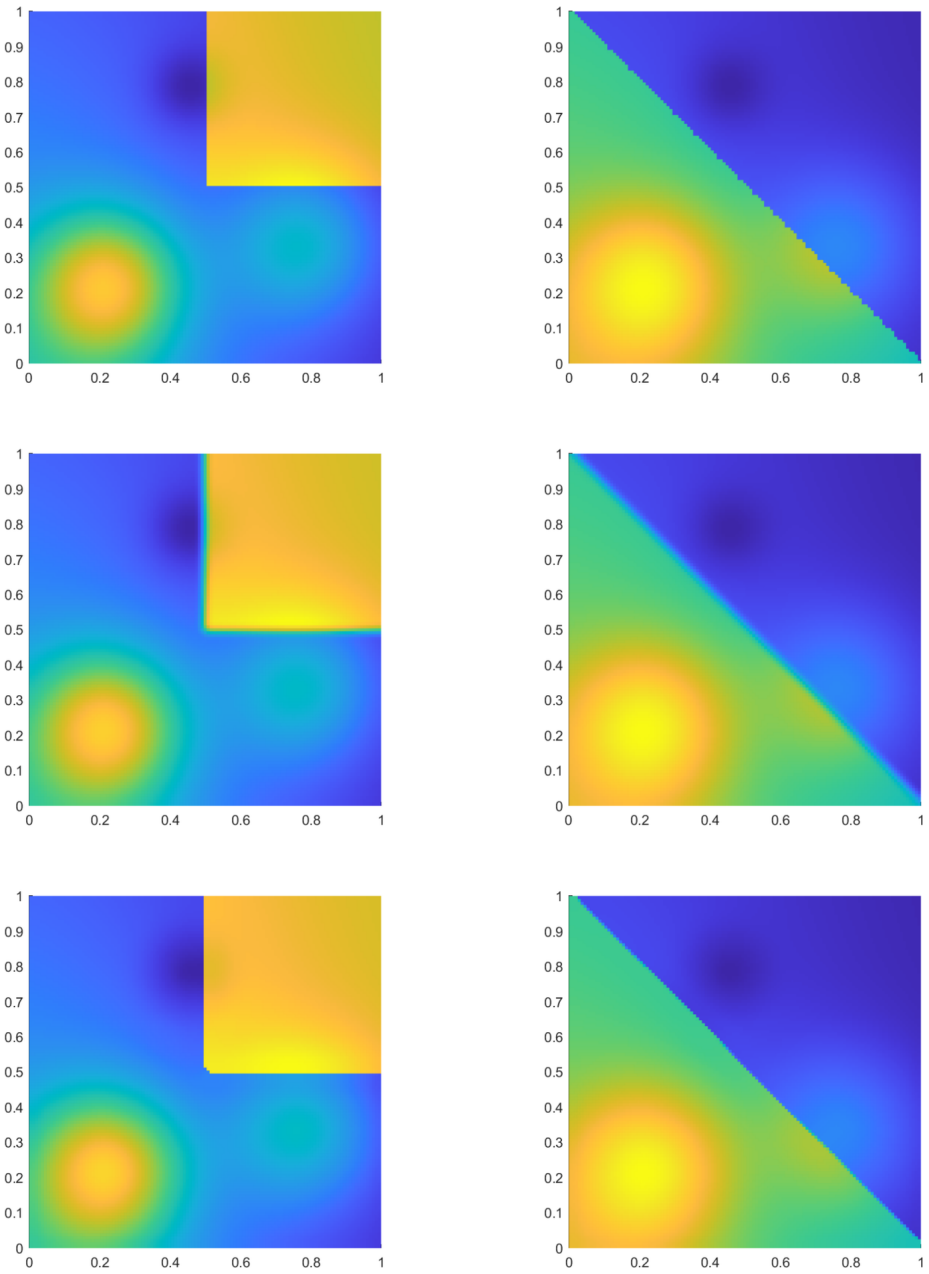

Fig. 3 First row: Cenital view of the original bivariate function $\tilde{f}$, (10) with discontinuity curve the square with vertices (0.5, 0.5), (0.5, 1), (1, 0.5), (1, 1) (left) and $\gamma_2(x, y) = 1 - x - y$ (right). Second row: cenital view of the approximation using Shepard's method. Third row: cenital view of the approximation using WENO-Shepard. Original data points placed on a regular grid

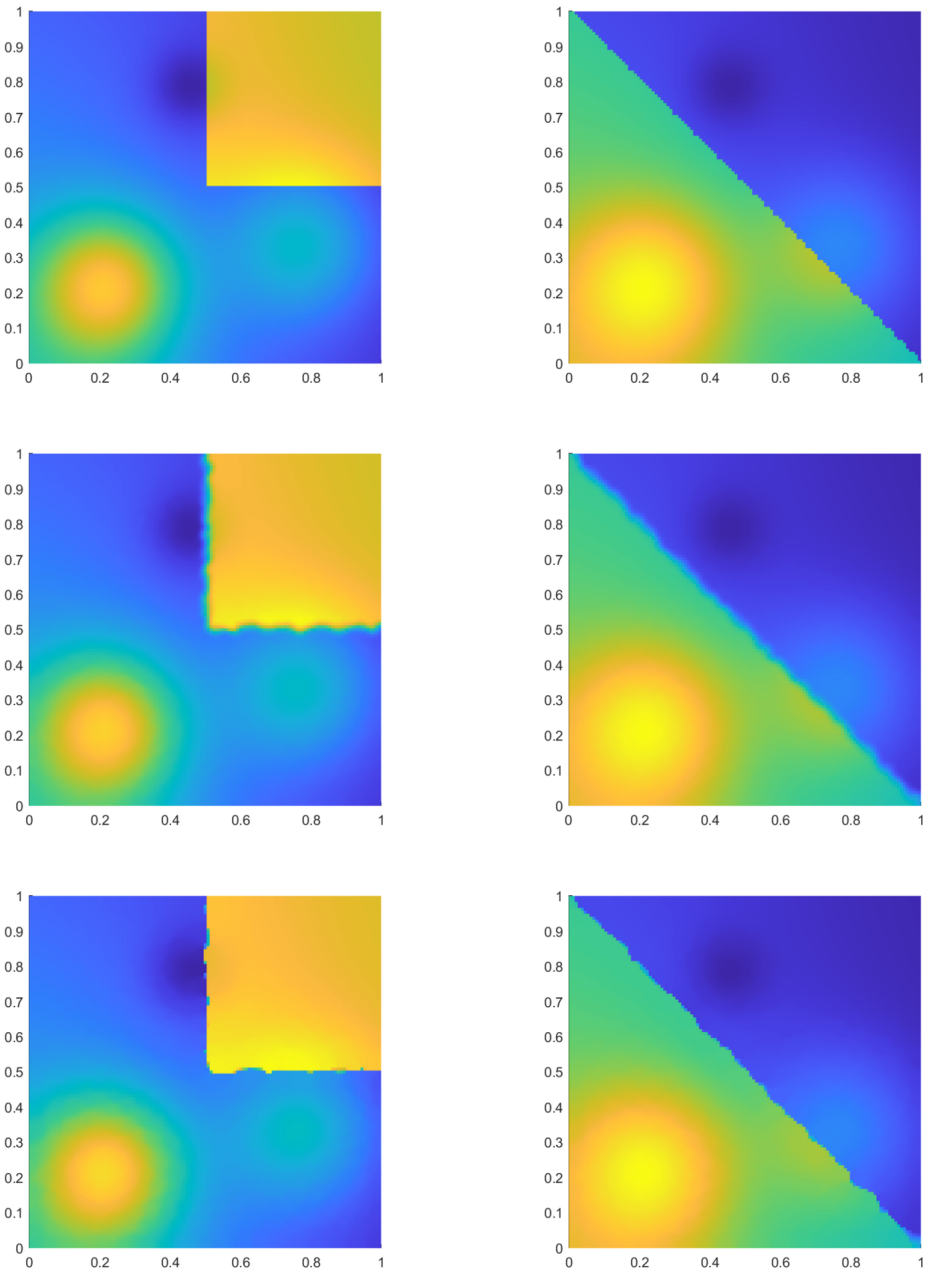

Fig. 4 First row: Cenital view of the original bivariate function $\tilde{f}$, (10) with discontinuity curve the square with vertices (0.5, 0.5), (0.5, 1), (1, 0.5), (1, 1) (left) and $\gamma_2(x, y) = 1 - x - y$ (right). Second row: cenital view of the approximation using Shepard's method. Third row: cenital view of the approximation using WENO-Shepard. Original data are Halton's points

we present the approximation of the surface defined in (10) through the linear method (left plot) and the non-linear algorithm (right plot). To contrast the smearing produced by the methods close to the discontinuities, we show a cenital view of the surfaces in Fig. 2. In this figure, the first row presents the original function, the second row presents Shepard's method and the third row presents the new algorithm. The left column is devoted to the experiment using a regular grid, and the right column is for Halton's points. It is evident that for non-linear method, the smearing of the discontinuity is reduced. This fact is clear also in the two following experiments for γ_2 and when the discontinuity is placed on a square. In Figs. 3 and 4, we represent a cenital view of the original function in the first row, Shepard's method in the second row, and WENO-Shepard's algorithm in the third row for a regular grid of data points and Halton's points, respectively. When the data points form a regular grid, the algorithm closely follows the discontinuity curve, as shown in Fig. 3. In contrast, when Halton points are used, as illustrated in Fig. 4, certain irregularities emerge due to the scattered distribution of the data. In any case, the smearing introduced by the non-linear method is smaller. This fact is also evident in the two following experiments for γ_2 and when the curve is a square, as presented in Figs. 3 and 4. In these figures, we show a cenital view of the original function in the first row, Shepard's method in the second row, and the WENO-Shepard algorithm in the third row, for both a regular grid of data points and Halton's points, respectively. When the data points form a regular grid, the algorithm closely follows to the discontinuity curve, as shown in Fig. 3. In contrast, when Halton points are used, as illustrated in Fig. 4, certain irregularities emerge. Nonetheless, the smearing introduced by the non-linear method is smaller in both cases.

5 Conclusions

The development of the WENO-Shepard's method presented in this article represents a significant advancement in the interpolation of scattered data, particularly in approximating piecewise smooth functions with discontinuities. Through a non-linear modification of the weight functions, the method demonstrates a remarkable ability to reduce diffusion effects near discontinuities, a common issue with the linear Shepard's method. Numerical experiments show that the proposed method maintains accuracy in smooth regions while substantially improving the quality of approximation near discontinuities. These features make it a versatile tool for scientific applications requiring the handling of complex datasets.

Furthermore, the theoretical analysis reveals that the method retains the essential properties of the linear approach, such as the order of accuracy, while introducing key improvements in handling sharp transitions. The inclusion of well-designed smoothness indicators dynamically adjusts the weights, ensuring more precise and stable interpolation in challenging scenarios. Visual and quantitative comparisons between regular grids and Halton points confirm the superiority of the WENO-Shepard's

method over its linear counterpart, establishing it as a significant contribution to the field of numerical approximation.

Author Contributions All the authors contributed equally to this work.

Funding Open Access funding provided thanks to the CRUE-CSIC agreement with Springer Nature. Dionisio F. Yáñez is supported by Spanish MINECO projects PID2020-117211GB-I00 and PID2023-146836NB-I00 funded by MCIN/AEI/10.13039/501100011033, and by GVA project CIAICO/2021/227.

Data Availability No datasets were generated or analysed during the current study.

Declarations

Competing Interests The authors declare no competing interests.

References

1. Shepard, D.: A two-dimensional interpolation function for irregularly-spaced data. In: Proceedings of the 1968 23rd ACM National Conference, pp. 517–524 (1968)
2. Rasmussen, C.E., Williams, C.K.I.: Gaussian Processes for Machine Learning. MIT Press, Cambridge, MA, USA (2006)
3. Hardy, R.L.: Multiquadric equations of topography and other irregular surfaces. J. Geophys. Res. **76**(8), 1905–1915 (1971)
4. Matérn, B.: Spatial Variation: Stochastic Models and Their Application to Some Problems in Forest Surveys and Other Sampling Investigations vol. 49, pp. 1–144. Meddelanden fran Statens Skogsforskningsinstitut, Stockholm, Sweden (1960)
5. Wendland, H.: Scattered Data Approximation. Cambridge University Press, Cambridge, UK (2004)
6. Wendland, H.: Fast evaluation of radial basis functions: Methods based on partition of unity. In: Chui, C.K., Schumaker, L.L., Stöcker, J. (eds.) Approximation Theory X: Wavelets. Splines and Applications. Vanderbilt University Press, Nashville, TN, USA (2002)
7. Fasshauer, G.E.: Meshfree Approximation Methods with MATLAB. World Scientifc, Singapore (2007). Chap. 23
8. Dell'Accio, F., Di Tommaso, F., Hormann, K.: On the approximation order of triangular shepard interpolation. IMA J. Numer. Anal. **36**(1), 359–379 (2016)
9. Cavoretto, R., De Rossi, A., Dell'Accio, F., Di Tommaso, F.: An efficient trivariate algorithm for tetrahedral shepard interpolation. J. Sci. Comput. **82**(3), 57 (2020)
10. Rosenblatt, M.: Remarks on some nonparametric estimates of a density function. Ann. Math. Stat. **27**, 832–837 (1956)
11. Parzen, E.: On estimation of a probability density function and mode. Annals of Mathematical Statistics **33**, 1065–1076 (1962)
12. Nadaraya, E.A.: On estimating regression. Theory Probab. Appl. **9**, 141–142 (1964)
13. Watson, G.S.: Smooth regression analysis. Sankhya, Series A **26**, 359–372 (1964)
14. Dell'Accio, F., Di Tommaso, F.: On the hexagonal shepard method. Appl. Numer. Math. **150**, 51–64 (2020)

15. Dell'Accio, F., Di Tommaso, F., Ala, G., Francomano, E.: Electric scalar potential estimations for non-invasive brain activity detection through multinode shepard method. In: MELECON 2022 – IEEE Mediterranean Electrotechnical Conference, Proceedings, pp. 1264–1268 (2022)
16. Levin, D.: The approximation power of moving least-squares. Math. Comput. **67**, 224 (1998)
17. Shu, C.-W.: High order weighted essentially nonoscillatory schemes for convection dominated problems. SIAM Rev. **51**(1), 82–126 (1999)
18. Aràndiga, F., Belda, A.M., Mulet, P.: Point-value WENO multiresolution applications to stable image compression. J. Sci. Comput. **43**(2), 158–182 (2010)
19. Halton, J.H.: On the efficiency of certain quasi-random sequences of points in evaluating multi-dimensional integrals. Numer. Math. **2**, 84–90 (1960)
20. Cavoretto, R., Rossi, A.D., Perracchione, E., Lancellotti, S.: Software implementation of the partition of unity method. Dolomites Res. Notes Approx. **15**(2), 35–46 (2022)
21. Wendland, H.: Piecewise polynomial, positive definite and compactly supported radial functions with minimal degree. Adv. Comput. Math. **4**, 389–396 (1995)

Appl. Numer. Math. 216 (2025) 56–75

Contents lists available at ScienceDirect

Applied Numerical Mathematics

journal homepage: www.elsevier.com/locate/apnum

Research Paper

Data-dependent moving least squares ☆

David Levin [a], José M. Ramón [b,*], Juan Ruiz-Álvarez [c], Dionisio F. Yáñez [b]

[a] School of Mathematical Sciences, Tel-Aviv University, Tel-Aviv, Israel
[b] Departamento de Matemáticas, Universidad de Valencia, Valencia, Spain
[c] Departamento de Matemática Aplicada y Estadística, Universidad Politécnica de Cartagena, Cartagena, Spain

ARTICLE INFO

MSC:
41A05
41A10
65D05
65M06
65N06

Keywords:
WENO
High accuracy approximation
Improved adaption to discontinuities
MLS

ABSTRACT

In this paper, we address a data-dependent modification of the moving least squares (MLS) problem. We propose a novel approach by replacing the traditional weight functions with new functions that assign smaller weights to nodes that are close to discontinuities, while still assigning smaller weights to nodes that are far from the point of approximation. Through this adjustment, we are able to mitigate the undesirable Gibbs phenomenon that appears close to the discontinuities in the classical MLS approach, and reduce the smearing of discontinuities in the final approximation of the original data. The core of our method involves accurately identifying those nodes affected by the presence of discontinuities using smoothness indicators, a concept derived from the data-dependent WENO method. Our formulation results in a data-dependent weighted least squares problem where the weights depend on two factors: the distances between nodes and the point of approximation, and the smoothness of the data in a region of predetermined radius around the nodes. We explore the design of the new data-dependent approximant, analyze its properties including polynomial reproduction, accuracy, and smoothness, and study its impact on diffusion and the Gibbs phenomenon. Numerical experiments are conducted to validate the theoretical findings, and we conclude with some insights and potential directions for future research.

1. Introduction and review

The Moving Least Squares (MLS) method, that was originally proposed by Shepard in [22] and further developed by Lancaster and Salkauskas in [12], is a powerful mathematical tool for generating smooth surfaces from scattered data points and for meshfree approximation of data. The MLS method has been widely applied in various fields such as data approximation [14], image processing [13], and geometric modelling [25], among others.

In the classical MLS approach, the goal is to approximate a function f given a set of scattered data points $\{(\mathbf{x}_i, f_i)\}_{i=1}^N$. The more general form of the MLS approximation $\hat{f}(\mathbf{x})$ at a point $\mathbf{x}$ is obtained by minimizing a weighted least squares error:

$$J(a(\mathbf{x})) = \sum_{i=1}^{N} \omega(\mathbf{x}-\mathbf{x}_i)\left(f_i - \sum_{j=0}^{m} a_j(\mathbf{x})\phi_j(\mathbf{x}-\mathbf{x}_i)\right)^2, \tag{1}$$

☆ The fourth author has been supported through project CIAICO/2021/227 (Proyecto financiado por la Conselleria de Innovación, Universidades, Ciencia y Sociedad digital de la Generalitat Valenciana), by grant PID2020-117211GB-I00 and by PID2023-146836NB-I00 funded by MCIN/AEI/10.13039/501100011033.

* Corresponding author.
E-mail addresses: levindd@gmail.com (D. Levin), Jose.Manuel.Ramon@uv.es (J.M. Ramón), juan.ruiz@upct.es (J. Ruiz-Álvarez), Dionisio.Yanez@uv.es (D.F. Yáñez).

https://doi.org/10.1016/j.apnum.2025.05.002
Received 19 December 2024; Received in revised form 21 February 2025; Accepted 4 May 2025

Available online 9 May 2025

where $\omega(\mathbf{x}-\mathbf{x}_i)$ is a weight function that decreases with the distance between $\mathbf{x}$ and $\mathbf{x}_i$, ϕ_j are basis functions, and $a_j(\mathbf{x})$ are the coefficients to be determined. The weight function $\omega(\mathbf{x}-\mathbf{x}_i)$ is designed so that points closer to $\mathbf{x}$ have a larger influence on the approximation.

Despite its effectiveness in smooth regions, the classical MLS method tends to produce oscillations near jump discontinuities. This limitation arises because the method assumes a smooth underlying function, which is not valid in the presence of discontinuities. Various strategies have been proposed to address this issue, including modifications to the weight function and the introduction of data-dependent techniques [24,8,20,21].

In this work, we propose a data-dependent modification to the classical MLS method, inspired by the Weighted Essentially Non-Oscillatory (WENO) algorithm [16,11]. Our purpose is to handle discontinuities more effectively including a data-dependent modification in the minimization problem (1). Our approach can be interpreted as an artificial adjustment of the distances of points near discontinuities, thereby reducing oscillations and improving the accuracy of the approximation. In the next subsection, we briefly introduce the WENO method, that will serve as inspiration for the data-dependent modification that we propose afterwards.

1.1. The Weighted Essentially Non-Oscillatory (WENO) method

The Weighted Essentially Non-Oscillatory (WENO) method was developed to solve hyperbolic partial differential equations with discontinuous solutions [11,16]. The WENO algorithm builds upon the Essentially Non-Oscillatory (ENO) scheme [18], aiming to achieve high-order accuracy in smooth regions while avoiding spurious oscillations near discontinuities in the solution of conservation laws. The key idea of the WENO method is to construct a weighted combination of several candidate stencils. For a given point, the WENO scheme selects the smoothest stencil by assigning weights that diminish the influence of stencils crossing discontinuities. The smoothness indicators are used to measure the smoothness of the function within each stencil, and the data-dependent weights are computed based on these indicators.

Consider a function $f(x)$ that we want to approximate at the point x_i. The WENO reconstruction for the function at x_i is given by:

$$\hat{f}(x_i) = \hat{f}_i = \sum_{k=0}^{r-1} \omega_k p_k(x_i), \tag{2}$$

where r is the number of stencils, $p(x_i)$ are the polynomial approximations from each stencil, and ω_k are the data-dependent weights. The weights ω_k are computed as:

$$\omega_k = \frac{\alpha_k}{\sum_{l=0}^{r-1} \alpha_l}, \tag{3}$$

with

$$\alpha_k = \frac{C_k}{(\epsilon + I_k)^p}, \tag{4}$$

where C_k are the linear weights, I_k are the smoothness indicators, ϵ is a small positive number to avoid division by zero, and p is a parameter typically set to 2 in order to obtain optimal accuracy at smooth zones. The smoothness indicators I_k were designed in [11] using a measure of the smoothness of the underlying data inspired in the total variation:

$$I_k = \sum_{l=1}^{r-1} \int_{x_{i-1/2}}^{x_{i+1/2}} \Delta x^{2l-1} \left(\frac{d^l}{dx^l} f_k(x) \right)^2 dx, \tag{5}$$

where Δx is the grid spacing. Given the nature of the problem we aim to solve, we will define the smoothness indicators differently. This approach is more suitable considering the scattered distribution of data points we are assuming. In the next subsection we explain the particular setting of our problem, including the description of the data and its distribution over the considered domain.

1.2. Our setting

We consider $\Omega \subseteq \mathbb{R}^n$ an open set, $\chi_N = \{\mathbf{x}_i \in \Omega : i = 1, \dots, N\}$, that contains N distinct nodes, and $\mathcal{F}_N = \{f_i = f(\mathbf{x}_i) : i = 1, \dots, N\}$, that is the corresponding set of function values, where $f : \Omega \to \mathbb{R}$ is unknown. Throughout this paper, we assume that the nodes are quasi-equally spaced (or equally spaced), and we define the fill distance (see, e.g. [9,25,26]) as:

$$h = \sup_{x \in \Omega} \min_{\mathbf{x}_i \in \chi_N} \|\mathbf{x} - \mathbf{x}_i\|, \tag{6}$$

we also choose a non-negative and compactly supported radial function $\omega : \Omega \to \mathbb{R}$, and define $\omega_i(\mathbf{x}) = \omega(\frac{\|\mathbf{x}_i - \mathbf{x}\|}{h})$, where $\|\cdot\|$ is the Euclidean norm in $\mathbb{R}^n$ (but any other norm can be used).

Let us consider a point $\mathbf{x}_0 \in \Omega$. We particularize the moving least squares problem described in equation (1), to the polynomial approximation of the values $\{f(\mathbf{x}_i)\}_{i=1}^N$. This involves calculating a polynomial of degree less than or equal to d that closely approximates the given values $f(\mathbf{x}_i)$ at the points $\mathbf{x}_i$, and that satisfies the classical least squares problem:

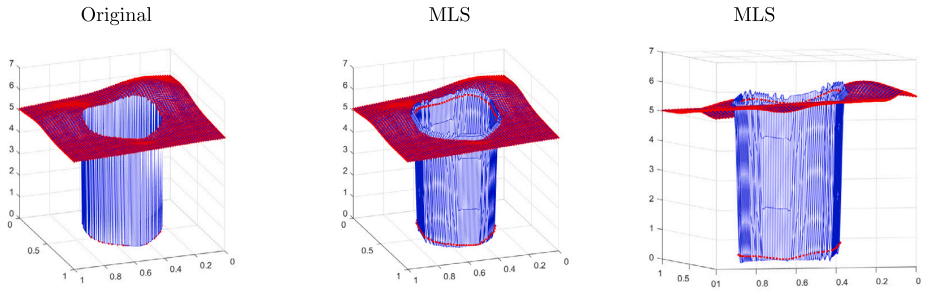

Fig. 1. Approximation to the function f, Eq. (9), where f_1 is the Franke's function, f_2 is the Franke's function plus a constant, and the discontinuity curve is defined by the zero level of the level-set function $\gamma(x,y) = 0.25^2 - x^2 - y^2$. We have used the MLS with $\omega(x)$ the C^2 Wendland function [26] and the class of polynomials $\Pi_2(\mathbb{R}^2)$. Red points: original function, blue lines: approximation. (For interpretation of the colors in the figure(s), the reader is referred to the web version of this article.)

$$\hat{p}_{\mathbf{x}_0} = \underset{p \in \Pi_d(\mathbb{R}^n)}{\arg\min} \sum_{i=1}^{N} (f(\mathbf{x}_i) - p(\mathbf{x}_i))^2 \omega_i(\mathbf{x}_0). \tag{7}$$

Then, it is evaluated at $\mathbf{x}_0$, obtaining the approximation

$$f(\mathbf{x}_0) \approx \hat{p}_{\mathbf{x}_0}(\mathbf{x}_0).$$

We can replace the condition that the function $\omega(r)$ is compactly supported with the requirement that it decreases rapidly as $r \to \infty$. In this case, interpolation is achieved if $\omega(0) = \infty$, [14]. There are many formulations for this problem in approximation theory (see e.g., [4–6,9,14]) and in statistics, where it is known as *local polynomial regression* (see e.g., [9,17]). The core idea of the method is to give more importance to the nodes near the point where we want to approximate. This method is effective because it can reproduce polynomials of degree d, which implies an accuracy order of $d+1$, and its smoothness depends on the chosen function ω. However, if the data points have a strong gradient or come from a discontinuous function, some oscillations may appear near the discontinuity, as shown in Fig. 1.

In particular, this paper considers a curve Γ defined as the zero level set of a continuous level-set function $\gamma : \Omega \to \mathbb{R}$. This function γ delineates two distinct sets within the domain Ω

$$\begin{aligned} \Omega^+ &= \{\mathbf{x} \in \Omega : \gamma(\mathbf{x}) \geq 0\}, \\ \Omega^- &= \Omega \setminus \Omega^+. \end{aligned} \tag{8}$$

The unknown function f is defined as:

$$f(\mathbf{x}) = \begin{cases} f_1(\mathbf{x}), & \mathbf{x} \in \Omega^+, \\ f_2(\mathbf{x}), & \mathbf{x} \in \Omega \setminus \Omega^+, \end{cases} \tag{9}$$

with $f_1 \in C^{d+1}(\overline{\Omega^+})$ and $f_2 \in C^{d+1}(\overline{\Omega^-})$. In this paper, we replace the functions ω_i in (7), which determine the importance of each node, with a new function $\mathcal{W}_i$ that assigns a greater weight if the nodes are far from the discontinuity. In this way, we avoid the undesired effects produced by these nodes, and the Gibbs phenomenon is mitigated. The key to the method is to correctly detect the *infected* nodes using *smoothness indicators*, a concept defined in the context of data-dependent methods such as WENO (see e.g., [23]). Therefore, our problem is a weighted least squares problem where the weights depend on different aspects, in this case, two: the distances between the nodes and the point to approximate, and the distance between the isolated discontinuity and the nodes. We could change these particular requirements to others, such as the density of points or the monotonicity of the data.

We divide the paper into four sections: We start by defining the ingredients to design the new data-dependent approximation operator in Section 2. The next section is devoted to analyzing the properties of the method, such as the reproduction of polynomials, the accuracy, and the smoothness presented by the new operator. Additionally, a study about the diffusion and the Gibbs phenomenon is shown. Some numerical experiments are performed to check the theoretical results in Section 4. Finally, some conclusions and future work are indicated in the last section.

2. The data-dependent MLS method

The MLS problem that we consider, Eq. (7), can be reformulated from an algebraic point of view (see e.g., [17,15]). We explain it for $n = 2$, but it is similar for any n. Thus, we consider $\Omega \subset \mathbb{R}^2$, $\chi_N = \{\mathbf{x}_i = (x_i, y_i) \in \Omega : i = 1, \dots, N\}$, the set of polynomials of degree less than or equal to d

$$\Pi_d(\mathbb{R}^2) = \{ \sum_{0 \leq |\boldsymbol{\alpha}| \leq d} a_{(\alpha_0,\alpha_1)} x^{\alpha_0} y^{\alpha_1} : a_{\boldsymbol{\alpha}} \in \mathbb{R}, \boldsymbol{\alpha} = (\alpha_0, \alpha_1) \in \mathbb{N}^2 \},$$

and a basis of $\Pi_d(\mathbb{R}^2)$ defined by (see [19] for a deeper discussion about the use of this base in the minimization problem):

$$B^d_{\mathbf{x}_0} = \{1, (x-x_0), (y-y_0), (x-x_0)^2, (y-y_0)^2, (x-x_0)(y-y_0), \dots, (x-x_0)^d, \dots, (y-y_0)^d\}.$$

Let $\mathbf{x}_0 = (x_0, y_0) \in \Omega$, we define the matrices $\mathbb{X}(\mathbf{x}_0) \in \mathbb{R}^{N \times \binom{d+2}{2}}$, $\mathbb{W}(\mathbf{x}_0) \in \mathbb{R}^{N \times N}$ as:

$$\mathbb{X}(\mathbf{x}_0) = \begin{bmatrix} 1 & (x_1-x_0) & (y_1-y_0) & \dots & (y_1-y_0)^d \\ 1 & (x_2-x_0) & (y_2-y_0) & \dots & (y_2-y_0)^d \\ 1 & (x_3-x_0) & (y_3-y_0) & \dots & (y_3-y_0)^d \\ \vdots & \vdots & \vdots & \ddots & \vdots \\ 1 & (x_N-x_0) & (y_3-y_0) & \dots & (y_N-y_0)^d \end{bmatrix}, \quad \mathbb{W}(\mathbf{x}_0) = \begin{bmatrix} \omega_1(\mathbf{x}_0) & 0 & 0 & \dots & 0 \\ 0 & \omega_2(\mathbf{x}_0) & 0 & \dots & 0 \\ 0 & 0 & \omega_3(\mathbf{x}_0) & \dots & 0 \\ \vdots & \vdots & \vdots & \ddots & \vdots \\ 0 & 0 & 0 & \dots & \omega_N(\mathbf{x}_0) \end{bmatrix}.$$

If we write

$$\hat{p}_{\mathbf{x}_0}(\mathbf{x}) = \sum_{i=1}^{\binom{d+2}{2}} c_i(\mathbf{x}_0) A_i(\mathbf{x}),$$

with

$$A(\mathbf{x}) = [1, (x-x_0), (y-y_0), (x-x_0)^2, (y-y_0)^2, (x-x_0)(y-y_0), \dots, (x-x_0)^d, \dots, (y-y_0)^d],$$

then the problem defined in Eq. (7) can be expressed as:

$$\mathbf{c}(\mathbf{x}_0) = \underset{\boldsymbol{\beta} \in \mathbb{R}^{\binom{d+2}{2} \times 1}}{\arg\min} \ \|\mathbb{W}^{\frac{1}{2}}[f(\mathbf{x}_1), \dots, f(\mathbf{x}_N)]^T - \mathbb{W}^{\frac{1}{2}}\mathbb{X}\boldsymbol{\beta}\|_2^2, \tag{10}$$

whose solution is

$$\mathbf{c}(\mathbf{x}_0) = (\mathbb{X}(\mathbf{x}_0)^T \mathbb{W}(\mathbf{x}_0)\mathbb{X}(\mathbf{x}_0))^{-1}\mathbb{X}(\mathbf{x}_0)^T \mathbb{W}(\mathbf{x}_0)[f(\mathbf{x}_1), \dots, f(\mathbf{x}_N)]^T.$$

So we get that

$$\mathcal{I}_{\text{MLS}}(\mathbf{x}_0) \equiv \hat{p}_{\mathbf{x}_0}(\mathbf{x}_0) = c_0 = [1, 0, \dots, 0](\mathbb{X}(\mathbf{x}_0)^T \mathbb{W}(\mathbf{x}_0)\mathbb{X}(\mathbf{x}_0))^{-1}\mathbb{X}(\mathbf{x}_0)^T \mathbb{W}(\mathbf{x}_0)[f(\mathbf{x}_1), \dots, f(\mathbf{x}_N)]^T. \tag{11}$$

Remark 1. Note that if ω is compactly supported, then there could exist some points $\mathbf{x}_i$ far away from $\mathbf{x}_0$ such that $\omega_i(\mathbf{x}_0) = 0$. In these cases, we denote as:

$$\tilde{\chi}_{N_0} = \{\mathbf{x}_i \in \chi_N : \omega_i(\mathbf{x}_0) > 0\} = \{\mathbf{x}_{0_i} : i = 1, \dots, N_0\},$$

and construct the same problem, but replacing χ_N by χ_{N_0}. In the rest of the paper, we consider that $\omega_i(\mathbf{x}_0) > 0$ if ω is of compact support and $\omega_i(\mathbf{x}_0) > \sigma$ otherwise, for all $i = 1, \dots, N$. In our experiments, Section 4, we have chosen $\sigma = 10^{-10}$.

In the solution of the MLS problem exposed before, we can see that the relevance of the matrix $\mathbb{W}$ is checked, such that weights are assigned depending on the distance of the nodes with respect to the point where we want to obtain the approximation. If the data points present an isolated discontinuity described by an unknown curve γ, then not only the distance but also the position of the nodes with respect to this curve are relevant. Therefore, in order to take into account these two variables, we construct a different problem by replacing the weight function with a data-dependent one. Thus, we define

$$\tilde{\omega}_i(\mathbf{x}) = \frac{\omega_i(\mathbf{x})}{(\epsilon + I_i)^t} = \frac{\omega(\frac{\|\mathbf{x}-\mathbf{x}_i\|}{h})}{(\epsilon + I_i)^t}, \tag{12}$$

where ϵ and t are two parameters. We use ϵ to avoid zero values in the denominator. Typically, ϵ is set to the machine precision (we take $\epsilon = 10^{-16}$ in our experiments). The purpose of t is to reach the maximum order of accuracy of the approximation at smooth zones (see [23] for a discussion about the use of both parameters in WENO method). Typically, we use $t = 4$, (but we will prove the value needed for t in Theorem 3.4). Finally, the values I_i with $i = 1, \dots, N$ are the *smoothness indicators*, i.e., the values which mark if one node is close to the discontinuity or not. In our case, we determine a ball centered at the node $\mathbf{x}_i$ with a fixed radius δ denoted by

$$\mathcal{S}_i = \mathcal{S}(\mathbf{x}_i) = B(\mathbf{x}_i, \delta) \cap \chi_N = \{\mathbf{x}_{i_j} \in \chi_N : j = 1, \dots, N_i\},$$

and impose the following conditions (see e.g. [3]):

P1 The order of a smoothness indicator that is free of discontinuities is h^2, i.e. $I_i = O(h^2)$ if f is smooth in $\mathcal{S}_i$.
P2 When the stencil $\mathcal{S}_i$ crosses a discontinuity, then $I_i \nrightarrow 0$ as $h \to 0$.

Table 1
Examples of RBFs.

$\omega(r)$	RBF	
e^{-r^2}	Gaussian C^∞	G
$\left(1+r^2\right)^{-1/2}$	Inverse MultiQuadratic C^∞	IMQ
e^{-r}	Matérn C^0	M0
$e^{-r}(1+r)$	Matérn C^2	M2
$e^{-r}\left(3+3r+r^2\right)$	Matérn C^4	M4
$(1-r)_+^2$	Wendland C^0	W0
$(1-r)_+^4(4r+1)$	Wendland C^2	W2
$(1-r)_+^6\left(35r^2+18r+3\right)$	Wendland C^4	W4

In this paper, we define the smoothness indicators in the following way: First we solve the linear least squares problem:

$$p_i = \underset{p\in\Pi_1(\mathbb{R}^2)}{\arg\min} \sum_{i_j=1}^{N_i} (f(\mathbf{x}_{i_j}) - p(\mathbf{x}_{i_j}))^2, \tag{13}$$

and compute the smoothness indicators as:

$$I_i = \frac{1}{N_i} \sum_{j_i=1}^{N_i} |f(\mathbf{x}_{j_i}) - p_i(\mathbf{x}_{j_i})|. \tag{14}$$

With this definition, I_i satisfies **P1** and **P2**. Now, with the new functions $\tilde{\omega}_i$, defined in (12), we can pose the weighted least squares problem and find its solution. To do so, we define

$$\tilde{\mathbb{W}}(\mathbf{x}_0) = \begin{bmatrix} \tilde{\omega}_1(\mathbf{x}_0) & 0 & 0 & \dots & 0 \\ 0 & \tilde{\omega}_2(\mathbf{x}_0) & 0 & \dots & 0 \\ 0 & 0 & \tilde{\omega}_3(\mathbf{x}_0) & \dots & 0 \\ \vdots & \vdots & \vdots & \ddots & \vdots \\ 0 & 0 & 0 & \dots & \tilde{\omega}_N(\mathbf{x}_0) \end{bmatrix},$$

and get the new data-dependent approximation DD-MLS as in Eq. (11):

$$\mathcal{I}_{\text{DD-MLS}}(\mathbf{x}_0) \equiv \tilde{\tilde{p}}_{\mathbf{x}_0}(\mathbf{x}_0) = \tilde{c}_0 = [1,0,\dots,0](\mathbb{X}(\mathbf{x}_0)^T\tilde{\mathbb{W}}(\mathbf{x}_0)\mathbb{X}(\mathbf{x}_0))^{-1}\mathbb{X}(\mathbf{x}_0)^T\tilde{\mathbb{W}}(\mathbf{x}_0)[f(\mathbf{x}_1),\dots,f(\mathbf{x}_N)]^T. \tag{15}$$

If we write $\lambda_i = (\epsilon + I_i)^{-t}$, then we have that $\tilde{\omega}_i$ is a radial function since

$$\tilde{\omega}_i(\mathbf{x}) = \lambda_i\omega_i(\mathbf{x}) = \lambda_i\omega\left(\frac{\|\mathbf{x}-\mathbf{x}_i\|}{h}\right),$$

with compact support, which assigns small weights (or zero) when the point $\mathbf{x}$ is far from $\mathbf{x}_i$, but also, from the fact that $\lambda_i = O(1)$ or $\lambda_i = O(h^{-2t})$ depending on whether $\mathbf{x}_i$ is close to or far from a discontinuity, the function $\tilde{\omega}_i$ assigns larger weights to *non-infected* points and smaller (close to zero) weights to *infected* ones (meaning by *infected*, nodes that are at a distance smaller than δ from the discontinuity). In other words, we can interpret this data-dependent modification as a change in the distance to the nodes that are close to discontinuities. All the nodes close to the discontinuity are considered to be far from any point and their importance is neglected in the final approximation. With these ingredients, in the next section we prove some properties of the new approximation technique.

3. Properties of the new method

In this section, we prove some properties of the approximation technique described in the previous section. In particular, we focus on the smoothness, the reproduction of polynomials, the order of accuracy and the mitigation of Gibbs phenomenon:

- Let us start with the smoothness. It is clear by Eq. (15) that if $\mathbb{X}(\mathbf{x}_0)$ has maximum rank, i.e. $m = \binom{d+2}{2}$, then the matrix $\mathbb{X}(\mathbf{x}_0)^T\tilde{\mathbb{W}}(\mathbf{x}_0)\mathbb{X}(\mathbf{x}_0)$ is non-singular, since all the entries of the matrix $\tilde{\mathbb{W}}(\mathbf{x}_0)$ are positive by Remark 1. Therefore, the smoothness of the new approximation operator depends only on the function ω since $\tilde{\omega}_i = \lambda_i\omega$. We summarize this property in the next Theorem (Theorem 3.1).

  Theorem 3.1. *Let $\nu \in \mathbb{N}$, $\Omega \subset \mathbb{R}^n$, ω be a function with $\omega \in C^\nu(\Omega)$, then the new approximation defined in Eq. (15) is $C^\nu(\Omega)$.*

  In the literature there are many functions ω which are used in radial basis approximation. We summarize some of them in Table 1 (see e.g. [9,26]).

- The second property is polynomial reproduction. As $\mathbb{X}(\mathbf{x}_0)^T\tilde{\mathbb{W}}(\mathbf{x}_0)\mathbb{X}(\mathbf{x}_0)$ is non-singular, the system has a unique solution. If the data are the discretization of a polynomial of degree less than or equal to d, then the solution of the problem Eq. (7) with $\tilde{\omega}_i$ instead of ω_i is the same. Therefore, the interpolation operator reproduces $\Pi_d(\mathbb{R}^n)$. The next result collects this property.

Theorem 3.2. *Let $\Omega \subset \mathbb{R}^n$ be an open set, $\mathbf{x}_0 \in \Omega$, $\chi_N = \{\mathbf{x}_i \in \Omega : i = 1, \dots, N\}$ a set of N distinct nodes and $\mathcal{F}_N = \{f_i = f(\mathbf{x}_i) : i = 1, \dots, N\}$ a corresponding set of function values with $f \in \Pi_d(\mathbb{R}^n)$. Then the data-dependent MLS approximation defined in Eq. (15) satisfies*

$$\tilde{\tilde{p}}_{\mathbf{x}_0}(\mathbf{x}_0) = f(\mathbf{x}_0).$$

A direct consequence of the last Theorem, Theorem 3.2, is the order of accuracy. If we consider the fill distance h, Eq. (6), then we can assure that if the function is $d+1$ continuous, the order of accuracy is $O(h^{d+1})$. Thus, we can enunciate the following corollary.

Corollary 3.3. *Let $\Omega \subset \mathbb{R}^n$. If $f \in C^{d+1}(\overline{\Omega})$, $\chi_N = \{\mathbf{x}_i \in \Omega : i = 1, \dots, N\}$ are quasi-uniformly distributed with fill distance h, the weight function ω is compactly supported with support size c, then the new approximation defined in Eq. (15) fulfills*

$$|f(\mathbf{x}_0) - \tilde{\tilde{p}}_{\mathbf{x}_0}(\mathbf{x}_0)| \le C h^{d+1} \max_{\xi \in \overline{\Omega}} |D^{\boldsymbol{\alpha}} f(\xi)|, \quad |\boldsymbol{\alpha}| = d+1, \ \forall \mathbf{x}_0 \in \Omega,$$

where C is a constant independent of h.

- Finally, we analyze the approximation when some points far enough from the discontinuities are used mixed with *infected* points. In this way, we will suppose that we have at least $m = \binom{d+2}{2}$ data points not marked as *infected*.

Theorem 3.4. *Let $\Omega \subset \mathbb{R}^2$ be an open set, $\chi_N = \{\mathbf{x}_i \in \Omega : i = 1, \dots, N\}$ a set of N distinct nodes with fill distance h, and $\mathcal{F}_N = \{f_i = f(\mathbf{x}_i) : i = 1, \dots, N\}$ the corresponding set of function values with f defined in Eq. (9). Let $\mathbf{x}_0 \in \Omega^+$ and let*

$$\tilde{\chi}_{N_0} = \{\mathbf{x}_i \in \chi_N : \omega_i(\mathbf{x}_0) > 0\} = \{\mathbf{x}_{0_i} \in \chi_N : i = 1, \dots, N_0\},$$

as the set of points used to calculate the approximation at $\mathbf{x}_0$, with $N_0 \ge \binom{d+2}{2}$. We assume there exist at least $m = \binom{d+2}{2}$ points belonging to $\tilde{\chi}_{N_0}$, denoted by P_d, such that their smoothness indicators are of order h^2, all located within Ω^+. We further assume that the interpolation operator in $\Pi_d(\mathbb{R}^2)$ defined using these points is well-defined, and that a constant independent of h bounds its norm. Then the data-dependent MLS approximation satisfies:

$$|f(\mathbf{x}_0) - I_{DD\text{-}MLS}(\mathbf{x}_0)| = O(h^{\min\{d+1,\kappa\}}),$$

with $\kappa \ge t$.

Proof. Let $\mathbf{x}_0$ be a point in Ω. We divide the set

$$\tilde{\chi}_{N_0} = \tilde{\chi}^f_{N_0} \cup \tilde{\chi}^d_{N_0},$$

with $\tilde{\chi}^f_{N_0} = \{\mathbf{x}_i \in \chi_N : \omega_i(\mathbf{x}_0) > 0 \ \wedge \ I_i = O(h^2)\}$ and $\tilde{\chi}^d_{N_0} = \tilde{\chi}_{N_0} \setminus \tilde{\chi}^f_{N_0}$. Let us define $\pi_1 \in \Pi_d(\mathbb{R}^2)$ to be polynomial interpolating f at the points P_d and, as all the non-infected data are at one side of the discontinuity, then

$$f(\mathbf{x}_i) = f_1(\mathbf{x}_i) = \pi_1(\mathbf{x}_i) + O(h^{d+1}), \quad \forall \mathbf{x}_i \in \tilde{\chi}^f_{N_0}.$$

The MLS solution $\tilde{\tilde{p}}_{\mathbf{x}_0}$ is defined by

$$\tilde{\tilde{p}}_{\mathbf{x}_0} = \operatorname*{arg\,min}_{p \in \Pi_d(\mathbb{R}^2)} \sum_{i=1}^{N_0} (f(\mathbf{x}_{0_i}) - p(\mathbf{x}_{0_i}))^2 \tilde{\omega}_{0_i}(\mathbf{x}_0) = \operatorname*{arg\,min}_{p \in \Pi_d(\mathbb{R}^2)} \left(\sum_{\mathbf{x}_{0_i} \in \tilde{\chi}^d_{N_0}} (f(\mathbf{x}_{0_i}) - p(\mathbf{x}_{0_i}))^2 \tilde{\omega}_{0_i}(\mathbf{x}_0) + \sum_{\mathbf{x}_{0_i} \in \tilde{\chi}^f_{N_0}} (f(\mathbf{x}_{0_i}) - p(\mathbf{x}_{0_i}))^2 \tilde{\omega}_{0_i}(\mathbf{x}_0) \right).$$

Since $\pi_1 \in \Pi_d(\mathbb{R}^2)$ we get that,

$$\sum_{i=1}^{N_0} (f(\mathbf{x}_{0_i}) - \tilde{\tilde{p}}_{\mathbf{x}_0}(\mathbf{x}_{0_i}))^2 \tilde{\omega}_{0_i}(\mathbf{x}_0) \le \sum_{i=1}^{N_0} (f(\mathbf{x}_{0_i}) - \pi_1(\mathbf{x}_{0_i}))^2 \tilde{\omega}_{0_i}(\mathbf{x}_0).$$

Now using that

$$\tilde{\omega}_{0_i}(\mathbf{x}_0) = \begin{cases} O(h^{-2t}), & \mathbf{x}_{0_i} \in \tilde{\chi}^f_{N_0}, \\ O(1), & \mathbf{x}_{0_i} \in \tilde{\chi}^d_{N_0}, \end{cases} \tag{16}$$

we have that:

$$\sum_{i=1}^{N_0}(f(\mathbf{x}_{0_i})-\pi_1(\mathbf{x}_{0_i}))^2\tilde{\omega}_{0_i}(\mathbf{x}_0)=$$
$$\sum_{\mathbf{x}_{0_i}\in\tilde{\chi}^d_{N_0}}(f(\mathbf{x}_{0_i})-\pi_1(\mathbf{x}_{0_i}))^2\tilde{\omega}_{0_i}(\mathbf{x}_0)+\sum_{\mathbf{x}_{0_i}\in\tilde{\chi}^f_{N_0}}(f_1(\mathbf{x}_{0_i})-\pi_1(\mathbf{x}_{0_i}))^2\tilde{\omega}_{0_i}(\mathbf{x}_0)=$$
$$=\sum_{\mathbf{x}_{0_i}\in\tilde{\chi}^d_{N_0}}(f(\mathbf{x}_{0_i})-\pi_1(\mathbf{x}_{0_i}))^2\tilde{\omega}_{0_i}(\mathbf{x}_0)+\sum_{\mathbf{x}_{0_i}\in\tilde{\chi}^f_{N_0}}(f_1(\mathbf{x}_{0_i})-\pi_1(\mathbf{x}_{0_i}))^2O(h^{-2t}).$$

Finally, as π_1 is a polynomial approximation of degree d, the order of accuracy in the smooth zones is $O(h^{d+1})$ (see e.g. [9,14]), thus

$$\sum_{\mathbf{x}_{0_i}\in\tilde{\chi}^d_{N_0}}(f(\mathbf{x}_{0_i})-\pi_1(\mathbf{x}_{0_i}))^2\tilde{\omega}_{0_i}(\mathbf{x}_0)+\sum_{\mathbf{x}_{0_i}\in\tilde{\chi}^f_{N_0}}(f_1(\mathbf{x}_{0_i})-\pi_1(\mathbf{x}_{0_i}))^2O(h^{-2t})=$$
$$=\sum_{\mathbf{x}_{0_i}\in\tilde{\chi}^d_{N_0}}(f(\mathbf{x}_{0_i})-\pi_1(\mathbf{x}_{0_i}))^2\tilde{\omega}_{0_i}(\mathbf{x}_0)+O(h^{2(d-t+1)}).$$

Thus, it follows

$$\sum_{\mathbf{x}_{0_i}\in\tilde{\chi}^d_{N_0}}(f(\mathbf{x}_{0_i})-\tilde{\tilde{p}}_{\mathbf{x}_0}(\mathbf{x}_{0_i}))^2\tilde{\omega}_{0_i}(\mathbf{x}_0)+\sum_{\mathbf{x}_{0_i}\in\tilde{\chi}^f_{N_0}}(f_1(\mathbf{x}_{0_i})-\tilde{\tilde{p}}_{\mathbf{x}_0}(\mathbf{x}_{0_i}))^2\tilde{\omega}_{0_i}(\mathbf{x}_0)\leq$$
$$\leq\sum_{\mathbf{x}_{0_i}\in\tilde{\chi}^d_{N_0}}(f(\mathbf{x}_{0_i})-\pi_1(\mathbf{x}_{0_i}))^2\tilde{\omega}_{0_i}(\mathbf{x}_0)+O(h^{2(d-t+1)})\Rightarrow$$

$$\sum_{\mathbf{x}_{0_i}\in\tilde{\chi}^f_{N_0}}(f_1(\mathbf{x}_{0_i})-\tilde{\tilde{p}}_{\mathbf{x}_0}(\mathbf{x}_{0_i}))^2\tilde{\omega}_{0_i}(\mathbf{x}_0)\leq\sum_{\mathbf{x}_{0_i}\in\tilde{\chi}^d_{N_0}}(f(\mathbf{x}_{0_i})-\pi_1(\mathbf{x}_{0_i}))^2\tilde{\omega}_{0_i}(\mathbf{x}_0)$$
$$-\sum_{\mathbf{x}_{0_i}\in\tilde{\chi}^d_{N_0}}(f(\mathbf{x}_{0_i})-\tilde{\tilde{p}}_{\mathbf{x}_0}(\mathbf{x}_{0_i}))^2\tilde{\omega}_{0_i}(\mathbf{x}_0)+O(h^{2(d-t+1)})$$
$$=\sum_{\mathbf{x}_{0_i}\in\tilde{\chi}^d_{N_0}}(\pi_1(\mathbf{x}_{0_i})-\tilde{\tilde{p}}_{\mathbf{x}_0}(\mathbf{x}_{0_i}))(\pi_1(\mathbf{x}_{0_i})-f(\mathbf{x}_{0_i})+\tilde{\tilde{p}}_{\mathbf{x}_0}(\mathbf{x}_{0_i})-f(\mathbf{x}_{0_i}))\tilde{\omega}_{0_i}(\mathbf{x}_0)$$
$$+O(h^{2(d-t+1)}).$$

From (16), we know that the right-hand side of the inequality is bounded, then there exists a constant C such that

$$\sum_{\mathbf{x}_{0_i}\in\tilde{\chi}^d_{N_0}}(\pi_1(\mathbf{x}_{0_i})-\tilde{\tilde{p}}_{\mathbf{x}_0}(\mathbf{x}_{0_i}))(\pi_1(\mathbf{x}_{0_i})-f(\mathbf{x}_{0_i})+\tilde{\tilde{p}}_{\mathbf{x}_0}(\mathbf{x}_{0_i})-f(\mathbf{x}_{0_i}))\tilde{\omega}_{0_i}(\mathbf{x}_0)\leq C, \tag{17}$$

independent of h. By (16), $\tilde{\omega}_{0_i}(\mathbf{x}_0)=O(h^{-2t})$ if $\mathbf{x}_{0_i}\in\tilde{\chi}^f_{N_0}$, and this implies that

$$\sum_{\mathbf{x}_{0_i}\in\tilde{\chi}^f_{N_0}}(f_1(\mathbf{x}_{0_i})-\tilde{\tilde{p}}_{\mathbf{x}_0}(\mathbf{x}_{0_i}))^2\tilde{\omega}_{0_i}(\mathbf{x}_0)=O(h^{-2t})\sum_{\mathbf{x}_{0_i}\in\tilde{\chi}^f_{N_0}}(f_1(\mathbf{x}_{0_i})-\tilde{\tilde{p}}_{\mathbf{x}_0}(\mathbf{x}_{0_i}))^2\leq C+O(h^{2(d-t+1)}),$$

then

$$(f_1(\mathbf{x}_{0_i})-\tilde{\tilde{p}}_{\mathbf{x}_0}(\mathbf{x}_{0_i}))^2=O(h^{2\kappa})\Rightarrow|f_1(\mathbf{x}_{0_i})-\tilde{\tilde{p}}_{\mathbf{x}_0}(\mathbf{x}_{0_i})|=O(h^{\kappa}),\quad\forall\,\mathbf{x}_{0_i}\in\tilde{\chi}^f_{N_0},$$

with $\kappa\geq t$. Therefore,

$$|\pi_1(\mathbf{x}_{0_i})-\tilde{\tilde{p}}_{\mathbf{x}_0}(\mathbf{x}_{0_i})|=|\pi_1(\mathbf{x}_{0_i})-f_1(\mathbf{x}_{0_i})+f_1(\mathbf{x}_{0_i})-\tilde{\tilde{p}}_{\mathbf{x}_0}(\mathbf{x}_{0_i})|$$
$$\leq|\pi_1(\mathbf{x}_{0_i})-f_1(\mathbf{x}_{0_i})|+|f_1(\mathbf{x}_{0_i})-\tilde{\tilde{p}}_{\mathbf{x}_0}(\mathbf{x}_{0_i})|=O(h^{d+1})+O(h^{\kappa}),\quad\forall\,\mathbf{x}_{0_i}\in\tilde{\chi}^f_{N_0}.$$

Since, the interpolation operator is well-defined with respect to the points P_d and its inverse is bounded by a constant independent of h then

$$||\pi_1-\tilde{\tilde{p}}_{\mathbf{x}_0}||_{\infty,\Omega^+}=O(h^{d+1})+O(h^{\kappa}).$$

Therefore,

$$\begin{aligned}|f(\mathbf{x}_0) - \tilde{\tilde{p}}_{\mathbf{x}_0}(\mathbf{x}_0)| &= |f_1(\mathbf{x}_0) - \pi_1(\mathbf{x}_0) + \pi_1(\mathbf{x}_0) - \tilde{\tilde{p}}_{\mathbf{x}_0}(\mathbf{x}_0)| \\ &\leq |f_1(\mathbf{x}_0) - \pi_1(\mathbf{x}_0)| + |\pi_1(\mathbf{x}_0) - \tilde{\tilde{p}}_{\mathbf{x}_0}(\mathbf{x}_0)| = O(h^{d+1}) + O(h^{d+1}) + O(h^{\kappa}) \\ &= O(h^{\min\{d+1,\kappa\}}). \quad \blacksquare\end{aligned}$$

In our case, we only have to take $t = d + 1$ in order to get the maximum order of accuracy.

Remark 2 *(Diffusion and oscillations in the MLS method).* When applying the linear MLS method to discontinuous data with a radial weight function ω of support c, the resulting approximation exhibits significant diffusion and oscillations within a region of width $\leq ch$ near the discontinuity curve Γ.

The following theorem demonstrates that the diffusion region is significantly reduced when using the data-dependent MLS method, and, additionally, oscillations are eliminated. We use the above definitions of Γ, Ω^+ and Ω^- and of f defined in Eq. (9). We consider a weight function ω of support size c, $c \geq 2$, and such that $\omega(c - \epsilon_0) \geq C_0 > 0$. We further assume that Γ is a smooth curve. We adopt below the assumptions in Theorem 3.4 and the notation within its proof. Let D_r denote the domain consisting of all points within a distance $\leq r$ from Γ, and let $\bar{D}_r$ denote its complement.

Theorem 3.5. *Assume the data points $\tilde{\chi}^d_{N_0}$ are within D_{kh} and let $\mathbf{x}_0 \in \Omega^+ \cap \bar{D}_{ch-kh}$. Then the data-dependent MLS approximation of degree d with ω of support size $c \geq d/2 + k$ satisfies $|\tilde{f}(\mathbf{x}_0) - \mathcal{I}_{DD\text{-}MLS}(\mathbf{x}_0)| = O(h^{d+1})$.*

Proof. Define the support of data points respect to $\mathbf{x}_0$ as $S(\mathbf{x}_0) = \{\mathbf{x}_i \in : \omega_i(\mathbf{x}_0) > 0\}$. For any point $\mathbf{x}_i \in S(\mathbf{x}_0) \cap \Omega^-$ the smoothness indicator I_i is $O(1)$. Additionally, within a circular segment of width dh there are points $\mathbf{x}_i \in S(\mathbf{x}_0) \cap \Omega^+$ for which the smoothness indicator I_i is $O(h^2)$ as $h \to 0$. Recalling that h is the fill distance of the points χ_N, it follows that there exist at least $m = \binom{d+2}{2}$ points $\mathbf{x}_i \in S(\mathbf{x}_0) \cap \Omega^+$ for which the smoothness indicator I_i is $O(h^2)$ as $h \to 0$. For these points, the interpolation operator, defined using them, is well-defined and its norm is bounded by a constant independent of h. Then, by Theorem 3.4, using $t = d + 1$, the data-dependent MLS approximation satisfies:

$$|f(\mathbf{x}_0) - \mathcal{I}_{\text{DD-MLS}}(\mathbf{x}_0)| = O(h^{d+1}). \quad \blacksquare$$

Corollary 3.6 *(Reduced diffusion region and reduced oscillations). The linear MLS provides full approximation order for points at a distance $\geq ch$ from Γ. By applying Theorem 3.5 we observe that the data-dependent MLS extends this full approximation order to a larger region, specifically to points at a distance $\geq ch - kh$ from Γ.*

The oscillations observed near Γ in the linear MLS approximation arise because it incorporates data from both sides of Γ and applies both positive and negative weights. This occurs for points at a distance $< ch$ from Γ. As argued in Theorem 3.5, for points within the range $ch - hk < dist < ch$, the data-dependent MLS approximation uses data only from one side of Γ. Since the weights in the approximation sum to 1 and are applied exclusively to data from one side of Γ, no oscillations will occur within this range.

4. Numerical experiments

In this section, we check numerically the theoretical properties shown in Section 3: order of accuracy, reproduction of polynomials, reduction of Gibbs oscillations, and reduction of the smearing around discontinuities.

The algorithm that we use is similar to the one designed in Chapter 22, page 220, of [9], we only introduce a detection of discontinuity points by calculating the smoothness indicator of each data point, i.e., we solve the problems in Eq. (13) and evaluate Eq. (14). For this problem, we fix the following parameter as in [7]:

$$\delta = \frac{\sqrt{2}}{\lfloor \frac{\sqrt{N}}{2} \rfloor}, \quad i = 1, \ldots, N,$$

where $\lfloor x \rfloor$ is the floor function, which returns the greatest integer less than or equal to $x \in \mathbb{R}$. This part is not very expensive computationally because it only involves solving a simple linear least squares problem. Therefore, the algorithms for the linear and data-dependent cases are very similar in terms of computational cost.

We will use the acronyms MLS^d_F or DD-MLS^d_F to call the linear and data-dependent moving least squares methods, where F represents the weight function, chosen from Table 1, and d is the maximum degree of the polynomial used. We have selected the Wendland $W2$, $W4$ functions and Gaussian function G to perform the experiments. We apply these functions in the following way, $\omega_i(\mathbf{x}) = \omega(\varepsilon \|\mathbf{x} - \mathbf{x}_i\|)$ with the *shape parameter* $\varepsilon \propto \frac{1}{h}$. In our experiments, we take for $W2$, $W4$ (see [7]):

$$\varepsilon = \frac{1}{2} \left\lfloor \frac{\sqrt{N}}{2} \right\rfloor,$$

Table 2
Errors and rates using linear and data-dependent MLS methods for Franke's test function evaluated at grid points.

	MLS^2_{W2}		$\text{DD-MLS}^2_{\text{W2}}$		MLS^2_{W2}		$\text{DD-MLS}^2_{\text{W2}}$	
l	MAE_l	r_l^∞	MAE_l	r_l^∞	RMSE_l	r_l^2	RMSE_l	r_l^2
4	2.9459e-02		6.2989e-02		4.5011e-03		1.2700e-02	
5	3.4607e-03	3.1049	9.5840e-03	2.7299	4.0810e-04	3.4805	1.5139e-03	3.0837
6	2.5977e-04	3.7728	9.5542e-04	3.3594	2.7858e-05	3.9111	1.3019e-04	3.5747
7	1.7035e-05	3.9115	5.1915e-05	4.1814	1.7626e-06	3.9629	5.6006e-06	4.5168
	MLS^2_{W4}		$\text{DD-MLS}^2_{\text{W4}}$		MLS^2_{W4}		$\text{DD-MLS}^2_{\text{W4}}$	
l	MAE_l	r_l^∞	MAE_l	r_l^∞	RMSE_l	r_l^2	RMSE_l	r_l^2
4	2.1519e-02		4.7609e-02		3.0906e-03		9.0872e-03	
5	2.2812e-03	3.2538	6.5667e-03	2.8721	2.6332e-04	3.5707	1.0050e-03	3.1924
6	1.6727e-04	3.8069	6.3657e-04	3.4002	1.7560e-05	3.9451	8.5276e-05	3.5941
7	1.0846e-05	3.9276	3.3648e-05	4.2210	1.1183e-06	3.9536	3.6034e-06	4.5425
	MLS^2_{G}		$\text{DD-MLS}^2_{\text{G}}$		MLS^2_{G}		$\text{DD-MLS}^2_{\text{G}}$	
l	MAE_l	r_l^∞	MAE_l	r_l^∞	RMSE_l	r_l^2	RMSE_l	r_l^2
4	1.1701e-02		3.0202e-02		1.5423e-03		4.9530e-03	
5	1.0906e-03	3.4403	3.4672e-03	3.1383	1.2017e-04	3.7001	4.8617e-04	3.3654
6	7.8215e-05	3.8392	3.1008e-04	3.5176	8.0812e-06	3.9330	3.9902e-05	3.6427
7	5.2402e-06	3.8807	1.5806e-05	4.2732	5.6088e-07	3.8300	1.6869e-06	4.5417

Table 3
Errors and rates using linear and data-dependent MLS methods for Franke's test function evaluated at Halton's points.

	MLS^2_{W2}		$\text{DD-MLS}^2_{\text{W2}}$		MLS^2_{W2}		$\text{DD-MLS}^2_{\text{W2}}$	
l	MAE_l	r_l^∞	MAE_l	r_l^∞	RMSE_l	r_l^2	RMSE_l	r_l^2
4	3.0411e-02		5.3557e-02		4.5092e-03		1.2182e-02	
5	3.9097e-03	3.3987	9.7501e-03	2.8224	5.1659e-04	3.5898	1.5725e-03	3.3920
6	4.9130e-04	3.4450	1.0768e-03	3.6595	5.4169e-05	3.7456	1.4011e-04	4.0161
7	6.2966e-05	3.4057	1.3020e-04	3.5022	6.7078e-06	3.4627	9.2877e-06	4.4986
	MLS^2_{W4}		$\text{DD-MLS}^2_{\text{W4}}$		MLS^2_{W4}		$\text{DD-MLS}^2_{\text{W4}}$	
l	MAE_l	r_l^∞	MAE_l	r_l^∞	RMSE_l	r_l^2	RMSE_l	r_l^2
4	2.3547e-02		4.3721e-02		3.3430e-03		8.6294e-03	
5	2.7803e-03	3.5398	6.7029e-03	3.1071	3.8656e-04	3.5744	1.0595e-03	3.4750
6	4.1415e-04	3.1625	7.9889e-04	3.5329	4.3740e-05	3.6192	9.6392e-05	3.9815
7	6.4247e-05	3.0891	1.0343e-04	3.3890	5.8562e-06	3.3333	7.2394e-06	4.2916
	MLS^2_{G}		$\text{DD-MLS}^2_{\text{G}}$		MLS^2_{G}		$\text{DD-MLS}^2_{\text{G}}$	
l	MAE_l	r_l^∞	MAE_l	r_l^∞	RMSE_l	r_l^2	RMSE_l	r_l^2
4	1.8162e-02		3.1263e-02		2.2047e-03		4.8132e-03	
5	2.2788e-03	3.4391	4.5951e-03	3.1769	2.7608e-04	3.4424	5.6946e-04	3.5364
6	3.8683e-04	2.9455	5.4298e-04	3.5472	3.3817e-05	3.4875	5.4933e-05	3.8842
7	5.6293e-05	3.1951	8.6890e-05	3.0376	4.8183e-06	3.2301	5.2895e-06	3.8797

and for G,

$$\varepsilon = 2\left\lfloor \frac{\sqrt{N}}{2} \right\rfloor.$$

Also, in the Gaussian case, another condition is imposed: we only consider the values $\mathbf{x}_i \in \chi_N$ such that $\omega_i(\mathbf{x}) > 10^{-10}$. We divide our experiments in three subsections: we examine the order of accuracy in smooth zones for the values $d = 0, 1, 2$. After that, we analyze the behavior of the approximations close to the discontinuities, and, finally, we study intensively the smearing of discontinuities when $d = 0$ (Shepard's method, [22]) and $d = 1$.

4.1. Order of accuracy

We start by analyzing the order of accuracy using the well-known Franke's function, defined as

$$f(x,y) = \frac{3}{4}e^{-1/4((9x-2)^2+(9y-2)^2)} + \frac{3}{4}e^{-1/49(9x+1)^2-1/10(9y+1)} + \frac{1}{2}e^{-1/4((9x-7)^2+(9y-3)^2)} - \frac{1}{5}e^{-(9x-4)^2-(9y-7)^2}, \tag{18}$$

Table 4
Errors and rates using linear and data-dependent MLS methods for Franke's test function evaluated at grid points.

	MLS^1_{W2}		$\text{DD-MLS}^1_{\text{W2}}$		MLS^1_{W2}		$\text{DD-MLS}^1_{\text{W2}}$	
l	MAE_l	r_l^∞	MAE_l	r_l^∞	RMSE_l	r_l^2	RMSE_l	r_l^2
4	1.1379e-01		1.9511e-01		2.9208e-02		4.1874e-02	
5	3.1759e-02	1.8502	5.4100e-02	1.8597	8.2129e-03	1.8395	9.5939e-03	2.1364
6	8.5522e-03	1.9115	1.1477e-02	2.2591	2.1242e-03	1.9703	2.1849e-03	2.1557
7	2.2003e-03	1.9490	2.3391e-03	2.2835	5.3588e-04	1.9773	5.3824e-04	2.0114
	MLS^1_{W4}		$\text{DD-MLS}^1_{\text{W4}}$		MLS^1_{W4}		$\text{DD-MLS}^1_{\text{W4}}$	
l	MAE_l	r_l^∞	MAE_l	r_l^∞	RMSE_l	r_l^2	RMSE_l	r_l^2
4	8.9718e-02		1.5742e-01		2.3062e-02		3.2179e-02	
5	2.4477e-02	1.8833	4.3323e-02	1.8707	6.3336e-03	1.8737	7.1698e-03	2.1769
6	6.5848e-03	1.9130	8.3406e-03	2.4005	1.6265e-03	1.9807	1.6580e-03	2.1334
7	1.6836e-03	1.9580	1.7678e-03	2.2273	4.0947e-04	1.9802	4.1084e-04	2.0030
	MLS^1_{G}		$\text{DD-MLS}^1_{\text{G}}$		MLS^1_{G}		$\text{DD-MLS}^1_{\text{G}}$	
l	MAE_l	r_l^∞	MAE_l	r_l^∞	RMSE_l	r_l^2	RMSE_l	r_l^2
4	5.5298e-02		9.7249e-02		1.4210e-02		1.8864e-02	
5	1.4845e-02	1.9067	2.5712e-02	1.9288	3.7812e-03	1.9195	4.0917e-03	2.2158
6	3.9269e-03	1.9375	4.6121e-03	2.5035	9.6173e-04	1.9947	9.7048e-04	2.0965
7	9.9534e-04	1.9705	1.0290e-03	2.1536	2.4153e-04	1.9837	2.4203e-04	1.9938

Table 5
Errors and rates using linear and data-dependent MLS methods for Franke's test function evaluated at Halton's points.

	MLS^1_{W2}		$\text{DD-MLS}^1_{\text{W2}}$		MLS^1_{W2}		$\text{DD-MLS}^1_{\text{W2}}$	
l	MAE_l	r_l^∞	MAE_l	r_l^∞	RMSE_l	r_l^2	RMSE_l	r_l^2
4	1.0485e-01		1.9775e-01		2.8246e-02		4.2458e-02	
5	3.4265e-02	1.8530	4.9345e-02	2.3000	8.2717e-03	2.0348	9.6733e-03	2.4507
6	9.7104e-03	2.0943	1.1974e-02	2.3520	2.1446e-03	2.2420	2.2221e-03	2.4431
7	2.4667e-03	2.2716	2.4842e-03	2.6073	5.4304e-04	2.2769	5.4552e-04	2.3282
	MLS^1_{W4}		$\text{DD-MLS}^1_{\text{W4}}$		MLS^1_{W4}		$\text{DD-MLS}^1_{\text{W4}}$	
l	MAE_l	r_l^∞	MAE_l	r_l^∞	RMSE_l	r_l^2	RMSE_l	r_l^2
4	8.3978e-02		1.5293e-01		2.2556e-02		3.2350e-02	
5	2.8296e-02	1.8024	3.7951e-02	2.3092	6.4277e-03	2.0800	7.2640e-03	2.4748
6	8.1573e-03	2.0659	8.9301e-03	2.4031	1.6564e-03	2.2522	1.6989e-03	2.4132
7	2.1030e-03	2.2471	2.0241e-03	2.4606	4.1929e-04	2.2774	4.1958e-04	2.3183
	MLS^1_{G}		$\text{DD-MLS}^2_{\text{G}}$		MLS^1_{G}		$\text{DD-MLS}^1_{\text{G}}$	
l	MAE_l	r_l^∞	MAE_l	r_l^∞	RMSE_l	r_l^2	RMSE_l	r_l^2
4	5.7777e-02		8.1826e-02		1.4432e-02		1.8700e-02	
5	2.1624e-02	1.6284	2.5200e-02	1.9514	3.9649e-03	2.1406	4.2732e-03	2.4458
6	6.1526e-03	2.0876	6.3276e-03	2.2953	1.0226e-03	2.2508	1.0340e-03	2.3568
7	1.5647e-03	2.2698	1.5688e-03	2.3118	2.5971e-04	2.2719	2.5859e-04	2.2975

using as nodes two types of sets: a regular grid defined by $\chi_{N=2^l+1} = \{(i/2^l, j/2^l) : i, j = 0, \dots, 2^l\}$, and a collection of $N = (2^l + 1)^2$ Halton's scattered data points, as described in [10]. We denote the fill distance by h_l, and the associated errors by $e_i^l = |f(\mathbf{z}_i) - \mathcal{I}^l(\mathbf{z}_i)|$, where $\{\mathbf{z}_i : 1 \le i \le N_{\text{eval}}\}$ is a regular grid in $[0.025, 0.975]^2$, and represents the set of evaluation points at which the function is approximated with $N_{eval} = 120^2$ points. Finally, we define the maximum discrete ℓ^2 norms and their respective convergence rates as follows:

$$\text{MAE}_l = \max_{i=1,\dots,N_{\text{eval}}} e_i^l, \quad \text{RMSE}_l = \left(\frac{1}{N_{\text{eval}}} \sum_{i=1}^{N_{\text{eval}}} (e_i^l)^2 \right)^{\frac{1}{2}}, \quad r_l^\infty = \frac{\log(\text{MAE}_{l-1}/\text{MAE}_l)}{\log(h_{l-1}/h_l)}, \quad r_l^2 = \frac{\log(\text{RMSE}_{l-1}/\text{RMSE}_l)}{\log(h_{l-1}/h_l)}.$$

When $d = 2$, we can see in Tables 2 and 3 that the order of accuracy reached is greater than 3. In fact, when the data points are placed on a regular grid, the order of accuracy is close to 4 in both linear and data-dependent cases. These results are shown in Table 2. We can see that the error is slightly small when the linear version of the MLS is employed. This effect can be reduced if we choose a value of the parameter t in (12) smaller, but then some oscillations can appear in the final approximation. When $d = 1$, Tables 4 and 5, the order of accuracy is 2 when using a regular grid, as it can be observed in Table 4, and also when using pseudo-random points, Table 5. Again, the error is slightly greater in the data-dependent case. Finally, when $d = 0$ the order of accuracy with regular data points is larger than the one expected, as it is shown in Table 6, but smaller when Halton's data points are used, as shown in

Table 6
Errors and rates using linear and data-dependent MLS methods for Franke's test function evaluated at grid points.

	MLS^0_{W2}		$\text{DD-MLS}^0_{\text{W2}}$		MLS^0_{W2}		$\text{DD-MLS}^0_{\text{W2}}$	
l	MAE_l	r_l^∞	MAE_l	r_l^∞	RMSE_l	r_l^2	RMSE_l	r_l^2
4	1.1379e-01		2.1215e-01		2.9355e-02		7.9470e-02	
5	3.1754e-02	1.8504	9.1316e-02	1.2222	8.3385e-03	1.8247	3.0115e-02	1.4069
6	8.5514e-03	1.9115	3.1215e-02	1.5640	2.1290e-03	1.9891	8.2379e-03	1.8887
7	2.2009e-03	1.9485	5.6983e-03	2.4417	5.3596e-04	1.9803	1.0663e-03	2.9352
	MLS^0_{W4}		$\text{DD-MLS}^0_{\text{W4}}$		MLS^0_{W4}		$\text{DD-MLS}^0_{\text{W4}}$	
l	MAE_l	r_l^∞	MAE_l	r_l^∞	RMSE_l	r_l^2	RMSE_l	r_l^2
4	8.9721e-02		1.8258e-01		2.3203e-02		6.5426e-02	
5	2.4474e-02	1.8835	7.5082e-02	1.2884	6.3935e-03	1.8688	2.4098e-02	1.4481
6	6.5832e-03	1.9132	2.4913e-02	1.6074	1.6274e-03	1.9936	6.4179e-03	1.9277
7	1.6845e-03	1.9569	4.4363e-03	2.4773	4.0959e-04	1.9806	8.1827e-04	2.9570
	MLS^0_{G}		$\text{DD-MLS}^0_{\text{G}}$		MLS^0_{G}		$\text{DD-MLS}^0_{\text{G}}$	
l	MAE_l	r_l^∞	MAE_l	r_l^∞	RMSE_l	r_l^2	RMSE_l	r_l^2
4	5.5301e-02		1.3307e-01		1.4256e-02		4.4167e-02	
5	1.4844e-02	1.9068	5.0079e-02	1.4169	3.7889e-03	1.9212	1.5365e-02	1.5308
6	3.9248e-03	1.9382	1.5705e-02	1.6896	9.6178e-04	1.9976	3.8797e-03	2.0053
7	9.9655e-04	1.9679	2.6784e-03	2.5393	2.4169e-04	1.9828	4.8548e-04	2.9838

Table 7
Errors and rates using linear and data-dependent MLS methods for Franke's test function evaluated at Halton's points.

	MLS^0_{W2}		$\text{DD-MLS}^0_{\text{W2}}$		MLS^0_{W2}		$\text{DD-MLS}^0_{\text{W2}}$	
l	MAE_l	r_l^∞	MAE_l	r_l^∞	RMSE_l	r_l^2	RMSE_l	r_l^2
4	1.0586e-01		2.4268e-01		2.8270e-02		8.4870e-02	
5	3.4724e-02	1.8469	9.8871e-02	1.4877	9.3858e-03	1.8269	3.1069e-02	1.6650
6	1.3981e-02	1.5109	3.3478e-02	1.7986	2.8053e-03	2.0059	9.1451e-03	2.0313
7	6.1264e-03	1.3678	9.2646e-03	2.1296	1.0559e-03	1.6198	1.6218e-03	2.8673
	MLS^0_{W4}		$\text{DD-MLS}^0_{\text{W4}}$		MLS^0_{W4}		$\text{DD-MLS}^0_{\text{W4}}$	
l	MAE_l	r_l^∞	MAE_l	r_l^∞	RMSE_l	r_l^2	RMSE_l	r_l^2
4	8.2583e-02		2.0157e-01		2.2883e-02		7.0341e-02	
5	3.3019e-02	1.5189	8.3508e-02	1.4600	7.8197e-03	1.7791	2.5145e-02	1.7044
6	1.5863e-02	1.2176	3.1235e-02	1.6334	2.6272e-03	1.8116	7.4538e-03	2.0196
7	6.7009e-03	1.4285	9.0153e-03	2.0599	1.1405e-03	1.3833	1.5213e-03	2.6344
	MLS^0_{G}		$\text{DD-MLS}^0_{\text{G}}$		MLS^0_{G}		$\text{DD-MLS}^0_{\text{G}}$	
l	MAE_l	r_l^∞	MAE_l	r_l^∞	RMSE_l	r_l^2	RMSE_l	r_l^2
4	7.5331e-02		1.4497e-01		1.6087e-02		4.8153e-02	
5	3.2711e-02	1.3821	6.3294e-02	1.3731	6.3405e-03	1.5427	1.6858e-02	1.7389
6	1.8551e-02	0.9421	2.8400e-02	1.3311	2.7718e-03	1.3743	5.3489e-03	1.9067
7	8.8940e-03	1.2187	1.0852e-02	1.5948	1.4143e-03	1.1155	1.5756e-03	2.0262

Table 7. It is clear that the results when the data-dependent MLS method is used are very close to the linear ones, and that it works correctly for smooth functions and, therefore, in the smooth zones.

4.2. Avoiding oscillations

In this subsection, we approximate some functions with discontinuities as we have defined in Eq. (9). We start by approximating the function, g on $[0,1]^2$, defined in [2]:

$$g(x,y) = \begin{cases} -(x+y+1)\cos(4x) + \sin(4(x+y)), & (x-0.5)^2 + (y-0.5)^2 \geq 0.1, \\ \exp\left(-10\left((x-0.5)^2 + (y-0.5)^2\right)\right), & (x-0.5)^2 + (y-0.5)^2 < 0.1, \end{cases} \tag{19}$$

using $N = 65^2$ grid data points, Fig. 2.a) using the linear method, and Fig. 2.b), using W2 (note that the figures in the second row are just a rotation of those in the first row). When a polynomial of degree $d \geq 2$ is used, we can see that some oscillations appear close to the discontinuities, Fig. 2.a), in the linear case. This phenomenon is not avoided even if we refine the mesh. We can observe that these non-desired oscillations disappear when the data-dependent method is employed, Fig. 2.b). This result is very similar when the data points are pseudorandom, Figs. 2.c) and 2.d). If the approximation operator is C^∞, Figs. 2.e) and 2.f), then the result is similar, but in the DD-MLS we can observe that some smearing of the discontinuities appears.

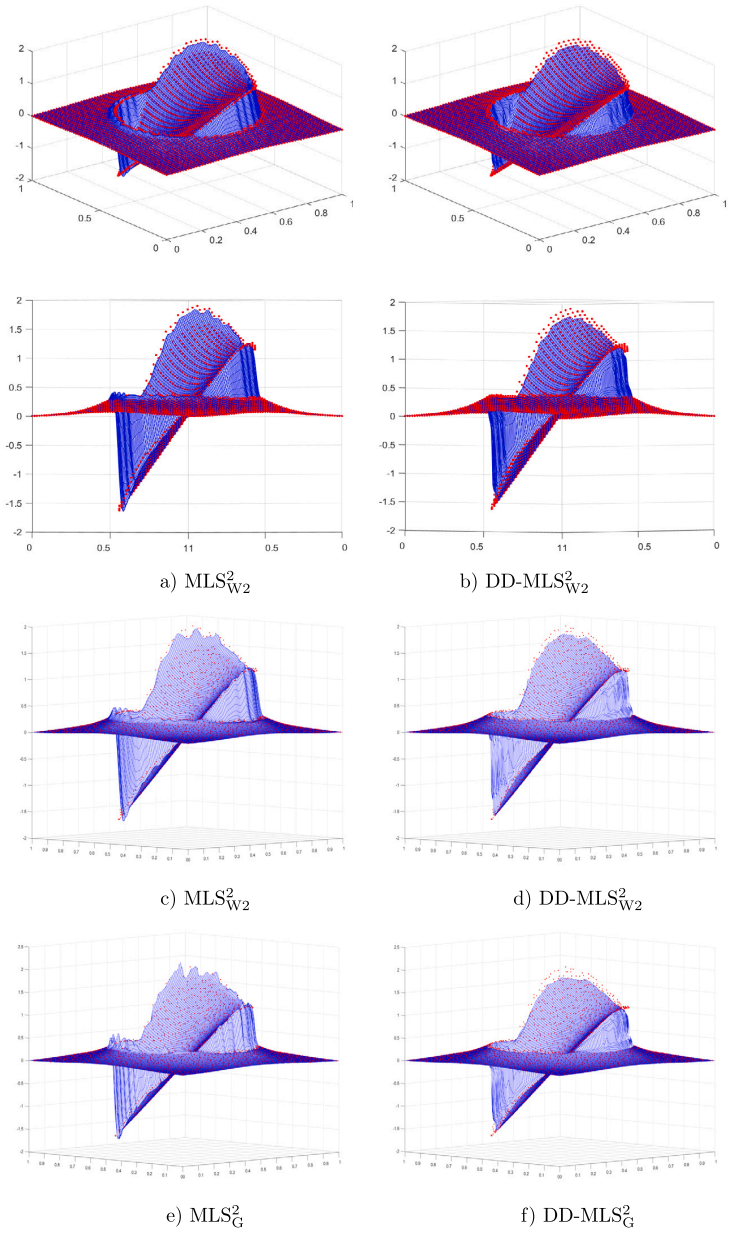

Fig. 2. Approximation to the function g, Eq. (19), using linear and data-dependent MLS with different $\omega(x)$ functions [26] and the class of polynomials $\Pi_2(\mathbb{R}^2)$. Red points: original function, blue lines: approximation.

In order to analyze the behavior when the discontinuity is more pronounced, we perform the example designed in [1] with the following function

$$z(x,y) = \begin{cases} \cos(xy), & (x-0.5)^2 + (y-0.5)^2 \le 0.25^2, \\ \sin(xy), & (x-0.5)^2 + (y-0.5)^2 > 0.25^2. \end{cases} \tag{20}$$

In this experiment, Figs. 3 and 4, we show the result using $N = 65^2$ and $N = 33^2$ data points, and the error between the original function and the approximated one. We can observe that the non-desired oscillations disappear for W2 and G cases.

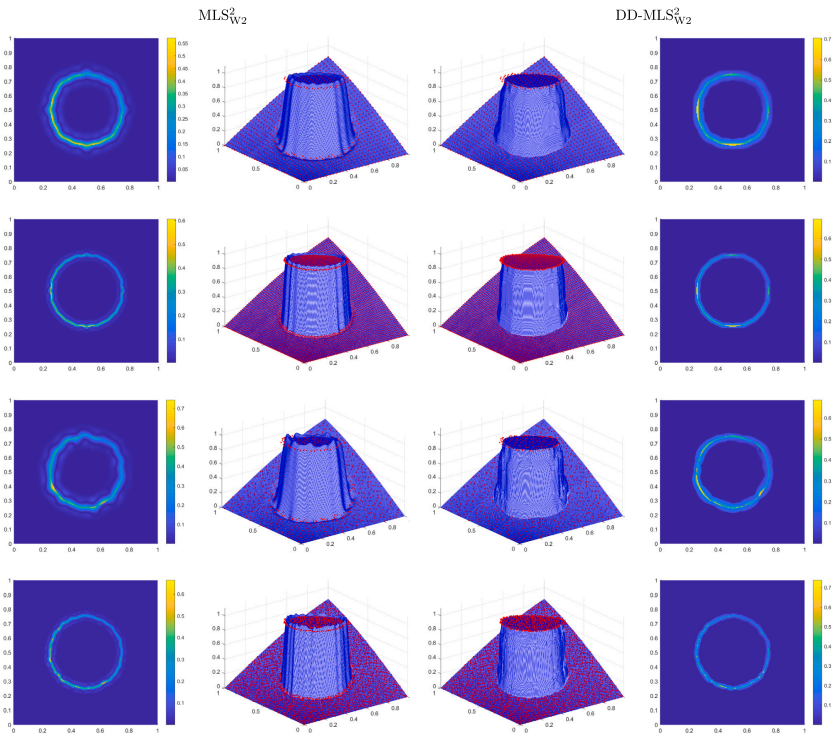

Fig. 3. Approximation to the function z, Eq. (20), using linear and data-dependent MLS with $\omega(x)$ the C^2 Wendland function [26] and the class of polynomials $\Pi_2(\mathbb{R}^2)$. Red points: original function, blue lines: approximation.

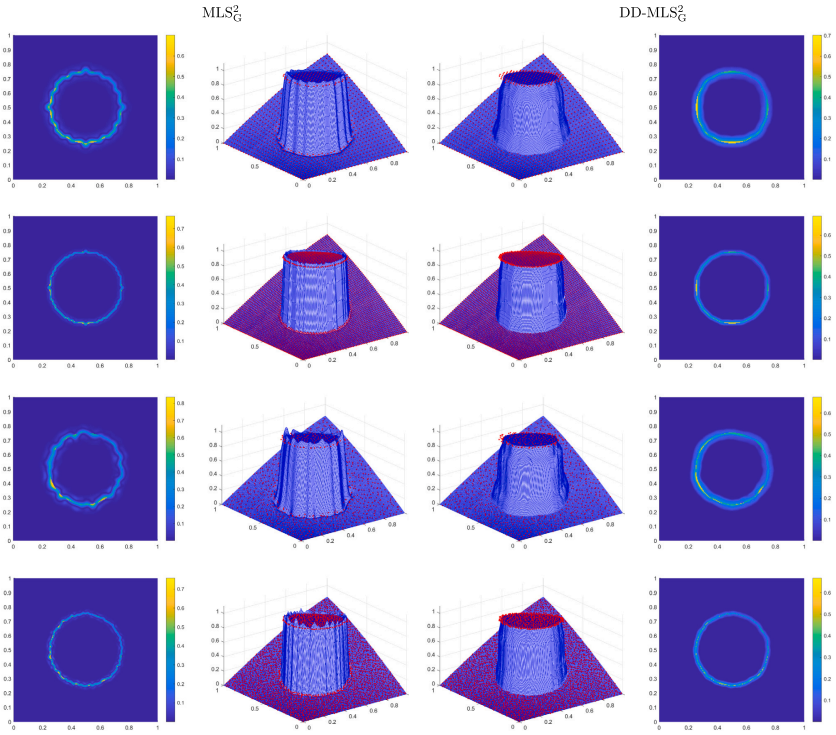

Fig. 4. Approximation to the function z, Eq. (20), using linear and data-dependent MLS with $\omega(x)$ the C^∞ Gauss function [26] and the class of polynomials $\Pi_2(\mathbb{R}^2)$. Red points: original function, blue lines: approximation.

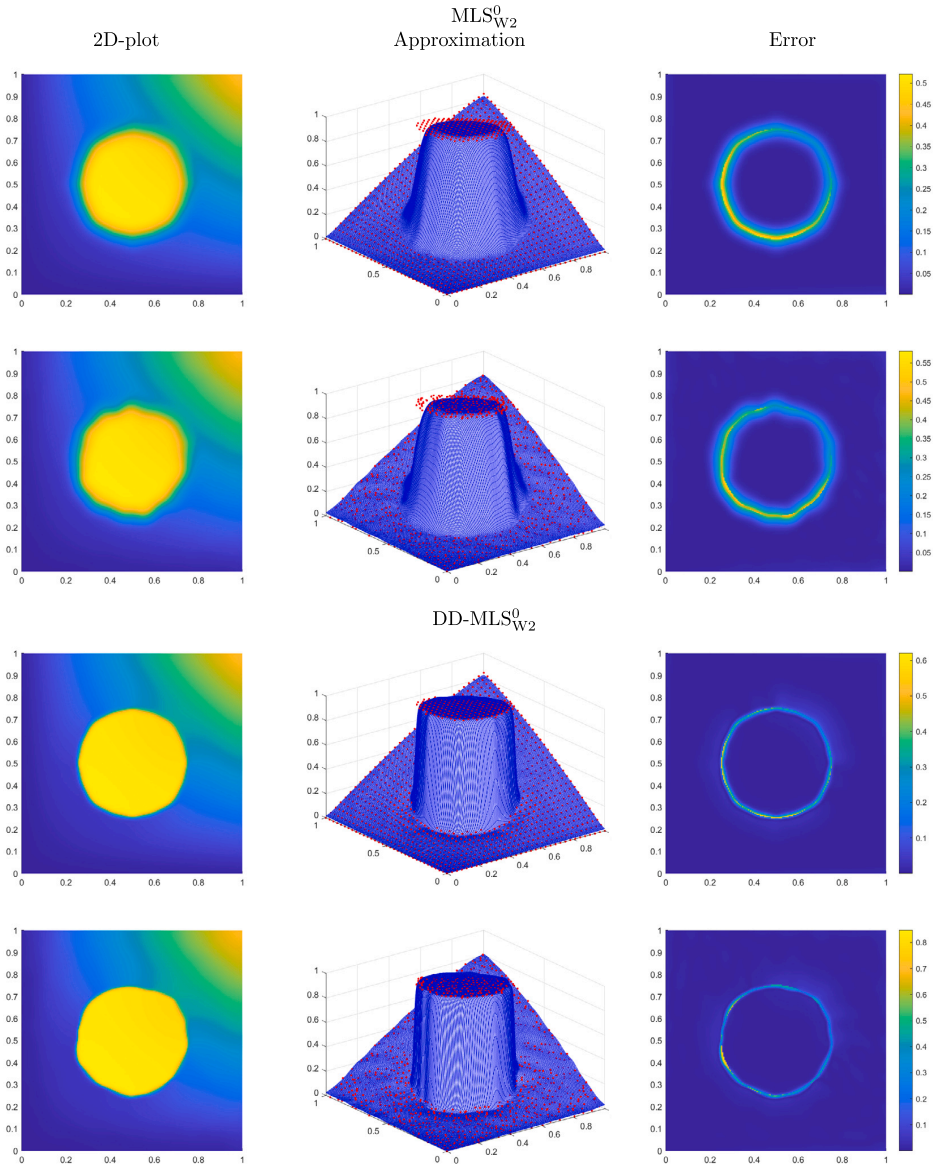

Fig. 5. Approximation to function z, Eq. (20), using W2, (linear MLS method in rows one and two, and data-depend MLS in rows three and four), $d = 0$ with $N = 33^2$. The first row and the third row correspond to uniform gridded data. The second and fourth row correspond to Halton points.

4.3. Reduction of the smearing zone across the discontinuity

In this section we study the results obtained when we employ the set of polynomials of degree $d = 0$, general Shepard's method (see [9]), or $d = 1$. In these cases, the non-desired oscillations do not occur, but some diffusion effects appear when the linear MLS algorithms are used. We compare these linear algorithms with the data-dependent ones using the same function, z, Eq. (20). We perform experiments with $N = 33^2$, Figs. 5 and 7 and $N = 65^2$, Figs. 6 and 8, using W2 and G functions, and for gridded and Halton's data points. In all the results, we can observe that the discontinuity is perfectly delineated in both the case of regular meshes and with Halton's points. Particularly striking is the result obtained for the function G, Figs. 7 and 8, where the band of diffusion around the discontinuity is reduced considerably.

Finally, some examples with $d = 1$ are shown in Figs. 9 and 10. Again, the diffusion effects decrease using DD-MLS.

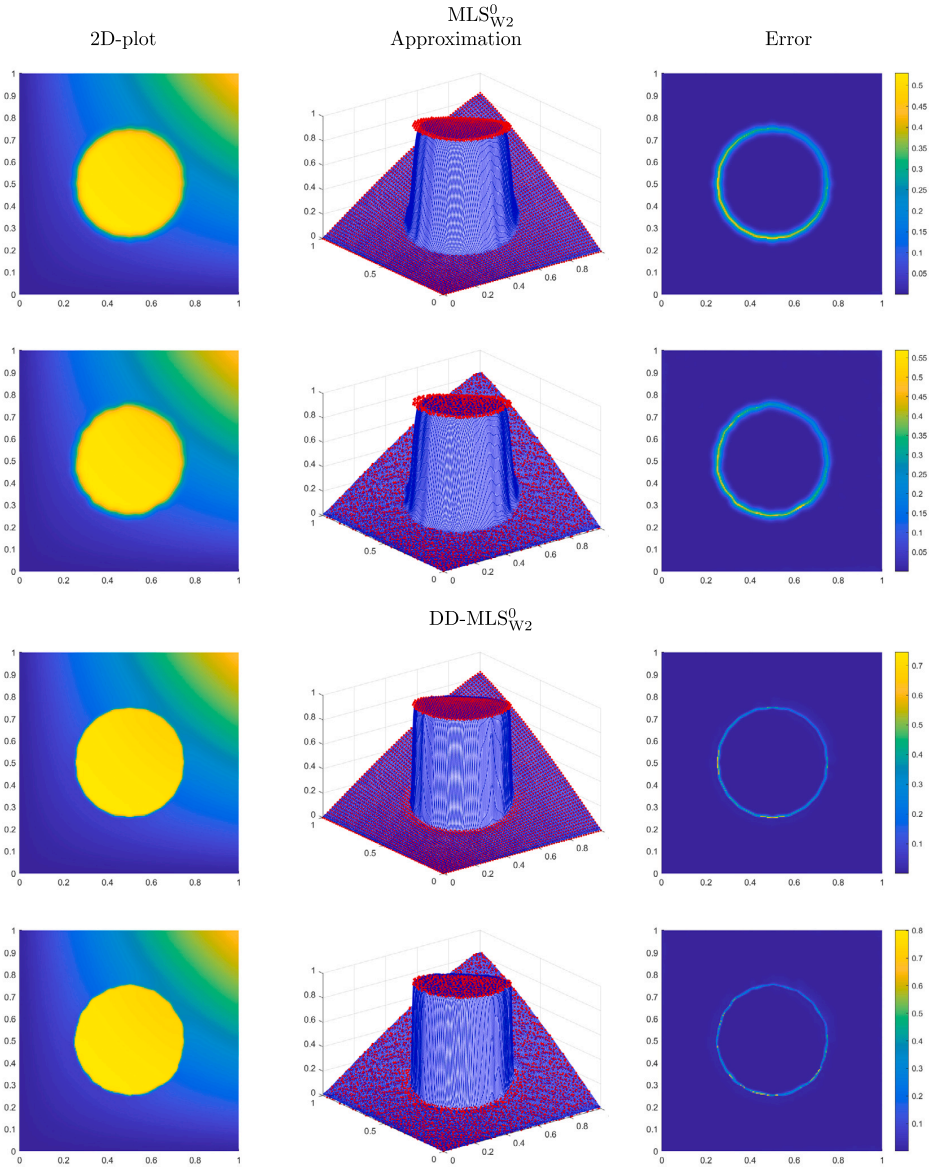

Fig. 6. Approximation to function z, Eq. (20), using W2, (linear MLS method in rows one and two, and data-depend MLS in rows three and four), $d = 0$ with $N = 65^2$. The first row and the third row correspond to uniform gridded data. The second and fourth row correspond to Halton points.

5. Conclusions and future work

In this study, we have introduced a novel approach to the moving least squares (MLS) problem (7) by replacing the traditional weight functions with new functions that assign greater weight to nodes farther from discontinuities, while still assigning smaller weights to nodes far from the point of approximation. This adjustment effectively mitigates the Gibbs phenomenon and reduces the smearing of discontinuities in the final approximation of the original data.

Our method uses smoothness indicators to accurately identify *infected* nodes, i.e. those affected by the presence of discontinuities, in a way inspired by the WENO method. This results in a data-dependent weighted least squares problem where the weights are influenced by both the distances between nodes and the point of approximation, and the distances between isolated discontinuities

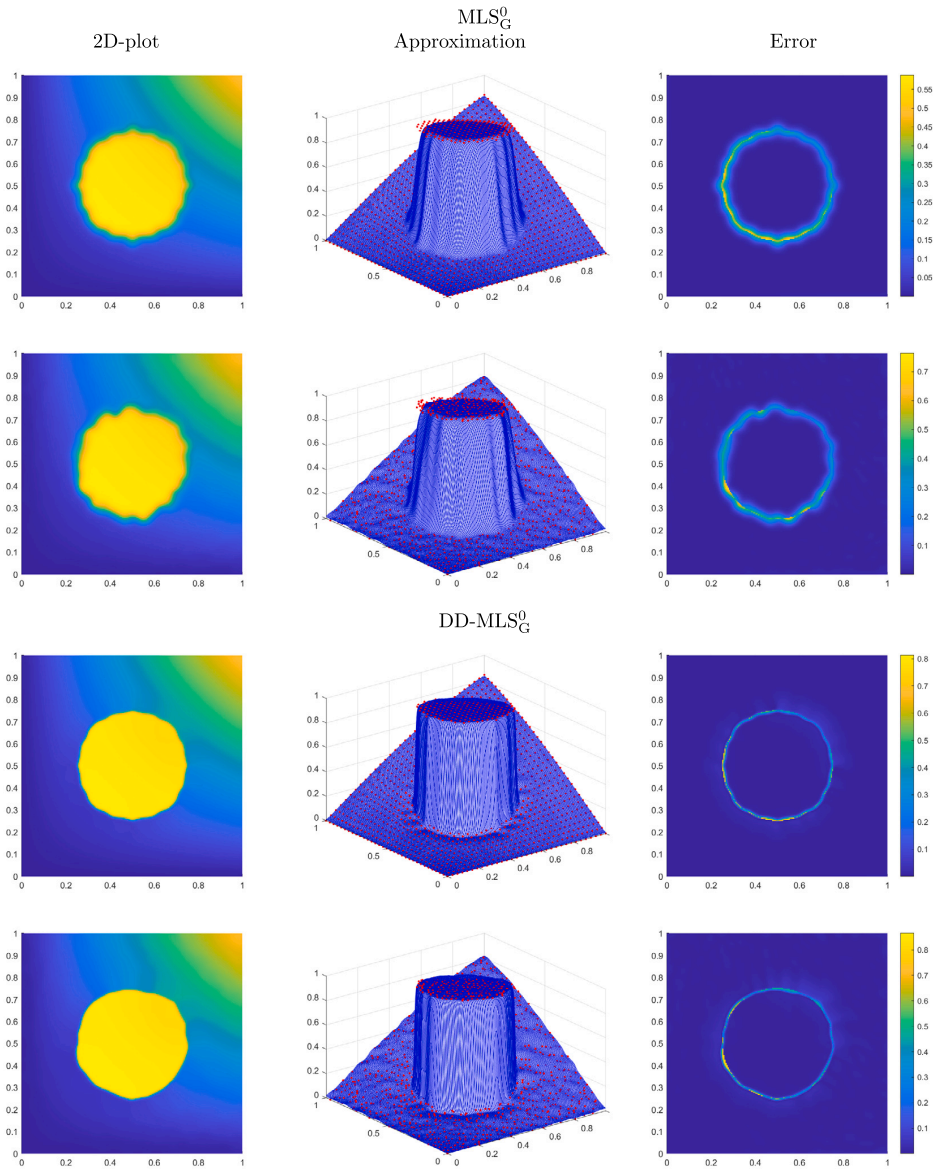

Fig. 7. Approximation to function z, Eq. (20), using G, (linear MLS method in rows one and two, and data-depend MLS in rows three and four), $d = 0$ with $N = 33^2$. The first row and the third row correspond to uniform gridded data. The second and fourth row correspond to Halton points.

and the nodes. We think these criteria could be adapted to other requirements, such as point density or monotonicity, but we leave these ideas for future explorations.

Through the design and analysis of the new data-dependent approximation, we have demonstrated its properties, including polynomial reproduction, accuracy, smoothness or mitigation of the Gibbs oscillations close to the discontinuities. Our numerical experiments validate the theoretical findings, showing the effectiveness of the proposed method.

CRediT authorship contribution statement

David Levin: Writing – review & editing, Writing – original draft, Supervision, Methodology, Investigation, Formal analysis, Data curation, Conceptualization. **José M. Ramón:** Writing – review & editing, Writing – original draft, Visualization, Validation, Su-

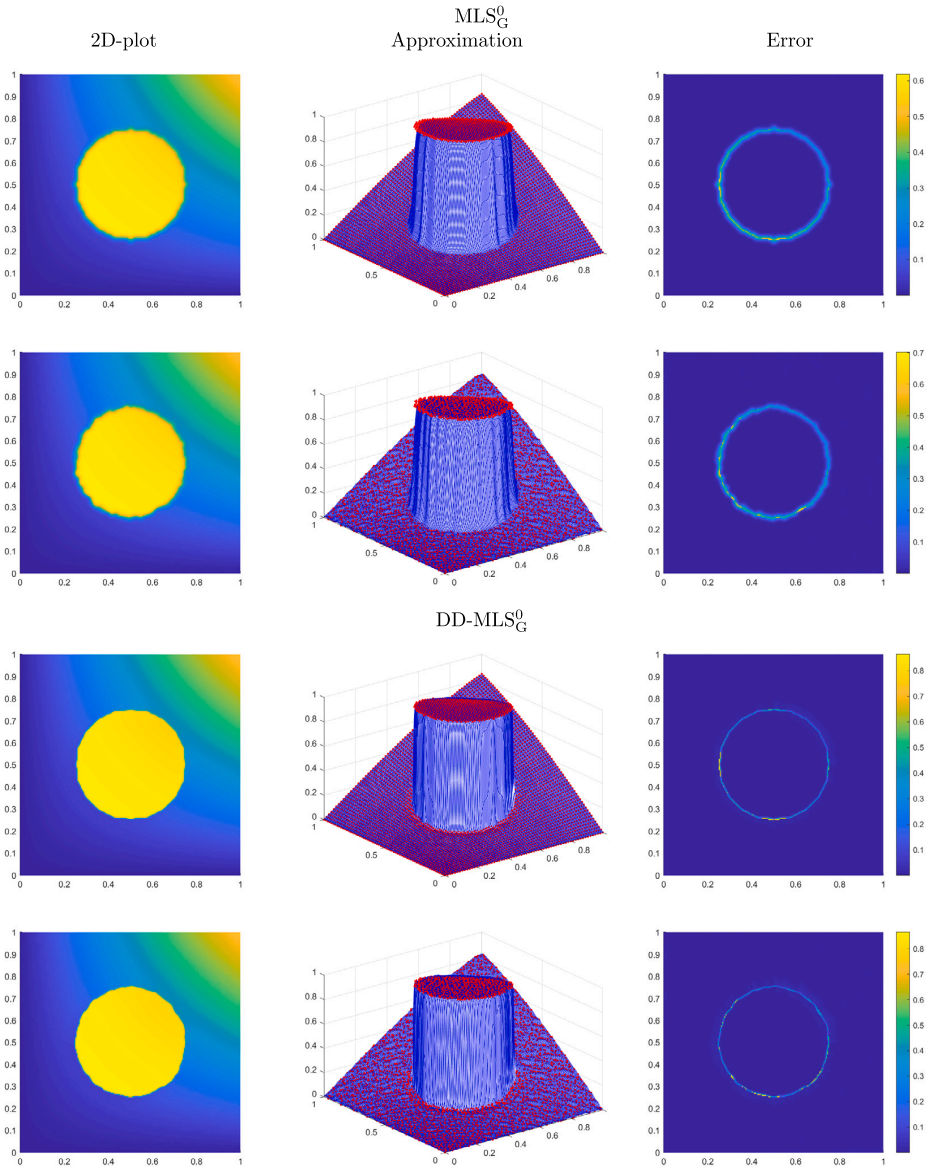

Fig. 8. Approximation to function z, Eq. (20), using G (linear MLS method in rows one and two, and data-depend MLS in rows three and four), $d = 0$ with $N = 65^2$. The first row and the third row correspond to uniform gridded data. The second and fourth row correspond to Halton points.

pervision, Software, Resources, Methodology, Investigation, Formal analysis, Data curation, Conceptualization. **Juan Ruiz-Álvarez:** Writing – review & editing, Writing – original draft, Visualization, Validation, Supervision, Software, Resources, Methodology, Investigation, Formal analysis, Data curation, Conceptualization. **Dionisio F. Yáñez:** Writing – review & editing, Writing – original draft, Visualization, Validation, Supervision, Software, Resources, Project administration, Methodology, Investigation, Funding acquisition, Formal analysis, Data curation, Conceptualization.

References

[1] S. Amat, D. Levin, J. Ruiz, D.F. Yáñez, Non-linear WENO B-spline based approximation method, Numer. Algorithms (2024).
[2] A. Amir, D. Levin, Reconstructing piecewise smooth bivariate functions from scattered data, Jaen J. Approx. 12 (2021) 155–173.

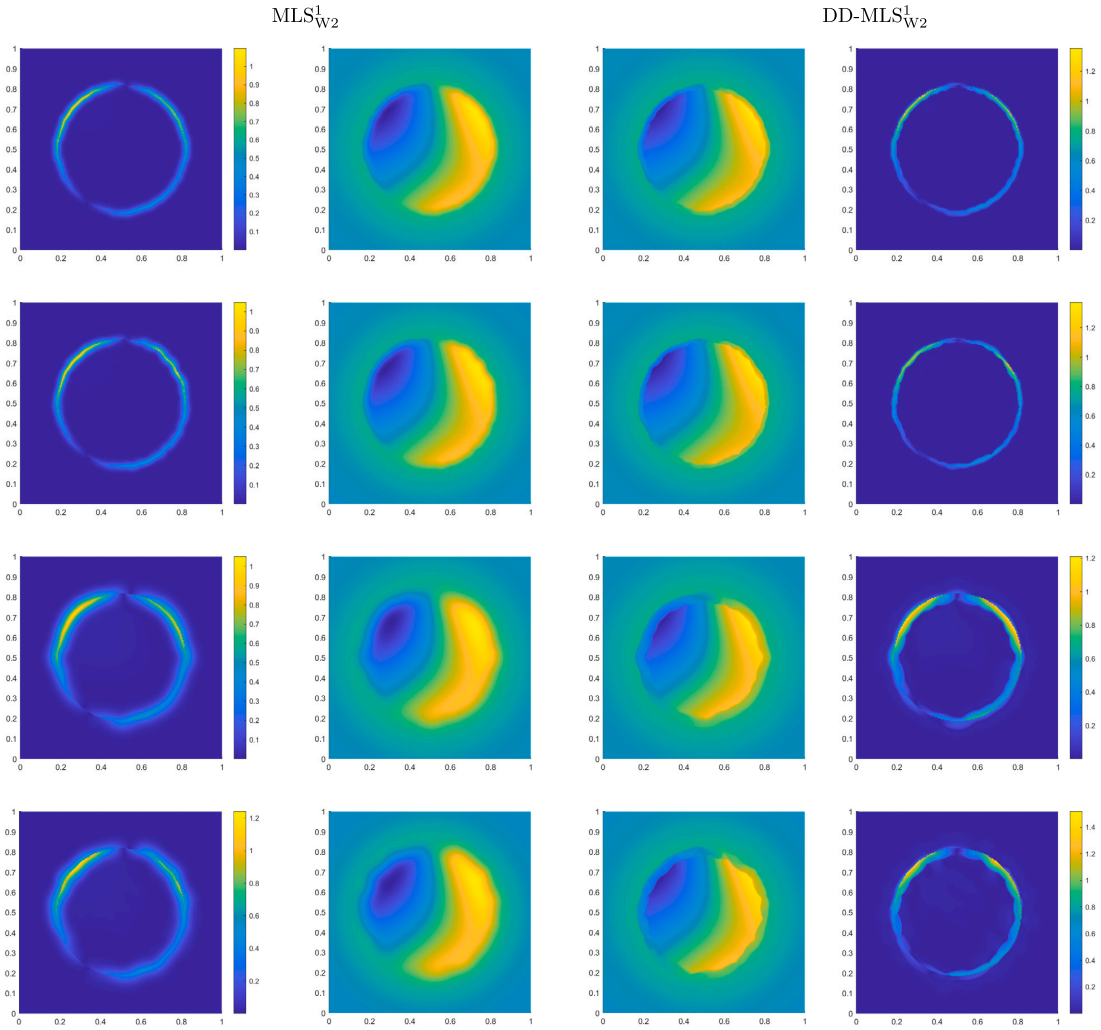

Fig. 9. Approximation to function f, Eq. (19), and errors in a 2-D plot using regular grid data points with $N = 65^2$ (first and second row) and $N = 33^2$ (third and fourth row). The first and fourth columns present the absolute error distribution and the second and third columns represent the approximation from a cenital view.

[3] F. Aràndiga, A.M. Belda, P. Mulet, Point-value WENO multiresolution applications to stable image compression, J. Sci. Comput. 43 (2) (2010) 158–182.
[4] G. Backus, F. Gilbert, Numerical applications of a formalism for geophysical inverse problems, Geophys. J. R. Astron. Soc. 13 (1967) 247–276.
[5] G. Backus, F. Gilbert, The resolving power of gross Earth data, Geophys. J. R. Astron. Soc. 16 (1968) 169–205.
[6] L. Bos, K. Salkauskas, Moving least-squares are Backus-Gilbert optimal, J. Approx. Theory 59 (1989) 267–275.
[7] R. Cavoretto, A. De Rossi, E. Perracchione, S. Lancellotti, Software implementation of the partition of unity method, Dolomites Res. Not. Approx. 15 (2) (2022) 35–46.
[8] M.K. Esfahani, S. De Marchi, F. Marchetti, Moving least squares approximation using variably scaled discontinuous weight function, arXiv preprint, arXiv: 2302.02707, 2023.
[9] G.E. Fasshauer, Meshfree Approximation Methods with Matlab, World Scientific Publishing, Singapore, 2007.
[10] J.H. Halton, On the efficiency of certain quasi-random sequences of points in evaluating multi-dimensional integrals, Numer. Math. 2 (1960) 84–90.
[11] G. Jiang, C.-W. Shu, Efficient implementation of weighted ENO schemes, J. Comput. Phys. 126 (1) (1996) 202–228.
[12] P. Lancaster, K. Salkauskas, Surfaces generated by moving least squares methods, Math. Comput. 37 (155) (1981) 141–158.
[13] Y.J. Lee, G. Wolberg, S.Y. Shin, Image morphing using moving least squares, in: Proceedings of the 24th Annual Conference on Computer Graphics and Interactive Techniques, ACM Press/Addison-Wesley Publishing Co., 1997, pp. 21–28.
[14] D. Levin, The approximation power of moving least-squares, Math. Comput. 67 (1998) 224.
[15] S. López-Ureña, D.F. Yáñez, Subdivision schemes based on weighted local polynomial regression. A new technique for the convergence analysis, J. Sci. Comput. 100 (10) (2024).
[16] X.-D. Liu, S. Osher, T. Chan, Weighted essentially non-oscillatory schemes, J. Comput. Phys. 115 (1994) 200–212.
[17] C. Loader, Local Regression and Likelihook, Springer, New York, 1999.

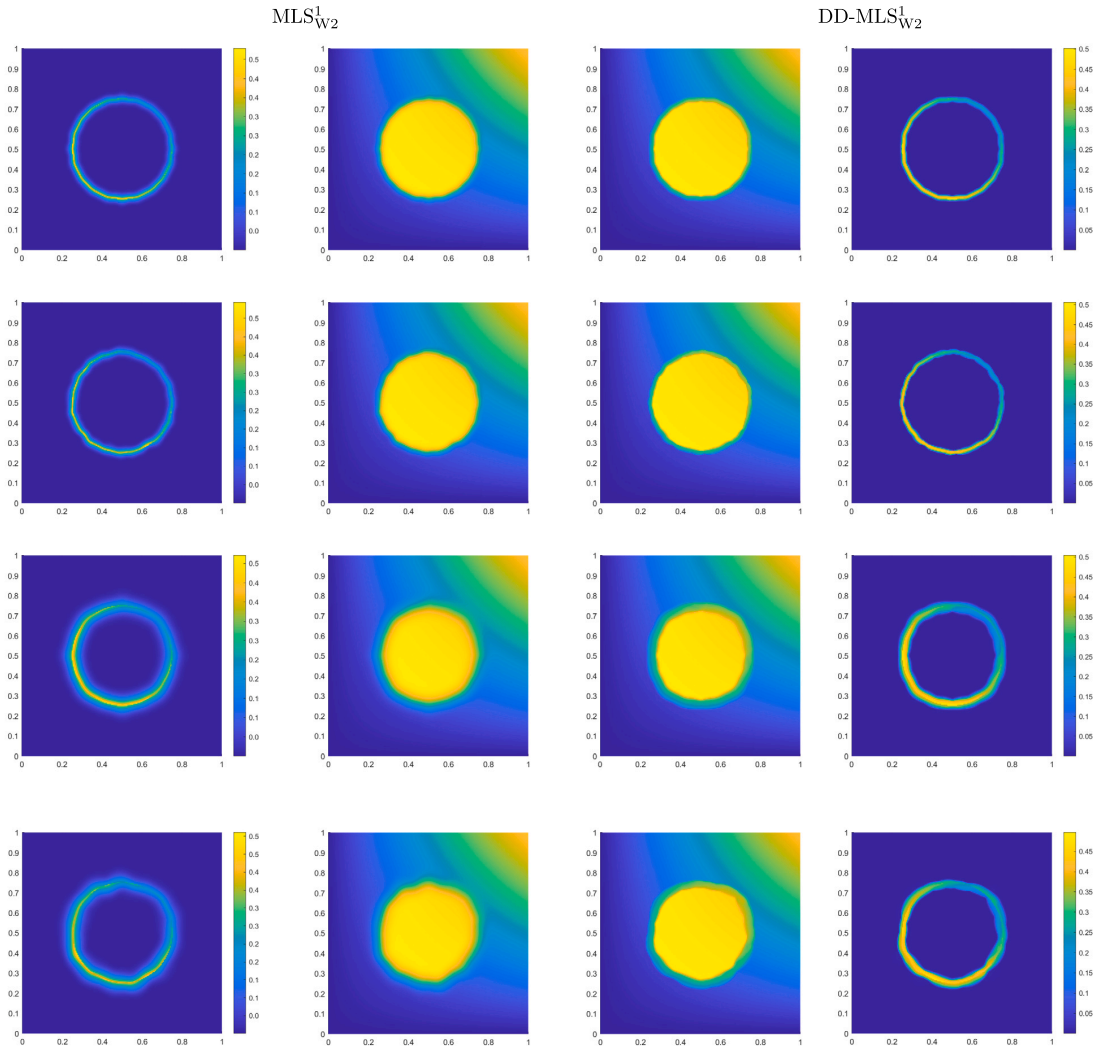

Fig. 10. Approximation to function z, Eq. (20), and errors in a 2-D plot using regular grid data points with $N = 65^2$ (first and second row) and $N = 33^2$ (third and fourth row). The first and fourth columns present the absolute error distribution and the second and third columns represent the approximation from a cenital view.

[18] A. Harten, B. Engquist, S. Osher, S.R. Chakravarthy, Uniformly high order accurate essentially non-oscillatory schemes, III, J. Comput. Phys. 71 (2) (1987) 231–303.
[19] F. Dell'Accio, F. Di Tommaso, N. Siar, On the numerical computation of bivariate Lagrange polynomials, Appl. Math. Lett. 112 (2021) 106885.
[20] S. De Marchi, G. Elefante, F. Marchetti, Stable discontinuous mapped bases: the Gibbs-Runge-Avoiding Stable Polynomial Approximation (GRASPA) method, Comput. Appl. Math. 40 (8) (2021) 299.
[21] S. De Marchi, Mapped Polynomials and Discontinuous Kernels for Runge and Gibbs Phenomena, SEMA SIMAI Springer Series, vol. 29, 2022, pp. 3–43.
[22] D. Shepard, A two-dimensional interpolation function for irregularly-spaced data, in: Proceedings of the 1968 23rd ACM National Conference, 1968, pp. 517–524.
[23] C.-W. Shu, High order weighted essentially nonoscillatory schemes for convection dominated problems, SIAM Rev. 51 (1) (1999) 82–126.
[24] W.Y. Tey, N.A.C. Sidik, Y. Asako, M.W. Muhieldeen, O. Afshar, Moving least squares method and its improvement: a concise review, J. Appl. Comput. Mech. 7 (2) (2021) 883–889, Shahid Chamran University of Ahvaz.
[25] H. Wendland, Scattered Data Approximation, Cambridge University Press, 2004.
[26] H. Wendland, Fast evaluation of radial basis functions: methods based on partition of unity, in: C.K. Chui, L.L. Schumaker, J. Stöcker (Eds.), Approximation Theory X: Wavelets, Splines and Applications, Vanderbilt University Press, 2002.

Journal of Computational and Applied Mathematics 473 (2026) 116891

Contents lists available at ScienceDirect

Journal of Computational and Applied Mathematics

journal homepage: www.elsevier.com/locate/cam

Non-linear Partition of Unity method ☆

José M. Ramón [a], Juan Ruiz-Álvarez [b], Dionisio F. Yáñez [a,*]

[a] Departamento de Matemáticas. Universidad de Valencia, Valencia, Spain
[b] Departamento de Matemática Aplicada y Estadística. Universidad Politécnica de Cartagena, Cartagena, Spain

ARTICLE INFO

Keywords:
WENO
High accuracy approximation
Improved adaption to discontinuities
RBF
41A05
41A10
65D05
65M06
65N06

ABSTRACT

This paper introduces the Non-linear Partition of Unity Method (NL-PUM), a novel technique integrating Radial Basis Function interpolation and Weighted Essentially Non-Oscillatory algorithms. As far as we know, this is the first time that a non-linear PUM method is introduced in the literature. The main advance of this proposal is providing an algorithm that keeps the properties of the PUM at smooth zones, while introducing a non-linear modification close to the discontinuities to avoid oscillations. This is done automatically computing estimations of the smoothness of the data and replacing the PUM by Sheppard method when all the data is affected by a discontinuity. Thus, the computation of smoothness indicators and the use of compactly supported base functions ensure precision in regions affected by the presence of discontinuities. Error bounds are calculated and validate the effectiveness of the new method, showing improved interpolation capabilities at discontinuity regions as well as at smooth zones. A battery of experiments is presented to check the theoretical results provided.

1. Introduction

Kernel-based methods are useful and powerful tools employed in several fields of science, such as computer-aided geometric design, the numerical solution of partial differential equations, image processing, and others. These schemes are satisfactorily used in interpolation, regression, and machine learning due to their easy and quick implementation and their simple generalization for any dimension.

The problem consists in finding a good approximation to an unknown function, $f : \mathbb{R}^n \to \mathbb{R}$, from some data values $F = \{f_i = f(\mathbf{x}_i),\ i = 1, \dots, N\}$ given a set of arbitrarily distributed points on an open and bounded domain $\Omega \subset \mathbb{R}^n$, $X = \{\mathbf{x}_i \in \Omega,\ i = 1, \dots, N\}$. The Radial Basis Function (RBF) method consists of developing the function as a linear combination of a basis of radial functions centered at the data points X. There exists a vast literature about it (see, e.g., [1–3]), however, the efficiency of the method can be improved in different ways. One approximation, called the *partition of unity method* (PUM or PU method) (see e.g., [1–5]), involves partitioning the entire domain into multiple smaller subdomains and applying the RBF method to each of them. Ultimately, a convex combination of these interpolants yields the final approximation. Satisfactory results are obtained when these methods are employed to data originating from continuous functions. For example, see the approximation presented in Fig. 1(a) where we approximate Franke's function:

$$\begin{aligned} f(x,y) = &\frac{3}{4}e^{-1/4((9x-2)^2+(9y-2)^2)} + \frac{3}{4}e^{-1/49(9x+1)^2-1/10(9y+1)} \\ &+ \frac{1}{2}e^{-1/4((9x-7)^2+(9y-3)^2)} - \frac{1}{5}e^{-(9x-4)^2-(9y-7)^2}, \end{aligned} \tag{1}$$

☆ Dionisio F. Yáñez has been supported through project CIAICO/2021/227, Spain (Proyecto financiado por la Conselleria de Innovación, Universidades, Ciencia y Sociedad digital de la Generalitat Valenciana), by grant PID2020-117211GB-I00 and by PID2023-146836NB-I00 funded by MCIN/AEI/10.13039/501100011033, Spain.

* Corresponding author.
E-mail addresses: Jose.Manuel.Ramon@uv.es (J.M. Ramón), juan.ruiz@upct.es (J. Ruiz-Álvarez), Dionisio.Yanez@uv.es (D.F. Yáñez).

https://doi.org/10.1016/j.cam.2025.116891
Received 16 January 2025; Received in revised form 23 April 2025
Available online 4 July 2025

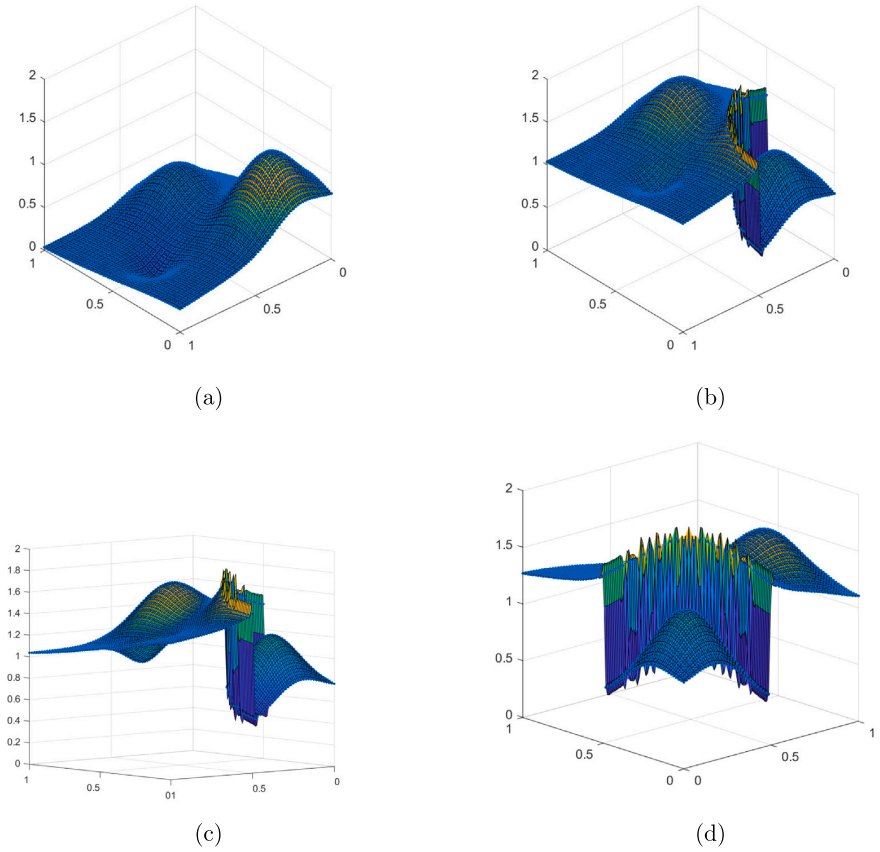

Fig. 1. (a) Approximation to Franke's function using PUM, (b), (c), (d) Approximation to function f_1, Eq. (2) using PUM.

using the PU method with data points located at $X = \{(i/64, j/64) : i, j = 0, \dots, 64\}$. However, these methods yield inadequate results when the data originates from functions with discontinuities. See for example Fig. 1(b), (c) and (d), where we present the result obtained when applying the PUM to the piecewise smooth function:

$$f_1(x, y) = \begin{cases} 1 + f(x, y), & x^2 + y^2 - 0.5^2 \geq 0, \\ f(x, y), & x^2 + y^2 - 0.5^2 < 0. \end{cases} \tag{2}$$

It is clear that we can observe some oscillations close to the discontinuities. These problems can also be found in more advanced implementations of the PUM method, for example the one presented in [6]. In order to avoid these undesirable effects, constructions inspired by those presented in [7,8] can be applied to approximate this kind of data. Thus, our aim in this work is to reformulate the classical PUM to make the weight functions used depend on the smoothness of the data. The objective is to mitigate oscillations and smearing around discontinuities. To reach this objective, the basic idea is to modify the weights of the partition of unity by replacing them with non-linear ones that depend on the data F. This way, when a discontinuity crosses a subdomain, the approximation is not considered. It is not difficult to prove that the order of accuracy is conserved in the entire domain, except in a band close to the discontinuity. As mentioned in the abstract, as far as we know, this is the first time that such a non-linear PUM method is presented.

The paper is divided in the following sections: In Section 2, we start by reviewing the RBF interpolation and showing some theorems where the error bounds are estimated, Section 3 is devoted to introduce the PUM and to prove the theoretical results related to the order of accuracy. Afterwards, in Section 4, we review WENO method from the PUM perspective, identifying each component of WENO with its corresponding component in PUM. The non-linear method is presented in Section 5, where we explain its theoretical properties and its implementation. Some numerical results are presented in Section 6, and some conclusions and future work are outlined in the last section.

2. Radial basis function interpolation

There is extensive literature on the RBF interpolation method (see e.g. [1–3]), we will principally employ the notation presented in [2,9]. We consider a set of scattered data $X = \{\mathbf{x}_i\}_{i=1}^N$ in a bounded domain $\Omega \subset \mathbb{R}^n$, with an associated set of data values $F = \{f_i := f(\mathbf{x}_i)\}_{i=1}^N$ which are the evaluations of certain unknown function $f : \Omega \to \mathbb{R}$ at the nodes $\mathbf{x}_i$. The scattered data interpolation problem is the following: to find an operator, $\mathcal{I}(f) : \Omega \to \mathbb{R}$, such that:

$$\mathcal{I}(f)(\mathbf{x}_i) = f(\mathbf{x}_i), \quad i = 1, \dots, N.$$

Ideally, we aim to minimize the distance between $\mathcal{I}(f)$ and f in a specified norm. First, we define a radial function $\boldsymbol{\Phi} : \Omega \to \mathbb{R}$ when there exists a univariate function $\phi : [0, \infty[\to \mathbb{R}$ such that

$$\boldsymbol{\Phi}(\mathbf{x}) = \phi(\|\mathbf{x}\|_2), \quad \forall\, \mathbf{x} \in \Omega,$$

with $\|\cdot\|_2$ the Euclidian norm in $\mathbb{R}^n$. Now, we denote as $\boldsymbol{\Phi}_i(\mathbf{x}) = \phi(\|\mathbf{x} - \mathbf{x}_i\|_2)$, $i = 1, \dots, N$ and use a radial basis function expansion to formulate the problem:

$$\mathcal{I}(f)(\mathbf{x}) = \sum_{i=1}^N c_i \boldsymbol{\Phi}_i(\mathbf{x}) = \sum_{i=1}^N c_i \phi(\|\mathbf{x} - \mathbf{x}_i\|_2), \quad \mathbf{x} \in \Omega, \tag{3}$$

being c_i the coefficients that solve the interpolation system $A\mathbf{c} = \mathbf{f}$ with

$$A = \begin{bmatrix} \phi(\|\mathbf{x}_1 - \mathbf{x}_1\|_2) & \phi(\|\mathbf{x}_1 - \mathbf{x}_2\|_2) & \cdots & \phi(\|\mathbf{x}_1 - \mathbf{x}_N\|_2) \\ \phi(\|\mathbf{x}_2 - \mathbf{x}_1\|_2) & \phi(\|\mathbf{x}_2 - \mathbf{x}_2\|_2) & \cdots & \phi(\|\mathbf{x}_2 - \mathbf{x}_N\|_2) \\ \vdots & \vdots & \ddots & \vdots \\ \phi(\|\mathbf{x}_N - \mathbf{x}_1\|_2) & \phi(\|\mathbf{x}_N - \mathbf{x}_2\|_2) & \cdots & \phi(\|\mathbf{x}_N - \mathbf{x}_N\|_2) \end{bmatrix}, \ \mathbf{c} = \begin{bmatrix} c_1 \\ c_2 \\ \vdots \\ c_N \end{bmatrix}, \ \mathbf{f} = \begin{bmatrix} f_1 \\ f_2 \\ \vdots \\ f_N \end{bmatrix}.$$

It is clear that A is symmetric, and certain conditions on ϕ must be imposed to ensure that the matrix A is positive definite, thereby guaranteeing a unique solution to the system. The following definition is useful for this purpose (see [2]).

Definition 1. [2] A real continuous function $\boldsymbol{\Phi} : \mathbb{R}^n \to \mathbb{R}$ is called positive definite on $\mathbb{R}^n$ if

$$\sum_{j=1}^N \sum_{i=1}^N c_j c_i \boldsymbol{\Phi}_i(\mathbf{x}_j) \geq 0 \tag{4}$$

for any N pairwise different points $\{x_i\}_{i=1}^N \subset \mathbb{R}^n$ and $\mathbf{c} = [c_1, \dots, c_N] \in \mathbb{R}^N$. It is strictly positive definite on $\mathbb{R}^n$ if the form (4) is zero only for $\mathbf{c} = \mathbf{0}$.

In the literature we can find many examples of functions ϕ which produce strictly positive definite functions, such as the Gaussian function $\phi_G(\|\mathbf{x}\|_2) = e^{-\|\mathbf{x}\|_2^2}$, that is also C^∞. Another example are Wendland functions, defined as

$$\begin{aligned} \phi_{W_0}(\|\mathbf{x}\|_2) &= (1 - \|\mathbf{x}\|_2)_+^2, \\ \phi_{W_2}(\|\mathbf{x}\|_2) &= (1 - \|\mathbf{x}\|_2)_+^4 (4\|\mathbf{x}\|_2 + 1), \\ \phi_{W_4}(\|\mathbf{x}\|_2) &= (1 - \|\mathbf{x}\|_2)_+^6 (35\|\mathbf{x}\|_2^2 + 18\|\mathbf{x}\|_2 + 3), \end{aligned} \tag{5}$$

based on the cutoff function

$$(x)_+ = \begin{cases} x & \text{for } x \geq 0, \\ 0 & \text{for } x < 0, \end{cases}$$

which are C^0, C^2 and C^4 respectively. Matérn functions are another example, that are defined as

$$\begin{aligned} \phi_{M_0}(\|\mathbf{x}\|_2) &= e^{-\|\mathbf{x}\|_2}, \\ \phi_{M_2}(\|\mathbf{x}\|_2) &= (1 + \|\mathbf{x}\|_2) e^{-\|\mathbf{x}\|_2}, \\ \phi_{M_4}(\|\mathbf{x}\|_2) &= \left(3 + 3\|\mathbf{x}\|_2 + \|\mathbf{x}\|_2^2\right) e^{-\|\mathbf{x}\|_2}, \end{aligned} \tag{6}$$

satisfying that $\phi_{M_k} \in C^k$, $k = 0, 2, 4$. Other classes of functions, such as generalized inverse multiquadrics or Poisson radial functions, also produce strictly positive definite functions, see [2] for more details.

The first characteristic of this interpolant, Eq. (3), is the smoothness, as it is a linear combination of smooth functions, $\boldsymbol{\Phi}_i$. Consequently, the continuity of the operator only depends on the continuity of the function $\phi(\|\cdot\|_2)$. Secondly, the error estimates and the order of accuracy for the interpolation process have been studied extensively (see [1–3] and the references cited therein for further details). To introduce the results, we need to present three relevant concepts: First of all, we define the fill distance, which measures the extent to which the data in the set X adequately cover the domain Ω, as

$$h = h_{X,\Omega} = \sup_{\mathbf{x} \in \Omega} \min_{\mathbf{x}_j \in X} \|\mathbf{x} - \mathbf{x}_j\|_2.$$

Following this, we refer to the space (see [2,5])

$$C_\nu^{2k}(\mathbb{R}^n) = \{f \in C^{2k} : D^{\boldsymbol{\beta}} f(\mathbf{x}) = O(\|\mathbf{x}\|_2^\nu), \text{ as } \|\mathbf{x}\|_2 \to 0 \text{ if } |\boldsymbol{\beta}| = 2k\},$$

and finally, we state that a region $\Omega \subseteq \mathbb{R}^n$ satisfies **an interior cone condition**, [2,3], if there exists an angle $\theta \in (0, \pi/2)$ and a radius $r > 0$ such that for every $\mathbf{x} \in \Omega$ there exists a unit vector $\boldsymbol{\xi}(\mathbf{x})$ such that the cone

$$C = \{\mathbf{x} + \lambda \mathbf{y} : \mathbf{y} \in \mathbb{R}^n,\ \|\mathbf{y}\|_2 = 1,\ \mathbf{y}^T \boldsymbol{\xi}(\mathbf{x}) \geq \cos\theta,\ \lambda \in [0, r]\}$$

is contained in Ω. The following lemma presented by Wendland in [3] indicates that a ball always satisfies an interior cone condition. This result will be relevant in our numerical experiments when we construct a particular partition of unity method.

Lemma 2.1. *Every ball with radius $\delta > 0$ satisfies an interior cone condition with radius $\delta > 0$ and angle $\theta = \pi/3$.*

With these three elements: the fill distance, the space $C_\nu^{2k}(\mathbb{R}^n)$ and the interior cone condition, we review the following result.

Theorem 2.2. *[2] Suppose $\Omega \subset \mathbb{R}^n$ is bounded and satisfies an interior cone condition. Suppose $\Phi \in C_\nu^{2k}(\mathbb{R}^n)$ strictly positive definite. Then, the error between $f \in \mathcal{N}_\Phi(\Omega) := span\{\Phi(\cdot - \mathbf{x}), \mathbf{x} \in \Omega\}$ and its interpolant $\mathcal{I}(f)$ defined in Eq. (3) can be bounded by*

$$|f(\mathbf{x}) - \mathcal{I}(f)(\mathbf{x})| \leq C h^{k+\frac{\nu}{2}} \|f\|_{\mathcal{N}_\Phi(\Omega)}$$

for all $\mathbf{x} \in \Omega$, h is sufficiently small and where C is a constant independent of $\mathbf{x}$, f and Φ.

In this work, we focus on studying the differences between the function and the interpolator. Error estimates for the derivatives are proved in [2,3]. To conclude this review section, we introduce the following results for Matérn function, Eq. (6), as they will be used in the numerical experiments. For this purpose, we need to define the Sobolev spaces $W_2^m(\mathbb{R}^n)$ introduced in [2] as

$$W_2^m(\Omega) = \{f \in L_2(\Omega) \cap C(\Omega) : D^\beta f \in L_2(\Omega) \ \text{ for all } \ |\beta| \leq m,\ \beta \in \mathbb{N}^n\}.$$

Proposition 2.3. *[2] For the strictly positive Matérn functions ϕ_{M_k}, $k = 0, 2, 4$, Eq. (6), and $\Omega \subseteq \mathbb{R}^2$ is satisfied that*

$$|f(\mathbf{x}) - \mathcal{I}_{M_k}(f)(\mathbf{x})| \leq C h^{\frac{k+1}{2}} \|f\|_{W_2^{(k+3)/2}(\Omega)}$$

for all $\mathbf{x} \in \Omega$, h is sufficiently small, and $f \in W_2^{(k+3)/2}(\Omega)$.

Next subsection is devoted to introduce the partition of unity method for radial basis functions, which is a well-known approximation method that is satisfactorily used when the number of data points is very large.

3. Partition of unity approximation

The partition of unity method (PUM) is proposed to facilitate efficient computation using meshfree approximation methods. The approach is straightforward: it involves decomposing the large problem into smaller subproblems while preserving the order of accuracy. Accordingly, using the same notation as above, let $\Omega \subset \mathbb{R}^n$ represent our open and bounded domain, which we partition into M subdomains Ω_j such that [5,10]:

- The domain is contained in the union of the subdomains, i.e.
$$\Omega \subseteq \bigcup_{j=1}^{M} \Omega_j.$$
- For every $\mathbf{x} \in \Omega$ the number of subdomains Ω_j with $\mathbf{x} \in \Omega_j$ is bounded by a global constant K.
- There exists a constant $C_r > 0$ and an angle $\theta \in (0, \pi/2)$ such that every patch $\Omega_j \cap \Omega$ satisfies an interior cone condition with angle θ and radius $r = C_r h_{X,\Omega}$.
- The local fill distance h_{X_j,Ω_j} with $X_j = \Omega_j \cup X$ is uniformly bounded by the global fill distance $h_{X,\Omega}$.

This is called a regular covering for (Ω, X), [3]. For this covering, we choose a partition of unity, i.e. a family of compactly supported, non-negative, continuous functions, $w_j : \Omega_j \to \mathbb{R}$ with

$$\sum_{j=1}^{M} w_j(\mathbf{x}) = 1 \ \forall\ \mathbf{x} \in \Omega, \quad \text{supp}(w_j) \subseteq \Omega_j,$$

and define the global interpolator as:

$$\mathcal{I}_{\text{PUM}}(f)(\mathbf{x}) = \sum_{j=1}^{M} w_j(\mathbf{x}) \mathcal{I}_j(f)(\mathbf{x}), \tag{7}$$

where $\mathcal{I}_j(f) : \Omega_j \to \mathbb{R}$ is a local RBF interpolant on each subdomain Ω_j.

In [2] some technical conditions over the partition of unity functions are imposed to establish error bounds. We assume that the partition of unity functions is k-stable. This is, each $w_j \in C^k(\mathbb{R}^n)$ and for every multi-index $\boldsymbol{\alpha}$ with $|\boldsymbol{\alpha}| \leq k$ the following inequality is satisfied:

$$\|D^{\boldsymbol{\alpha}} w_j\|_{\infty,\Omega_j} \leq \frac{C_{\boldsymbol{\alpha}}}{\delta_j^{|\boldsymbol{\alpha}|}},$$

where $C_{\boldsymbol{\alpha}}$ is some positive constant and δ_j is the diameter of Ω_j, i.e. $\delta_j = \sup_{\mathbf{x},\mathbf{y}\in\Omega_j} \|\mathbf{x}-\mathbf{y}\|_2$. With these restrictions over the covering and the partition of unity function, we show the following result, [2].

Theorem 3.1. *Suppose $\Omega \subseteq \mathbb{R}^n$ is open and bounded, and let $X = \{\mathbf{x}_i\}_{i=1}^N \subseteq \Omega$. Let $\Phi \in C_v^{2k}(\mathbb{R}^n)$ be strictly positive definite. Let $\{\Omega_j\}_{j=1}^M$ be a regular covering for (Ω, X) and let $\{w_j\}_{j=1}^M$ be k-stable for $\{\Omega_j\}_{j=1}^M$. Then the error between $f \in \mathcal{N}_\Phi(\Omega)$ and its partition of unity interpolant, Eq. (7), can be bounded by*

$$|f(\mathbf{x}) - \mathcal{I}_{PUM}(f)(\mathbf{x})| \leq Ch^{k+\frac{\nu}{2}} \|f\|_{\mathcal{N}_\Phi(\Omega)},$$

for all $\mathbf{x} \in \Omega$.

It is clear that the order of accuracy does not vary using PUM or RBF method, as we can see in Theorems 2.2 and 3.1. A simple way, suggested in [2,5], to construct PUM is to consider Shepard's approximation, i.e.

$$w_j(\mathbf{x}) = \frac{\varphi_j(\mathbf{x})}{\sum_{k=1}^M \varphi_k(\mathbf{x})}, \quad j = 1, \dots, M, \tag{8}$$

where φ_j are compactly supported, with their support contained in Ω_j, and can be chosen, for example, as Wendland functions, Eq. (5).

4. Reviewing weighted essentially non-oscillatory algorithm as a PUM

The WENO scheme has gained widespread recognition as an effective method for approximating data values, especially in contexts where discontinuities are prevalent (see e.g. [8]). Initially introduced for approximating the solution of hyperbolic partial differential equations, the WENO approach is structured to achieve high-order accuracy while mitigating the unwanted oscillations that typically occur near discontinuities [11]. This is accomplished through the adaptive assignment of weights that prioritize smoother portions of the data and diminish the contribution of stencils that intersect discontinuities.

In what follows, we review the WENO-2r method in the point-values context (see [12,13]) relating each of its components to those corresponding to the PUM. The analogy is done for the algorithms in one variable, but it can be generalized to several variables [14]. In this case, let $\{x_i\}_{i=0}^J$ be a uniform partition of the interval $[a,b]$ in J subintervals, $x_i = a + i \cdot h$, $\quad h = \frac{b-a}{J}$, and let $\{f_i\}_{i=0}^J$ be the point-values discretization of an unknown function f at the nodes x_i, to interpolate at $x \in (x_{i-1}, x_i)$. WENO-2r algorithm uses the stencil $X = \{x_{i-r}, \dots, x_{i+r-1}\}$, that is composed of $N = 2r$ nodes, we denote it by $\tilde{I}(f)$. We can divide the stencil X in r substencils of $r+1$ nodes, $S_j = \{x_{i-r+j}, \dots, x_{i+j}\}$, $j = 0, \dots, r-1$ and prove that there exist $\tilde{w}_j : [x_{i-1}, x_i] \to \mathbb{R}$, $j = 0, \dots, r-1$, [14], called optimal weights, such that:

$$\tilde{I}(f)(x) = \sum_{j=0}^{r-1} \tilde{w}_j(x) \tilde{I}_j(f)(x),$$

with $\tilde{w}_j(x) > 0$ and $\sum_{j=0}^{r-1} \tilde{w}_j(x) = 1$. This is a PU-like method, with $\Omega_j = [x_{i-r+j}, x_{i+j}]$ and $\tilde{I}_j(f)$ the Lagrange interpolatory polynomial using the nodes S_j. Now, the WENO method consists in replacing $\tilde{w}_j(x)$ by non-linear weights $\tilde{\mathcal{W}}_j(x)$, such that

$$\mathcal{I}_{\text{WENO}}(f)(x) = \sum_{j=0}^{r-1} \tilde{\mathcal{W}}_j(x) \tilde{I}_j(f)(x), \tag{9}$$

where the non-linear weights are defined as:

$$\tilde{\mathcal{W}}_j(x) = \frac{\tilde{\alpha}_j(x)}{\sum_{k=0}^{r-1} \tilde{\alpha}_k(x)}, \text{ with } \tilde{\alpha}_j(x) = \frac{\tilde{w}_j(x)}{(\epsilon + \tilde{I}_j)^t}, \tag{10}$$

being $\tilde{I}_j$ smoothness indicators which indicate if a discontinuity crosses Ω_j, ϵ is a small positive parameter to avoid divisions by zero, and t is typically a constant to enhance accuracy in smooth regions. The idea is to make a non-linear version of the interpolator $\mathcal{I}_{\text{PUM}}$, Eq. (7), (NL-PUM) using the ideas of WENO method. The key is to define an adequate smoothness indicator for our framework.

5. Non-linear partition of unity method

As we mentioned in the previous section, Section 4, we construct a non-linear PUM starting with the interpolator $\mathcal{I}_{\text{PUM}}(f)$, Eq. (7):

$$\mathcal{I}_{\text{PUM}}(f)(\mathbf{x}) = \sum_{j=1}^M w_j(\mathbf{x}) \mathcal{I}_j(f)(\mathbf{x}),$$

replacing the weight functions w_j described in Eq. (8) by non-linear ones in the same way as in Eq. (10), i.e.

$$\mathcal{W}_j(\mathbf{x}) = \frac{\alpha_j(\mathbf{x})}{\sum_{k=1}^{M} \alpha_k(\mathbf{x})}, \text{ with } \alpha_j(\mathbf{x}) = \gamma_j \varphi_j(\mathbf{x}) = \frac{\varphi_j(\mathbf{x})}{(\epsilon + I_j)^t},$$

where $0 < \gamma_j = (\epsilon + I_j)^{-t}$ is a positive constant, and φ_j are compactly supported functions with support on Ω_j. Note that the new functions α_j are compactly supported and, if we choose φ_j as Wendland functions, then α_j are Wendland functions too. The constant $\epsilon = 10^{-14}$ is set to avoid non-zero denominators. The parameter t is relevant to correctly detect the discontinuities and we choose $t = 6$. Finally, I_j, $j = 1, \dots, M$ are the smoothness indicators. To construct them, we consider

$$S_j = \Omega_j \cap X = \{\mathbf{x}_{j_i} \in \Omega_j \cap X : i = 1, \dots, N_j\},$$

with $N_j > 3$, and the linear least square problem

$$p_j = \underset{p \in \Pi_1(\mathbb{R}^2)}{\arg\min} \sum_{i=1}^{N_j} (f(\mathbf{x}_{j_i}) - p(\mathbf{x}_{j_i}))^2,$$

where $\Pi_1(\mathbb{R}^2)$ is the set of polynomials of degree less than or equal to one, and define

$$I_j = \frac{1}{N_j} \sum_{i=1}^{N_j} |f(\mathbf{x}_{j_i}) - p_j(\mathbf{x}_{j_i})|. \tag{11}$$

Then I_j satisfies the conditions:

- The order of the smoothness indicator that are free of discontinuities is h^2, i.e.

$$I_j = O(h^2) \text{ if } f \text{ is smooth in } \Omega_j. \tag{12}$$

- When a discontinuity crosses Ω_j then:

$$I_j \nrightarrow 0 \text{ as } h \to 0.$$

Therefore, the new non-linear operator will be:

$$\mathcal{I}_{\text{NL-PUM}}(f)(\mathbf{x}) = \sum_{j=1}^{M} \mathcal{W}_j(\mathbf{x}) \mathcal{I}_j(f)(\mathbf{x}). \tag{13}$$

The key to this new method is that it gives a greater weight to the data placed in smooth regions, while neglecting data located near the discontinuity, as this data is multiplied by a weight of order $O(h^{2t})$. In the next subsection we will analyze the properties of the interpolator.

5.1. Properties of the new NL-PUM

As the new interpolator, Eq. (13), is defined in the same way as PUM, multiplying the compactly supported functions by constants (that are dependent on the data $F = \{f_i\}_{i=1}^N$) then the smoothness of the new operator is similar to PUM, in the sense that its smoothness is solely determined by the smoothness of the functions $\varphi(\|\cdot\|_2)$ and $\phi(\|\cdot\|_2)$.

Secondly, we determine the order of accuracy when we apply $\mathcal{I}_{\text{NL-PUM}}(f)$ to data that comes from a function which is piecewise continuous, i.e. we suppose an open and bounded domain $\Omega \subset \mathbb{R}^n$ and consider a curve $\zeta : \mathbb{R}^n \to \mathbb{R}$, $\zeta \in C^1$ and the sets

$$\Gamma = \{\mathbf{x} \in \Omega : \zeta(\mathbf{x}) = 0\}, \quad \Omega^+ = \{\mathbf{x} \in \Omega : \zeta(\mathbf{x}) \geq 0\}, \quad \Omega^- = \Omega \setminus \Omega^+$$

that is to say that Ω is divided into two subsets, $\Omega = \Omega^+ \cup \Omega^-$. Let us assume that our data originates from a function of the type:

$$f(\mathbf{x}) = \begin{cases} f_+(\mathbf{x}), & \mathbf{x} \in \Omega_+, \\ f_-(\mathbf{x}), & \mathbf{x} \in \Omega_-, \end{cases}$$

with $f_\pm \in C^k(\overline{\Omega_\pm})$, $k \in \mathbb{N}$, but

$$\lim_{\mathbf{x} \to \mathbf{x}_0 \in \Gamma} f_-(\mathbf{x}) \neq f_+(\mathbf{x}_0),$$

then our scattered data $X = \{\mathbf{x}_i\}_{i=1}^N$ are divided in two $X_\pm = X \cap \Omega_\pm$. We select our partition $\{\Omega_j\}_{j=1}^M$ as in Section 3 and define patches that are contaminated by a discontinuity as follows.

Definition 2 (*Contaminated Patches*)**.** Using the notation presented above, $\Omega_k \in \{\Omega_j\}_{j=1}^M$ is a contaminated patch if there exist $\Omega_k \cap X_+ \neq \emptyset$ and $\Omega_k \cap X_- \neq \emptyset$.

We determine if a subset $\Omega_k \in \{\Omega_j\}_{j=1}^M$ is a contaminated patch if $I_k > h = h_{X,\Omega}$. Also, the points close to the discontinuity will be marked using the following definition.

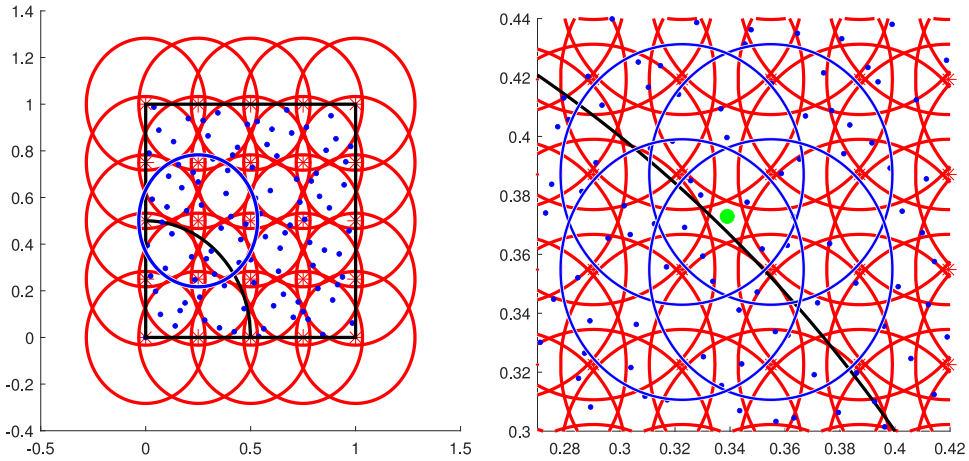

Fig. 2. Black square: frontier of Ω, red circumferences: frontiers of the patches, black curve: discontinuity, blue circumferences: contaminated patches, blue points: data, red stars: centers of the patches, green point (right): discontinuity point.

Definition 3 (*Discontinuity Points*)**.** Using the notation above presented, let $\mathbf{x} \in \Omega$ be a point of the domain, $\varepsilon > 0$ be a fixed threshold and

$$S(\mathbf{x}) = \{j \in \{1, \dots, M\} : \mathbf{x} \in \text{supp}(\Omega_j),\ \varphi_j(\mathbf{x}) > \varepsilon\},$$
$$\tilde{S}(\mathbf{x}) = \{j \in \{1, \dots, M\} : \mathbf{x} \in \text{supp}(\Omega_j),\ \Omega_k \cap X_+ \neq \emptyset,\ \Omega_k \cap X_- \neq \emptyset,\ \varphi_j(\mathbf{x}) > \varepsilon\},$$

then $\mathbf{x}$ is a discontinuity point if

$$S(\mathbf{x}) = \tilde{S}(\mathbf{x}).$$

This definition means that a point is a discontinuity point only if all the patches used to interpolate at that point are contaminated, Definition 2. Last definition, Definition 3, is quite relevant to design the new algorithm. This is due to the fact that, at the discontinuity points, the strategy to interpolate has to be changed due to the oscillations produced by the RBF method close to the discontinuity curve. Hence, the most problematic case is the one in which all the patches containing the point where the interpolation is desired, $\mathbf{x}$, are contaminated, except for one whose weight, $\varphi_j(\mathbf{x})$, is close to zero. For this reason, we impose the threshold condition in the previous definition, Definition 3. The value ε is also relevant for determining the parameter t, since if, for some subindex j_0, a discontinuity intersects Ω_{j_0} and $\varphi_{j_0}(\mathbf{x}) > \varepsilon$, albeit by a very small margin, it is necessary to ensure that the weight assigned to this patch is sufficiently large. Consequently, the parameter t must also be chosen to be high enough depending of h, Eq. (12). In Fig. 2 we can see a picture with the representation of the two previous concepts, Definitions 2 and 3. We represent the data points using blue dots, the patch boundaries with red circles, the discontinuity curve and the domain boundary with black lines, and the patch centers with red stars. In the figure on the left, the contaminated patch is indicated with a blue circle. In the figure on the right, the point at which the function is to be approximated is marked in green, while the patches used for interpolation are highlighted in blue. It can be observed that all the patches are contaminated, indicating that the green point is a discontinuity point.

With these definitions, the following result is straightforward based on Theorem 3.1, where an error bound is deduced dependent on the smoothness of the function Φ and its native space $\mathcal{N}_\Phi$.

Theorem 5.1. *Suppose $\Omega \subseteq \mathbb{R}^n$ is open and bounded, and let $X = \{\mathbf{x}_i\}_{i=1}^N \subseteq \Omega$. Let $\Phi \in C_\nu^{2k}(\mathbb{R}^n)$ be strictly positive definite. Let $\{\Omega_j\}_{j=1}^M$ be a regular covering for (Ω, X) and let $\{w_j\}_{j=1}^M$ be k-stable for $\{\Omega_j\}_{j=1}^M$. Then, if $\mathbf{x} \in \Omega_+$, it is not a discontinuity point, Def. 3, and $f_\pm \in \mathcal{N}_\Phi(\Omega_\pm)$, the error between f and its non-linear partition of unity interpolant, Eq. (13), with $t \geq k/2 + \nu/4$ can be bounded by*

$$|f(\mathbf{x}) - \mathcal{I}_{NL\text{-}PUM}(f)(\mathbf{x})| \leq C h^{k+\frac{\nu}{2}} \|f\|_{\mathcal{N}_\Phi(\Omega_+)}.$$

Analogously, if $\mathbf{x} \in \Omega_-$ and it is not a discontinuity point.

In other words, if $\mathbf{x} \in \Omega$ and there exists, at least, a patch Ω_k free of discontinuities, then the order of accuracy is conserved. Consequently, the discontinuity points have to be treated in a special manner. Also, if we suppose (without loss of generality) that

$$\lim_{\mathbf{x} \to \mathbf{x}_0 \in \Gamma} f_+(\mathbf{x}) < \lim_{\mathbf{x} \to \mathbf{x}_0 \in \Gamma} f_-(\mathbf{x}),$$

we cannot ensure that if $\tilde{\mathbf{x}} \in \Omega$ is a discontinuity point then

$$\lim_{\mathbf{x}\to\mathbf{x}_0\in\Gamma} f_+(\mathbf{x}) \leq \mathcal{I}_{\text{NL-PUM}}(f)(\tilde{\mathbf{x}}) \leq \lim_{\mathbf{x}\to\mathbf{x}_0\in\Gamma} f_-(\mathbf{x}).$$

For this reason, in order to avoid some oscillations of the interpolator $\mathcal{I}_{\text{NL-PUM}}(f)$ close to the discontinuities, we modify our algorithm and explain it in the next subsection.

5.2. On the implementation of the method. Avoiding oscillations close to the discontinuities

We compute our method using the implementation explained by Cavoretto et al. in [9], based on the partitioning data procedures proposed in [4]. Let $\{\hat{\mathbf{x}}_k\}_{k=1}^{L} \subset \Omega$ be a sample where we want to approximate the function f, we start with the covering of the domain Ω, consider some centers $P = \{\bar{\mathbf{x}}_j\}_{j=1}^{M} \subset \Omega$, fix a radius δ and construct the subdomains $\Omega_j = B(\bar{\mathbf{x}}_j, \delta)$ where $B(\bar{\mathbf{x}}_j, \delta)$ is a ball of center $\bar{\mathbf{x}}_j$ and radius δ. It is important to remark, as noted in [2,9], that if a nearby node distribution is chosen, M is an adequate number of PU subdomains if

$$\frac{N}{M} \approx 2^n,$$

then, the radius has to satisfy the condition, [9]:

$$\delta \geq \frac{1}{M^{\frac{1}{n}}}. \tag{14}$$

At this point, we estimate the smoothness indicators I_j, Eq. (11) and mark the contaminated patches, Definition 2. The interpolation data located in each subdomain j are found using the partitioning data structures explained in [9]. After this, we estimate the non-linear weights at each point $\hat{\mathbf{x}}_k$ using the smoothness indicators calculated, and label the discontinuity points, we called them $\tilde{\mathbf{x}}_j$. We apply the classical Shepard's method only for these points, with the same compactly supported function used in PUM. In summary, we describe the algorithm in two passes:

1. We use the software designed in [9] and mark the discontinuity points, $\tilde{\mathbf{x}}$.
2. We apply the Shepard's method to these discontinuity points.

Due to the partitioning data structures introduced in [9], which allow us to organize data very efficiently across different subdomains, the modifications inserted to make the algorithm non-linear are not too costly in terms of computational efficiency.

6. Numerical experiments

In this section, we perform some tests in order to check two principal properties of the new non-linear algorithm, NL-PUM, in comparison with the classical one, PUM. We will conduct the experiments using a uniform grid and Halton's points as data. Firstly, in Section 6.1, we employ our method with a continuous function, in particular with Franke's function, Eq. (1), to verify the order of accuracy. Next subsection is devoted to analyze the elimination of the non-desired oscillations close to the discontinuities, we come back to the example presented in the introduction, Section 1, and show the powerful capabilities of the new algorithm for this type of functions. We take the same parameters as [9] in all the experiments, i.e., the number of patches in one direction is $\lfloor\sqrt{N}/2\rfloor$ and the radius $\delta = \sqrt{2/M}$.

6.1. Order of accuracy

We begin by analyzing the order of accuracy using the widely recognized Franke's function, Eq. (1), using as data points a regular grid defined by $X_{N=2^l+1} = \{(i/2^l, j/2^l) : i, j = 0, \ldots, 2^l\}$, and a set of $N = (2^l+1)^2$ Halton's scattered data points, [15]. We denote the fill distance by h_l, and the errors by $e_k^l = |f(\hat{\mathbf{x}}_k) - \mathcal{I}^l(\hat{\mathbf{x}}_k)|$, where $\{\hat{\mathbf{x}}_k\}_{k=1}^{60}$ is a regular grid in $[0,1]^2$. We define the maximum discrete ℓ^2 norms and their respective convergence rates as follows:

$$\text{MAE}_l = \max_{i=1,\ldots,60} e_i^l, \quad \text{RMSE}_l = \left(\frac{1}{60}\sum_{i=1}^{60}(e_i^l)^2\right)^{\frac{1}{2}},$$
$$r_l^{\infty} = \frac{\log(\text{MAE}_{l-1}/\text{MAE}_l)}{\log(h_{l-1}/h_l)}, \quad r_l^2 = \frac{\log(\text{RMSE}_{l-1}/\text{RMSE}_l)}{\log(h_{l-1}/h_l)}.$$

In the first example, we choose Matèrn function, ϕ_{M_2} for the RBF problems, and the Wendland C^2 function ϕ_{W_2}, for the partition of unity. We present the results in Table 1, and it is clear that they are very similar for both the linear and non-linear methods. The expected theoretical order of accuracy, Prop. 2.3, is improved for the two algorithms in this example. With respect to the errors, the NLPUM yields slightly better results when the data is placed on an uniform grid.

To finish this subsection, we repeat the experiment using the functions ϕ_{M_4} for the RBF method and ϕ_{W_4} for the partition of unity. The results are shown in Table 2. Again, we can see that the errors and orders of accuracy are very similar.

Table 1
Errors and rates using PUM and NLPUM for Franke's test function: two first columns evaluated at grid points and two final columns evaluated at Halton's points. For RBF problems the C^2 Matérn function ϕ_{M_2} has been used, and for partition of unity the Wendland function ϕ_{W_2} is used, i.e. $\varphi_j = \phi_{W_2}$, for all j.

Grid points					Halton's points			
	PUM		NLPUM		PUM		NLPUM	
l	MAE_l	r_l^∞	MAE_l	r_l^∞	MAE_l	r_l^∞	MAE_l	r_l^∞
4	7.5944e−03	–	2.8436e−01	–	1.4157e−02	–	2.6937e−02	–
5	1.6541e−03	2.1989	8.6890e−02	1.7105	2.6921e−03	2.1831	2.9567e−03	2.9058
6	3.7494e−04	2.1413	8.8016e−05	9.9472	9.1058e−04	2.3481	6.6469e−04	3.2331
7	1.1278e−04	1.7332	2.6376e−05	1.7385	2.0617e−04	1.9743	3.0466e−04	1.0369
8	2.8906e−05	1.9640	7.0429e−06	1.9050	6.0296e−05	1.4750	7.9830e−05	1.6068
	PUM		NLPUM		PUM		NLPUM	
l	RMSE_l	r_l^2	RMSE_l	r_l^2	RMSE_l	r_l^2	RMSE_l	r_l^2
4	1.3800e−03	–	9.6360e−02	–	6.8732e−03	–	9.6360e−02	–
5	2.2904e−04	2.5910	4.7798e−03	4.3334	3.3489e−04	2.2581	4.7798e−03	3.9740
6	5.8939e−05	1.9583	1.5566e−05	8.2624	3.8497e−05	2.7589	1.5566e−05	4.6860
7	1.8977e−05	1.6350	1.9141e−06	3.0236	5.9659e−06	1.8766	1.9141e−06	2.4782
8	4.0380e−06	2.2325	2.5281e−07	2.9206	7.4670e−07	1.7219	2.5281e−07	2.4933

Table 2
Errors and rates using PUM and NLPUM for Franke's test function: two first columns evaluated at grid points and two final columns evaluated at Halton's points. For RBF problems the C^4 Matérn function ϕ_{M_4} has been used, and for partition of unity the Wendland function ϕ_{W_4} is used, i.e. $\varphi_j = \phi_{W_4}$, for all j.

Grid points					Halton's points			
	PUM		NLPUM		PUM		NLPUM	
l	MAE_l	r_l^∞	MAE_l	r_l^∞	MAE_l	r_l^∞	MAE_l	r_l^∞
4	6.4397e−03	–	2.9103e−01	–	8.1704e−03	–	8.7701e−03	–
5	7.6400e−04	3.0754	9.0838e−02	1.6798	8.9459e−04	2.9091	1.1375e−03	2.6863
6	7.3358e−05	3.3805	2.0297e−05	12.1278	3.0378e−04	2.3397	1.6615e−04	4.1672
7	9.0336e−06	3.0216	1.6754e−06	3.5986	2.2676e−05	3.4490	4.5792e−05	1.7129
8	1.5305e−06	2.5613	2.5780e−07	2.7002	2.3915e−06	2.6987	1.0517e−05	1.7650
	PUM		NLPUM		PUM		NLPUM	
l	RMSE_l	r_l^2	RMSE_l	r_l^2	RMSE_l	r_l^2	RMSE_l	r_l^2
4	1.0412e−03	–	1.0168e−01	–	9.6168e−04	–	2.6447e−03	–
5	1.0970e−04	3.2465	4.7209e−03	4.4289	1.0395e−04	2.9260	1.2230e−04	4.0427
6	1.2027e−05	3.1893	2.7164e−06	10.7631	1.3923e−05	4.3550	6.5149e−06	6.3522
7	1.8291e−06	2.7170	1.5998e−07	4.0858	1.7160e−06	2.7826	6.6212e−07	3.0389
8	1.9361e−07	3.2400	1.0651e−08	3.9088	2.0360e−07	2.5573	5.6579e−08	2.9512

6.2. Avoiding discontinuities

In this subsection, we conduct a series of experiments to analyze the behavior of the new interpolator near discontinuities. In all the experiments the initial number of data points is $N = 65^2$.

We begin with a set of experiments in which the original domain $[0,1]^2$ is divided into two subdomains. We assume that the data originates from Franke's function f, as defined in Eq. (1), in one subdomain, and from $1 + f$ in the other, i.e., we define the functions:

$$f_q(x,y) = \begin{cases} 1 + f(x,y), & (x,y) \in \Omega^+, \\ f(x,y), & (x,y) \in \Omega^-, \end{cases}$$

where $\Gamma_q = \{(x,y) \in [0,1]^2 : \zeta_q(x,y) = 0\}$, $\Omega^+ = \{\mathbf{x} \in [0,1]^2 : \zeta_q(\mathbf{x}) \geq 0\}$, $\Omega^- = [0,1]^2 \setminus \Omega^+$. In this series of experiments we employ ϕ_{M_2} as function for RBF problems and $\varphi = \phi_{W_2}$ for the partition of unity.

Let us start with the example presented in the introduction, Section 1, where the discontinuity curve is the following

$$\zeta_1(x,y) = x^2 + y^2 - 0.5^2.$$

In this case, we plot in Fig. 3 the result of the experiment with $L = 120^2$ equidistant points in the square $[0,1]^2$. It is clear, Fig. 3 right column, that the NL-PUM presents an adequate behavior close to the discontinuities whereas the PUM produces some oscillations. When the figure is rotated (Fig. 3 rows 2 and 3), the differences become even more evident.

We also discuss the results when the discontinuities are horizontal, vertical and diagonal lines. For this, we computed a first example with:

$$\Gamma_2 = (\{0.5\} \times [0.5,1]) \cup ([0,0.5] \times \{0.5\}),$$

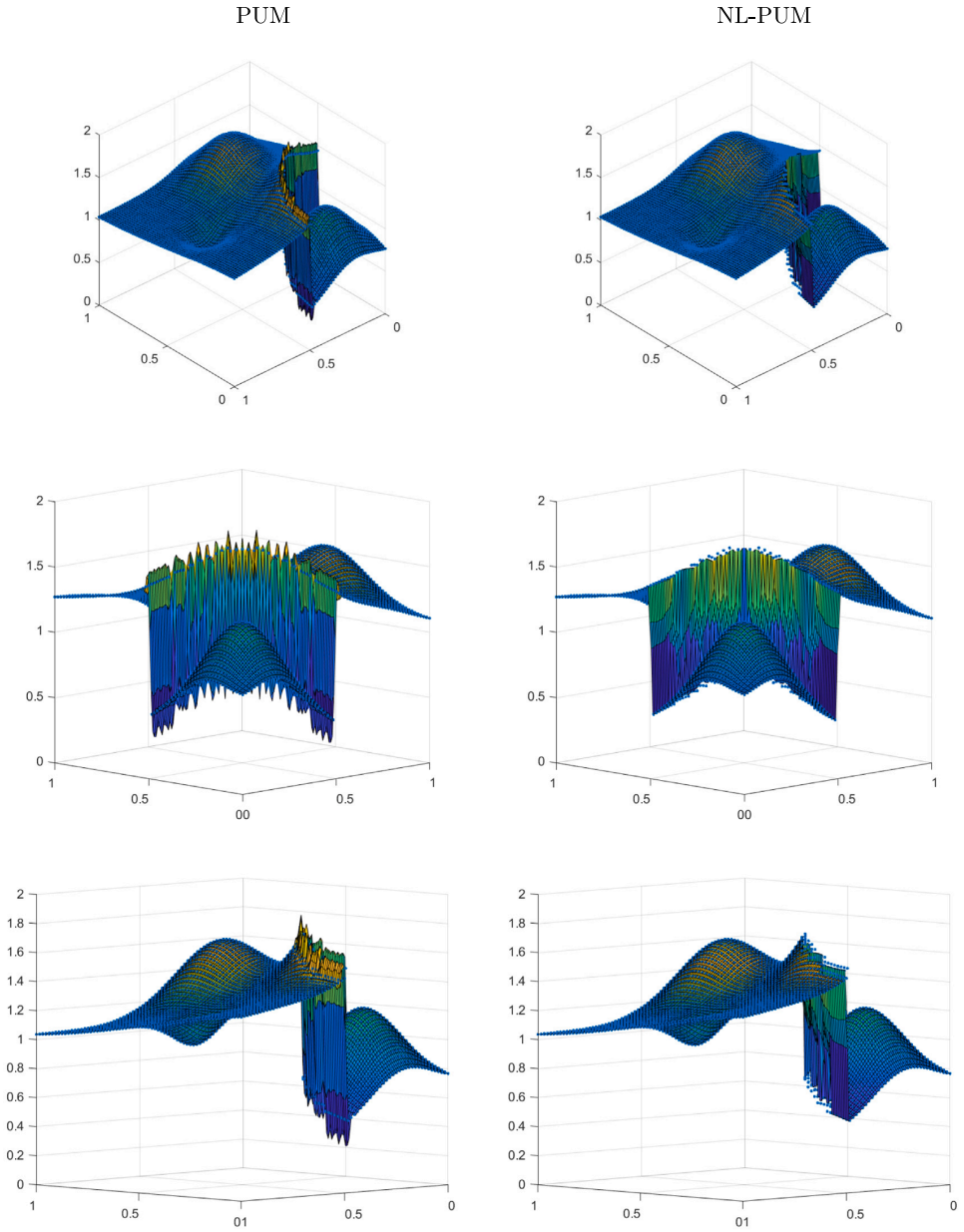

Fig. 3. Approximation of the function f_1 using PUM, and NL-PUM at grid points where we use ϕ_{M_2} for the RBF problems and ϕ_{W_2} for the partition of unity. Second and third rows are rotations of the plots presented in the first row.

and a second with

$$\zeta_3(x, y) = x + y - 1.$$

We illustrate the interpolators for the function f_2 in Fig. 4 and for f_3 in Fig. 5. In these cases we take $N = 65^2$ initial Halton's points and we approximate at $L = 120^2$ final points. Again, we can see that the new method avoids the oscillations.

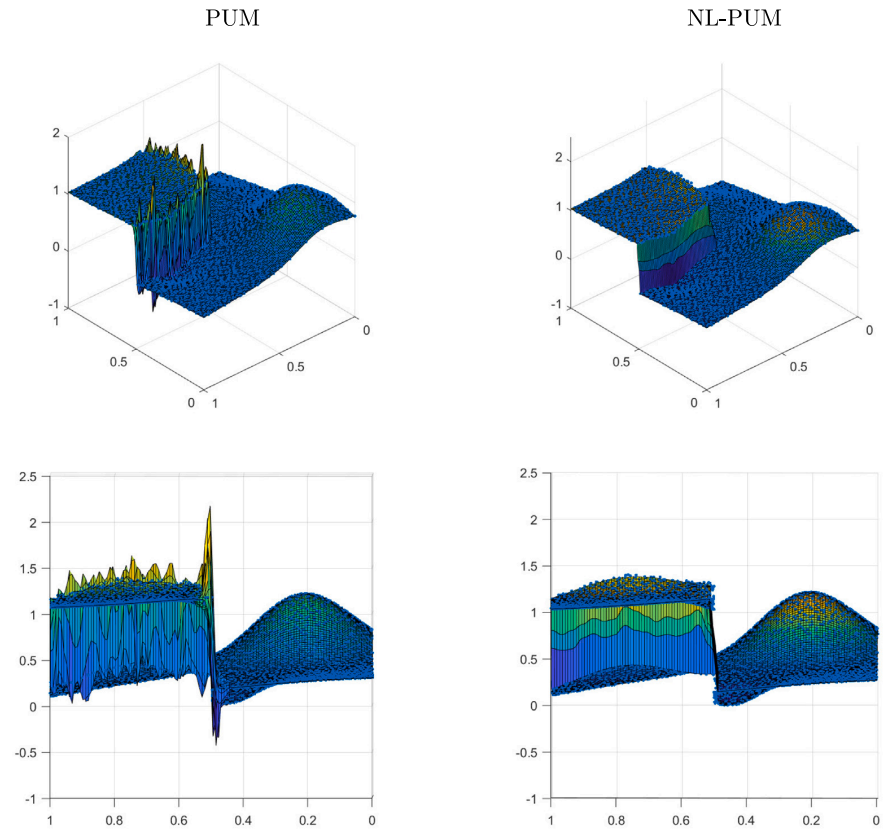

Fig. 4. Approximation to functions f_2 using PUM, and NL-PUM at Halton's points using for RBF problems ϕ_{M_2} and for partition of unity ϕ_{W_2}. The second row is a rotation of the plots presented in the first row.

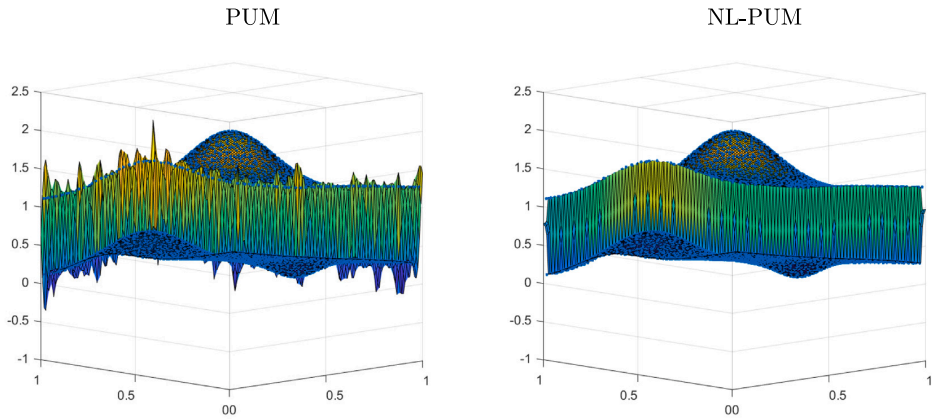

Fig. 5. Approximation to function f_3 using PUM, and NL-PUM at Halton's points using for RBF problems ϕ_{M_2} and for partition of unity ϕ_{W_2}.

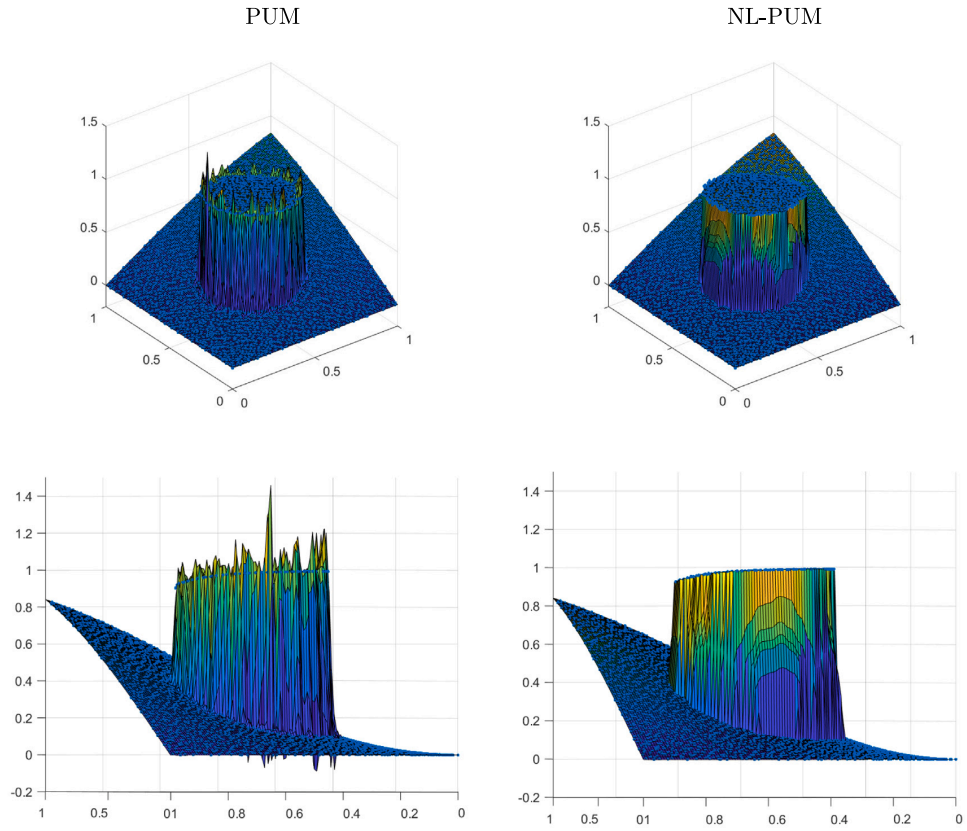

Fig. 6. Approximation to functions z using PUM, and NL-PUM at Halton's points using for RBF problems ϕ_{M_2} and for partition of unity ϕ_{W_2}. The second row is a rotation of the plots presented in the first row.

To end this subsection, we apply the algorithms to the same function employed in [16],

$$z(x,y) = \begin{cases} \sin(xy), & (x-0.5)^2 + (y-0.5)^2 \geq 0.25^2, \\ \cos(xy), & (x-0.5)^2 + (y-0.5)^2 < 0.25^2. \end{cases} \tag{15}$$

We plot the result using ϕ_{M_2} for RBF problems and ϕ_{W_2} for partition of unity in Fig. 6 using Halton's points. Finally, we illustrate the interpolants employing ϕ_{M_4} and ϕ_{W_4} in Fig. 7 using gridded data points in the two first rows, and Halton's points in the two last rows. The interpolators in both cases are very similar. Again, we can see that the new method improves the behavior close to the discontinuities. Furthermore, in Fig. 7 we perform the experiment for Halton and grided data points. The oscillations obtained when the classical PUM is applied are highly significant in contrast to the result obtained when the NL-PUM is employed.

7. Conclusions and future work

In this article, we have introduced a non-linear modification of the Partition of Unity Method (NL-PUM). We believe this is the first time such an approach has been presented in the literature. The design of the new method aims to mitigate the oscillations and smearing around discontinuity zones that the classical PUM method produces. Thus, the NL-PUM presented in this study marks a substantial improvement in PUM techniques, offering a robust solution to the numerical artifacts that appear when discontinuities are introduced in the datasets on which the classical PUM has been tested. The new method is founded on integrating Radial Basis Function (RBF) interpolation with Weighted Essentially Non-Oscillatory (WENO) techniques, improving the results obtained by traditional PUM algorithms close to the discontinuities. By dynamically adjusting weights through smoothness indicators, the NL-PUM selectively conserves accuracy in smooth regions while minimizing oscillations and smearing near discontinuities.

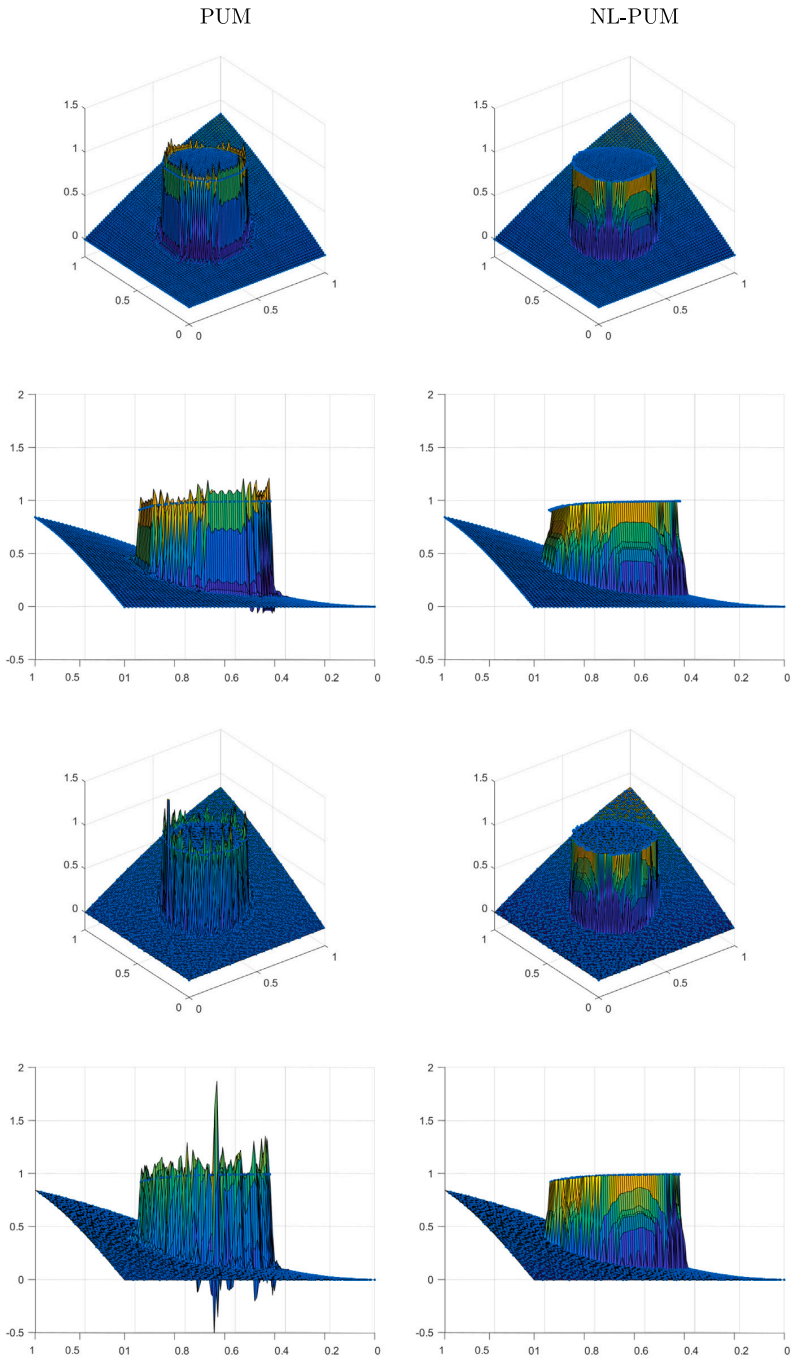

Fig. 7. Approximation to function z using PUM, and NL-PUM where we use ϕ_{M_4} for the RBF problems and ϕ_{W_4} for the partition of unity employing gridded data points (two first rows) and Halton's points (two last rows). The second and fourth rows are a rotation of the plots presented in the first row and third row respectively.

Numerical experiments confirmed that the NL-PUM maintains the order of accuracy expected from the traditional PUM method in continuous domains while exhibiting superior performance in discontinuous settings. This is achieved by identifying and treating *contaminated patches* near discontinuities, effectively eliminating oscillations that commonly arise in such scenarios. The method's ability to consistently produce reliable results, regardless of the orientation or complexity of discontinuities, emphasizes its robustness.

While the NL-PUM demonstrates promising capabilities, it also presents certain limitations, such as its reliance on well-tuned parameters. These factors highlight the need for further research to optimize and simplify the method. Future work could focus on automating parameter selection, extending the framework to higher-dimensional problems, and exploring its application in practical contexts such as image processing and fluid dynamics.

Data availability

No data was used for the research described in the article.

References

[1] M.D. Buhmann, Radial Basis Functions: Theory and Implementations, Cambridge University Press, 2003.
[2] G.E. Fasshauer, Meshfree Approximation Methods with Matlab, World Scientific Publishing, Singapore, 2007.
[3] H. Wendland, Scattered Data Approximation, Cambridge University Press, 2004.
[4] R. Cavoretto, A. De Rossi, A trivariate interpolation algorithm using a cube-partition searching procedure, SIAM J. Sci. Comput. 37 (2015) A1891–A1908.
[5] R. Cavoretto, A. De Rossi, E. Perracchione, Efficient computation of partition of unity interpolants through a block-based searching technique, Comput. Math. Appl. 71 (2016) 2568–2584.
[6] F. Dell'Accio, F. Di Tommaso, F. Larosa, The multinode shepard method: MATLAB implementation, J. Approx. Softw. 1 (2024).
[7] X.-D. Liu, S. Osher, T. Chan, Weighted essentially non-oscillatory schemes, J. Comput. Phys. 115 (1994) 200–212.
[8] C.-W. Shu, High order weighted essentially nonoscillatory schemes for convection dominated problems, SIAM Rev. 51 (1) (1999) 82–126.
[9] R. Cavoretto, A. De Rossi, E. Perracchione, S. Lancellotti, Software implementation of the partition of unity method, Dolomites Res. Notes Approx. 15 (2) (2022) 35–46.
[10] H. Wendland, Fast evaluation of radial basis functions: methods based on partition of unity, in: J. Stöckler C.K. Chui (Ed.), Approximation Theory X: Wavelets, Splines, and Applications, Vanderbilt Univ. Press, Nashville, TN, 2002, pp. 473–483.
[11] G. Jiang, C.-W. Shu, Efficient implementation of weighted ENO schemes, J. Comput. Phys. 126 (1) (1996) 202–228.
[12] S. Amat, J. Ruiz, C.W. Shu, D.F. Yáñez, A new WENO-2r algorithm with progressive order of accuracy close to discontinuities, SIAM J. Numer. Anal. 58 (6) (2020) 3448–3474.
[13] F. Aràndiga, A.M. Belda, P. Mulet, Point-value WENO multiresolution applications to stable image compression, J. Sci. Comput. 43 (2) (2010) 158–182.
[14] P. Mulet, J. Ruiz, C.W. Shu, D.F. Yáñez, A non-separable progressive multivariate WENO-2r point value, App. Numer. Math. 204 (2024) 26–47.
[15] J.H. Halton, On the efficiency of certain quasi-random sequences of points in evaluating multi-dimensional integrals, Numer. Math. 2 (1960) 84–90.
[16] S. Amat, D. Levin, J. Ruiz-Álvarez, D.F. Yáñez, Non-linear WENO B-spline based approximation method, Numer. Algor. 100 (10) (2024).